Mathematical modelling of polymer degradation in cellulose acetate artefacts in cultural heritage collections

Ida Rebecca Ahmad

University College London

Institute for Sustainable Heritage

Thesis submitted for the degree of Doctor of Philosophy

6th June 2022

I, Ida Rebecca Ahmad, confirm that the work presented in this thesis is my own. Where information has been derived from other sources, I confirm that this has been indicated in the thesis.

_____

Ida Rebecca Ahmad

ABSTRACT

Cellulose acetate (CA) is one of the earliest man-made polymers. The oldest CA artefacts housed in museum collections are no more than a century old. However, the degree and the rate of damage observed in these items, which may have appeared stable before acquisition, as well as in other objects stored near them, has resulted in its reputation as a "malignant" plastic. This PhD thesis presents the development of mathematical models to investigate the dynamics of polymer degradation in CA. Polymer degradation refers to irreversible changes in the polymer molecule due to chemical reactions. Two types of polymer degradation were investigated, deacetylation and chain scission. Both are believed to be due to reaction of the polymer with water, present as moisture in the object. Deacetylation produces acetic acid; acidic conditions are associated with catalysing both deacetylation and chain scission. The degree of deacetylation appears to impact the susceptibility of the polymer to chain scission. These causal relationships were modelled by developing systems of differential equations, which were solved computationally. Quantitative inputs, such as rate constants, were obtained by fitting to experimental data collected by other researchers, or by estimating values based on comparable reference systems found in the literature. The models were evaluated on their prediction errors on unseen data (data not used for training the models) and tended to outperform benchmarks. The results suggest that current guidelines for cellulose triacetate film conservation may be overestimating the benefits of cold storage to prolonging film lifetime. Finally, the thesis discusses the implications for museum professionals trying to conserve CA artefacts, based on the understanding of the system dynamics developed through this investigation.

ACKNOWLEDGEMENTS

IMPACT STATEMENT

This PhD was a part of the European Research Council Starting Grant funded project "COMPLEX: The Degradation of Complex Modern Polymeric Objects in Heritage Collections: A System Dynamics Approach", which aimed to develop new approaches to understanding and modelling the degradation of modern polymeric materials in collections. During my PhD, I had the opportunity to present my research to the stakeholders involved in the COMPLEX project. I presented my research at several Advisory Board and partners meetings, in which the following institutions were represented: University College London, University of Cambridge, University of Sussex, the Design Museum, the National Museum of Denmark, the National Physical Laboratory, Museum of London, Lacerta, Process Systems Enterprise, and Tate.

As a PhD in the Science and Engineering for Arts, Heritage and Archaeology (SEAHA) Centre for Doctoral Training, the PhD was expected to include collaboration with heritage and industry partners, who were represented in their roles as tertiary supervisors.

Tate was the heritage partner, with Dr Joyce H. Townsend and Deborah Cane as my supervisors. Benefits of collaboration with Tate included insight into the museum perspective on care of collections as well as on-site access to artefacts in storage facilities. The latter provided indispensable first-hand experience of real degrading CA artworks, such as *Construction in Space 'Two Cones'* (1927) by Naum Gabo (see Chapter 1, Figure 1.1).

Process Systems Enterprise (PSE) was the industry partner, with Dr Cristian Triana as my supervisor. PSE provided academic licenses for the gPROMS modelling software, which was used to implement a system model combining the deacetylation model presented in Chapter 4 of this thesis and a plasticiser model developed by COMPLEX researcher Argyro Gili. The system model, which was implemented by myself, is an example of how my PhD research contributed towards the COMPLEX project.

The research presented in this thesis could have benefits in several ways.

First, the discovery that cellulose triacetate cinematographic film lifetimes may be overestimated (Chapters 4 and 7) has urgent implications for film conservation guidelines. The results suggest that these films may be less stable than previously thought, and that it may be prudent to prioritise duplicating these films to a more stable medium. These findings were disseminated through publication of a peer-reviewed paper (1) in a scientific journal, a news article (2) on a popular science website, and the presentation of a talk at the American Institute for Conservation 48th Virtual Annual Meeting

Second, the mathematical model which accounts for monomer composition in the deacetylation kinetics of cellulose acetate (Chapter 5) is a new tool for analysing mechanisms in the chemical reactions it describes. This was demonstrated by the application of the model to experimental data published by other researchers. The results of this analysis appear to contradict some of the earlier theories about the reactions of acetyl groups in cellulose acetate. The model is quite general and could be applied to other substitution kinetics in cellulose derivatives. There is also already published data of other cellulose derivatives that could be used with this model, which were not considered in this thesis as the focus was cellulose acetate. The model could be used as a framework to analyse this data and provide new perspectives for understanding cellulose substitution kinetics. This research could be disseminated in the form of a peer-reviewed paper in a scientific journal.

Third, the mathematical model which couples substitution and depolymerisation kinetics (Chapter 6) could enhance future studies of polymer degradation. This could be within the field of heritage science—to better understand degradation of plastic heritage—or in a broader context. Cellulose and starch are of interest in the development of environmentally friendly plastics, due to their being plant-based as well as the possibility for biodegradation. Carbohydrate polymers are typically modified by substitutions of functional groups to engineer new materials with desirable properties. The model could be used to understand how these materials degrade in the natural environment, or even during manufacturing processes. It is possible that objects composed of such materials are eventually acquired into cultural heritage collections, where it could be beneficial for conservators to understand how these materials are expected to degrade. These impacts are more

speculative, and depend on incremental research, industry, and societal developments in the future. Nonetheless, the novel theoretical framework provided by the mathematical model should be shared to the research community, perhaps as a peer-reviewed paper in a scientific journal.

Conferences:

International Institute of Conservation – Palace Museums 2018 Beijing Symposium (1 – 2 November 2018)

Science and Engineering for Arts, Heritage and Archaeology Conference 2019 (1 – 3 April 2019)

Plastics Heritage Congress 2019 (29 – 31 April 2019)

American Institute for Conservation 48th Virtual Annual Meeting (19 May – 31 Aug 2020)

Publications:

1. Ahmad IR, Cane D, Townsend JH, Triana C, Mazzei L, Curran K. Are we overestimating the permanence of cellulose triacetate cinematographic films? A mathematical model for the vinegar syndrome. Polymer Degradation and Stability [Internet]. 2020 Feb;172:109050. Available from: https://doi.org/10.1016/j.polymdegradstab.2019.109050
2. Ahmad IR. Historical films may be decaying much faster than we thought thanks to "vinegar syndrome" [Internet]. The Conversation. 2020 [cited 2022 Feb 21]. Available from: https://theconversation.com/historical-films-may-be-decaying-much-faster-than-we-thought-thanks-to-vinegar-syndrome-131712

CONTENTS

LIST OF FIGURES

LIST OF TABLES

1 INTRODUCTION

1.1 THE PROBLEM OF DEGRADATION

Deterioration in cultural heritage artefacts is associated with causing a loss of value due to accumulation of damage over time. Value is a subjective quality, attributed by stakeholders such as historians, communities or individuals whose heritage is represented, curators, owners, museum visitors, and conservation professionals (1). Heritage has multiple values, which are mutable, incommensurable, and in conflict (1). Examples of different kinds of values include utility, aesthetic, economic, emotional, existence, and evidence (2,3). Acknowledging the complexity and nuance of determining heritage value, preserving heritage value is a key motivation for studying degradation in cellulose acetate (CA) artefacts. As with all scientific research, the study of degradation processes may also provide insight in other disciplines and sectors, in this case one example is those concerned with plastic performance.

Artefacts made of cellulose acetate are considered difficult to conserve due to their tendency to deteriorate relatively rapidly and unpredictably after long periods of apparent stability. The first sign of degradation in CA artefacts is the presence of an odour known to film archivists and museum conservators as the "vinegar syndrome" or "Pedigree Doll disease" (4–7). Acetic acid, commonly known as vinegar, is a degradation product generated by the reaction of water and cellulose acetate. Emissions of acetic acid may cause damage to storage materials or other nearby objects, lending cellulose acetate its reputation as a "malignant" plastic (8,9).

In CA films, other changes in film properties will typically follow the vinegar syndrome. These include reduction in tensile strength or toughness due to degradation of the polymer (*embrittlement*), buckling of emulsion away from the base layer (*shrinkage* and *channelling*), and surface deposits caused by the migration of plasticiser (*crystals* or *bubbles*) (10–14). Historical archives, including public records and cultural heritage institutes, are already seeing damage to their film collections due to the inherent instability of CA films (15,16).

Aside from film archives, CA plastics feature in sculptures by constructivist artists such as Naum Gabo, László Moholy-Nagy and Antoine Pevsner (17). *Construction in Space: Two Cones* (1927), a CA sculpture by Gabo, started disintegrating in 1967 while kept at the Philadelphia Museum of Art (18). The artist blamed the museum for not taking care of it properly and produced a replica in the same material, which is kept at Tate today (19). Presently, the replica (Figure 1.1) shows signs of deterioration such as *warping*, *crazing* and crystal growth, and is deemed too deteriorated to be displayed (20).
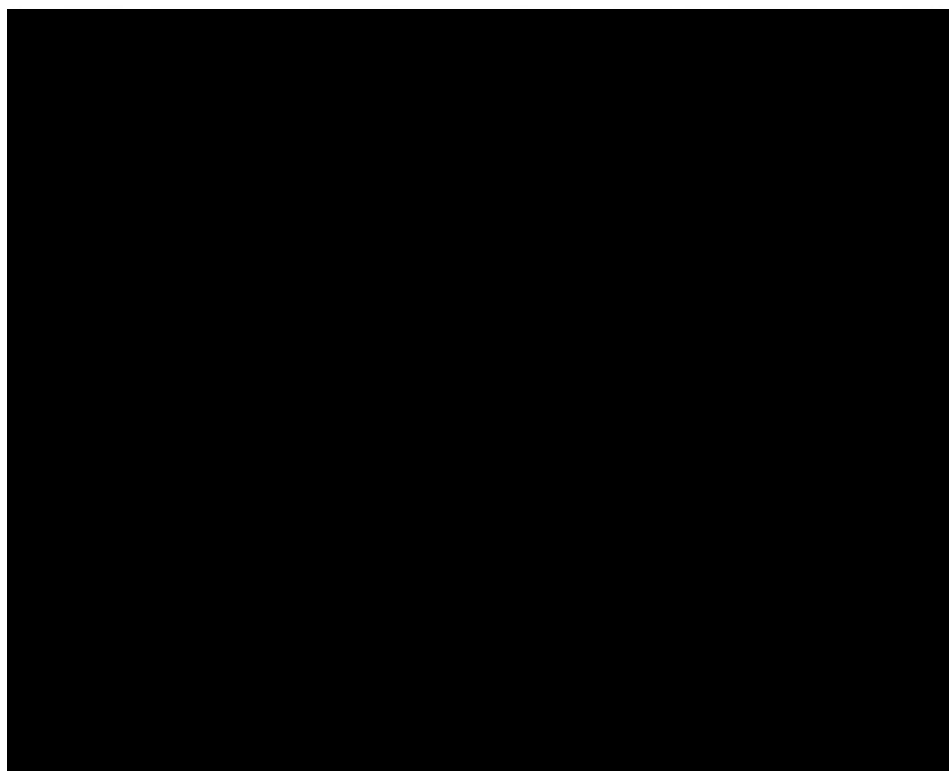
Figure 1.1   Naum Gabo 1890-1977. Tate T02143 *Construction in Space 'Two Cones'* 1927, this version a replica made by the artist in 1968 using the same materials as for the original. Cellulose acetate. The Work of Naum Gabo © Nina & Graham Williams/Tate, London 2022. Caption and photo (17).

Recognising the timeliness of the conservation of plastic objects, the European Commission funded the POPART: Preservation Of Plastics ARTefacts research project, a consortium of 13 partners from eight countries, which lasted from 2008 to 2012 (21). In the POPART survey (22) of plastic artefacts in three museums, about 20% of the objects surveyed were made of cellulose acetate or cellulose

nitrate, mostly fashion accessories at musée Galliera. About 37% of these were classified as being in "poor" or "severe" condition. The types and frequency of important or severe damages suggest that those due to internal decaying processes play a prominent role compared with external causes, confirming the physical and chemical instabilities of the materials (23).

1.2 DEGRADATION IN CELLULOSE ACETATE ARTEFACTS

Collins English Dictionary (24) defines degradation as "a breakdown of a molecule into atoms or smaller molecules" and "an irreversible process in which the energy available to do work is decreased". Considering how these concepts apply to cellulose acetate artefacts, this work employs a more context-specific definition of degradation, as irreversible change in the chemistry of the material from its initial composition. Degradation is therefore relative to an agreed-upon starting point. For example, fluctuations in moisture content due to cycling relative humidity conditions do not constitute degradation as this change is reversible. Plasticiser loss is included in this definition as it is not reversible. Cracking, while irreversible, is not degradation as it does not involve a change in chemical composition.

The material "cellulose acetate plastic" contains multiple components, including the polymer, plasticisers, other additives such as pigments and stabilisers, as well as water and other small molecules absorbed from the environment surrounding the plastic. These participate in several physicochemical processes identified in the degradation of CA artefacts, including:

- *Deacetylation*: Chemical reaction with water, resulting in a change in the composition of the individual monomers (anhydroglucose units, or AGUs) of which the CA polymer is composed (4).
- *Chain scission*: Also known as chain degradation, cleavage of the links connecting monomers results in large polymer molecules splitting into smaller polymer chains (26).
- *Loss of plasticiser*: Common plasticisers such as triphenyl phosphate (TPP) and diethyl phthalate (DEP) can diffuse out of the body of the plastic, evaporating from the surface and/or forming liquid or crystalline deposits (27,28).

17

- *Degradation of additives (including plasticisers and residual impurities)*: These molecules may undergo chemical changes over time. For example, TPP reacts with moisture to form a more acidic diphenyl phosphate and phenol (29).

Studies (4,30) on CA films and CA objects have found evidence that suggests deacetylation occurs first, with chain degradation following later. This has led to speculation that deacetylation is a necessary pre-requisite for chain scission. The retention of acidic products resulting from reactions such as deacetylation or degradation of additives have the effect of catalysing further degradation reactions (30,31). Changes in the polymer matrix may reduce its compatibility with plasticiser and increase moisture retention (32). It is not well-understood whether deacetylation precedes or follows plasticiser loss, or how other factors affect this (30).

1.3 RESEARCH AIM AND QUESTIONS

Mathematical models have been used in heritage conservation to understand the role of environmental factors on degradation, but these have limited use for materials whose rate of degradation appears to be influenced by the dynamics of intrinsic factors. These reductionist approaches appear to yield reasonable approximations for short timescales, little degradation, or one type of degradation, but fail to generalise for longer timescales, more advanced degradation, or multiple/combined forms of degradation.

The interactions and effects of the physicochemical processes listed in Section 1.2 are the scope of the COMPLEX research project, of which the research presented in this PhD forms a part. This PhD thesis focuses on polymer degradation, defined as processes that alter the composition of the CA molecule. Specifically, the research project aims to develop mathematical models of deacetylation and chain scission in CA cultural heritage artefacts.

The research questions are:

- How have analytical methods been used to study polymer degradation in CA artefacts, and what can these studies tell us about the underlying phenomena?

- How does polymer degradation in CA artefacts manifest in tangible signs of damage, and how does this influence which metrics of polymer degradation we should be concerned with as model outputs?

- How have mathematical models been used to understand polymer degradation in CA artefacts up until now?

- How can novel mathematical models represent causal relationships underlying CA deacetylation and chain scission?

- To what extent can novel mathematical models of deacetylation and chain scission enhance our understanding of CA polymer degradation?

- To what extent can these new mathematical models improve our ability to manage risk and conserve CA cultural heritage artefacts?

1.4 THESIS OUTLINE

This chapter introduced some of the gaps in our understanding of CA polymer degradation and the consequences that CA instability has for conservation of cultural heritage collections, that motivate the research aim and questions for this work.

In Chapter 2, a literature review establishes the current understanding of CA polymer degradation and its effects on heritage conservation. This establishes the causal relationships in polymer degradation that this work aims to model, the evidence for these, and the role of understanding CA degradation dynamics in conserving cultural heritage.

Chapter 3 discusses the role of mathematical models in heritage conservation, and approaches to mathematical modelling of polymer degradation in heritage and non-heritage contexts. Having reviewed the research context, methods, and opportunities in Chapters 2-3, Chapter 3 concludes by underlining the original contribution of this thesis.

Chapter 4 presents the development of an autocatalytic model of deacetylation. This model looks at how acetic acid produced by deacetylation causes acceleration of deacetylation. The model is trained and tested on published literature data on cellulose triacetate films.

In Chapter 5, a mathematical model of deacetylation which can simulate how AGU composition varies with time is described and analysed. As a proof-of-concept, the model is trained on published literature data of lab-prepared CA samples degraded in aqueous acidic solution.

Chapter 6 combines the deacetylation models in Chapters 4-5 and builds on the outputs (acetic acid concentration and AGU composition as a function of time) to develop the model of chain scission. This model is based on the theory that chain bonds between AGUs are more susceptible to scission after the AGUs have been deacetylated. The model is trained on cross-sectional data sampled from naturally aged CA artefacts. One dataset is from a published study and the second is from research carried out by other COMPLEX workers. Cross-validation is used to compare the performance of the novel model against a benchmark model for polymer degradation in historic artefacts.

Chapter 7 discusses the practical consequences of the models developed in Chapters 4-6, for conserving cultural heritage. Although it refers to some results obtained in earlier chapters, this chapter does not require deep familiarity with the mathematics of the models, and it includes overviews of the models for non-technical readers. I reflect on some of the challenges of developing models for heritage conservation and discuss the benefits and limitations of mathematical models based on my experiences while conducting this research project.

Chapter 8 summarises the main takeaways of the work, discusses whether the work succeeds in answering the research questions set out at the start, and proposes suggestions for future research directions.

2 CELLULOSE ACETATE DEGRADATION

This chapter is an introduction to polymer degradation in cellulose acetate (CA) artefacts in cultural heritage collections. The literature review aims to cover polymer degradation in depth, while presenting sufficient coverage of other aspects of CA degradation to establish:

- *key analytical methods to measure polymer degradation*
- *the motivation for focusing on polymer degradation*
- *factors affecting polymer degradation*
- *possible interactions of polymer degradation with other processes*
- *the conservation context of the research.*

2.1 INTRODUCTION

In this work, only tangible deterioration is considered. Tangible deterioration refers to phenomena that can be measured objectively using analytical methods used by natural scientists. Such phenomena can be assessed across a variety of aspects. For example, types of deterioration could be categorised by: agent (moisture, heat, light); degradation process (deacetylation, chain scission); or damage (cracking, warping, yellowing). There are clearly opportunities to propose links between the ways that deterioration is understood under each of these categories. One framework (Figure 2.1) is that agents induce microscopic degradation processes (or those which occur on an even smaller scale), which result in macroscopic property changes observed as damage. This framework underlies most of the proposed explanations in the literature covering damage in CA artefacts and will be applied in this thesis. The application of this framework has led to a set of hypothesised relationships between agents, degradation, and damage, several of which appear to have become accepted (to varying degrees) tacitly by researchers in the field. This is not to suggest that only explanations following this simplistic, linear format have been proposed, and indeed the possibility that more complex relationships may exist contributes to the challenges and opportunities in the field.
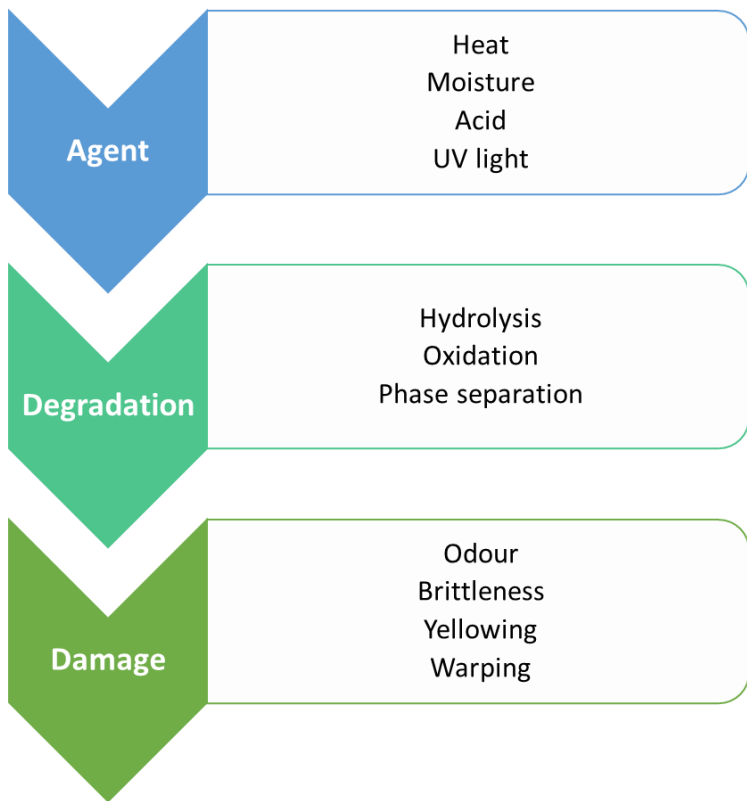
Figure 2.1 Agent-degradation-damage framework, with examples of each.

This review aims to uncover evidence and explanations of polymer degradation in CA-based artefacts. In this respect, the review aims to identify research opportunities presented by knowledge gaps in polymer degradation mechanisms and the relationships between polymer degradation, its causes (agents), and its effects (damage), in the context of cultural heritage collections. Research published in peer-reviewed scientific journals form the bulk of the references; however, other sources of information were also consulted—including patents, news reports, standards, guidelines, and condition surveys—as these offer rich insight into the practical consequences of degradation and beliefs about degradation in the heritage sector.

2.2 WHERE DO CELLULOSE ACETATE ARTEFACTS COME FROM?

Cellulose acetate was first synthesised in 1865 by French physician and chemist Paul Schützenberger (33,34). It is a derivative of the naturally occurring polymer cellulose, which is produced in plants (35). In cellulose acetate, the monomers are anhydroglucose units (AGUs) that are substituted by up to three acetyls (CH_3CO)

at carbon positions 2, 3, and 6 (Figure 2.2). The degree of substitution (DS) describes the average degree of acetylation in cellulose acetate and can vary from 0 to 3 (36). DS impacts the properties of cellulose acetate, such as its miscibility in different solvents: cellulose triacetate with a DS of 3.0 is easily soluble in chloroform, but cellulose diacetate with a DS of 2.3 is soluble in acetone (30,36). Consequently, CA is produced in a range of DSs which reflects its use in diverse products from cigarette filters to hair combs (37–39).
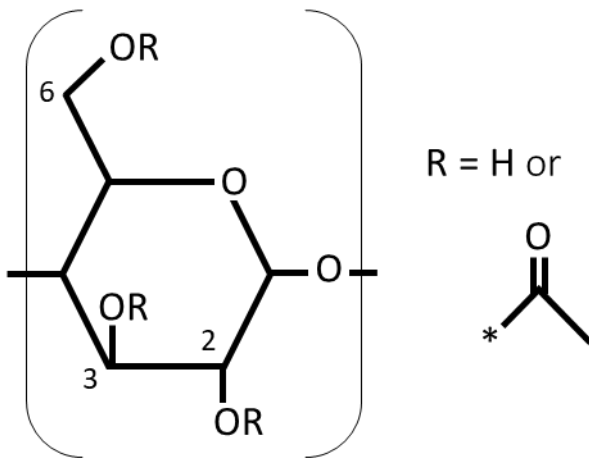
Figure 2.2 Chemical structure of CA monomer.

Cellulose acetate is produced by acetylation of cellulose sourced from wood pulp or cotton linters (40,41). The most common industrial manufacturing route today is the "Acetic Acid Process", with the "Methylene Chloride Process" and the "Heterogeneous Process" having fallen into disuse due to being less competitive in terms of cost and quality (42,43). These routes were established in the 1920/30s, but the latter two have never accounted for more than 10-15% (each) of world triacetate flake and were phased out at the end of the 20th century (42). Starting with wood pulp, the mixture is activated with acetic acid and sulphuric acid, which causes the morphology of the cellulose fibres to open up, promoting access to the hydroxyl groups. Acetic anhydride is added for the acetylation reaction. Cellulose triacetate is formed in the first step of the process, with a second hydrolysis step to obtain the desired degree of substitution. At the same time, chain degradation occurs as it is subject to acidic hydrolysis.

Plasticisers are added to cellulose acetate during processing to lower the melting temperature of the polymer further from the decomposition temperature, increasing its flexibility and durability (44). Common plasticisers in historic cellulose acetate include triphenyl phosphate (TPP) and diethyl phthalate (DEP), but can also include dimethyl phthalate, toluene sulphonamide, N-ethyl toluene sulphonamide, or mixtures of the same (45,46).

The first application of cellulose acetate was in the field of coatings for airplanes (39). Cellulose diacetate lacquer gave light, water, oil, and petrol resistance to the linen tissue wings, and improved the tension and flatness in the surface. Demand for plane applications dropped strongly after World War I, so manufacturers had to find new uses based on existing industrial capacities. This led to the development of textile cellulose diacetate (47). Fibre-grade CA requires a DS of about 2.6 (30).

Cellulose triacetate (CTA) is found in historical films, including cinematographic, photographic and microfilms (15,48,49). CTA is substituted to a specification of 2.7-3.0 (37). Also known as 'safety film', cellulose triacetate came into use in the 1950s as an alternative film base material to cellulose nitrate (often known as Celluloid) which, though widely used, was both unstable and highly flammable (50,51). Research and production of CTA photographic film base was advanced by the Eastman Kodak Company (52). As an example of the prevalence of CA films, the BFI Master Collection consists of over 450,000 cans of film, of which 59% are acetate films (53).

Moulded cellulose acetate is found in plastic objects such as spectacle frames, toys, jewellery, buttons, hair accessories, and combs (27,38,39,54,55). Typical DS for such applications are 2.5 to 2.7 (30). CA sculptures may be made of moulded CA, but artists often used as materials fabricated CA in the form of rod, sheet, or tube (56).

As mentioned at the start of this section, cellulose triacetate is used to make cigarette filters. Cigarette butts are the most common litter in the world (57). Another example of CA waste is osmotic filters, which must be continually replaced (58). While CA waste is not expected to feature prominently in museum

collections, it is useful to consider these objects as research on their degradation may provide information that is relevant to understanding CA degradation in museum artefacts and vice versa.

More recently, cellulose acetate has been studied due to its potential as a biodegradable polymer (59,60). Cellulose acetate is a bioplastic, meaning it is based on renewable resources and not on petrochemicals. Environmentally conscious policies and growing consumer interest in sustainability may have the effect of increasing the prevalence of cellulose acetate materials in museum collections of the future.

2.3 DEGRADATION PROCESSES IN CELLULOSE ACETATE ARTEFACTS

As mentioned in Chapter 1, the main chemical degradation processes in CA artefacts include deacetylation, chain scission, loss of plasticiser, and degradation of additives. This section reviews literature to establish the current understanding of these phenomena, how they affect CA artefacts, and the analytical methods used to study them.

2.3.1 Deacetylation

Deacetylation of cellulose acetate occurs by the reaction of water (H_2O) with a bound acetyl group (ROAc), resulting in hydroxyl substitution (ROH) and acetic acid (HOAc). In this notation, OAc represents CH_3COO (Ac is short for acetyl) and R represents the rest of the polymer (61). The chemical reaction is:

$$ROAc + H_2O \rightarrow HOAc + ROH \qquad\qquad (2.1)$$

Deacetylation of CTA in solution shows a first-order dependence on degree of substitution (62). It is known that the reactivity of acetyl groups varies with the carbon position, and this appears to affect the order in which they react, although this depends on the reaction conditions (63–69). In industrial processes, CTA is partially hydrolysed to yield different grades of CA, which may contain different distributions of acetylated carbons (36).

Deacetylation produces acetic acid and reduces the DS. Methods of detecting deacetylation have focused on measuring acetic acid or DS, directly or indirectly.

Evidence of deacetylation in CA museum artefacts has mainly focused on detecting acid (acetic or other) in the plastic or the surrounding air. Acid detector strips (A-D strips) are a popular option for conservators. Cheap, non-destructive, and easy to use, A-D strips give a rough indication of pH changes (70–72). Ion chromatography has been used to detect acetate ions in samples taken from CA museum artefacts (30,73). Solid phase microextraction gas chromatography/mass spectrometry (SPME-GC/MS) has been used to detect acetic acid from CA objects (20,74). Proton Transfer Reaction "Time-of-Flight" Mass Spectrometer (PTR-Tof-MS) was used to monitor volatile organic compounds (VOCs) emitted from CA movie films, with acetic acid the most abundant, but over 100 VOCs were detected (75).

Deacetylation in CTA film has been studied using measurements of the free acidity of the film. Free acidity, determined by the volume of 0.1 M NaOH required to neutralise one gram of film base, is considered the most sensitive indicator of degradation in CTA film (76).

Direct measurement of the degree of substitution is less common. GC/MS has been used to measure the % acetyl content of CTA and cellulose diacetate (CDA) animation cels, though it is inconclusive from this study whether differences in acetyl content were due to ageing or different initial DS of the cels (28).

Moisture regain is independent of molecular weight, but depends on other properties such as DS, distribution of acetyls in the chain, and extent of crystallisation (37). Reduction in DS is generally associated with increasing hygroscopicity of CA; therefore, equilibrium moisture content has been used to evaluate degradation in CA films, providing indirect evidence of deacetylation (13).

The term "vinegar syndrome" best exemplifies the effect of deacetylation on artefact stability and the role that this effect is considered to play within the narrative of cellulose acetate degradation. It has been extensively observed that one of the first signs of degradation in CTA films is emissions of acetic acid; this process is nicknamed the "vinegar syndrome" owing to its characteristic odour of acetic acid (4–7).

Emissions with a vinegar-like odour due to the production of acetic acid are typically the first sign of degradation in CTA film (14). While acidic film with no other visible signs of degradation has been observed, very badly degraded film is nearly always highly acidic (76). Other than the vinegar odour, the presence of acetic acid does not directly affect the film properties, though the acidity tends to increase prior to significant changes in the film properties.

Accelerated ageing experiments reveal that the free acidity in CTA film proceeds with an induction phase, where little change is observed over a period (the exact duration depends on the experiment conditions), followed by the so-called initiation of the vinegar syndrome, where the rate of change in free acidity increases dramatically (10).

Deacetylation is an ester hydrolysis, a type of chemical reaction which may be catalysed by an acid (77). At the initiation point, the deacetylation reaction is said to become autocatalytic, as increasing quantities of acetic acid become available to catalyse the reaction. According to conservation guidelines, a rule of thumb is that the reaction becomes autocatalytic at a free acidity of 0.5 (76). However, no scientific explanation has been proposed to explain why the acid-catalysed mechanism should not occur if there is acid present; nor why a free acidity of 0.5 is the characteristic point at which the dominant mechanism changes to acid-catalysed. A later analysis of the same published accelerated ageing data which was argued by the original authors to show this "autocatalytic point" found no evidence of a distinct change at 0.5 acidity (78). This will be discussed further in Chapter 3.

The "vinegar syndrome" is also known as "Pedigree Doll disease", which describes the same deacetylation degradation but observed in dolls (initially) and extends to other solid objects as found in museum collections (54). Damaging effects of deacetylation are primarily associated with the evolution of acetic acid, identified by a vinegar odour (4,79). The tendency for neighbouring objects to deteriorate faster in the presence of degrading CA objects is believed to be due to acetic acid catalysing degradation reactions in the nearby objects (8,80). Acetic acid may also autocatalyse or catalyse other degradation reactions within the CA object.

Advanced stages of deacetylation have been observed in museum artefacts. Samples from a highly degraded plastic sculpture by Naum Gabo were analysed using pyrolysis gas chromatography mass spectrometry (Py-GCMS) in conjunction with Fourier transform infrared microscopy (µFTIR) and other techniques, confirming that Gabo had used cellulose acetate and cellulose nitrate plastics (81). The original polymer has degraded almost completely to a cellulose-like structure through deacetylation.

Deacetylation is promoted by moisture (11). Increasing the temperature also increases the reaction rate (10). The reaction is acid-catalysed and so is autocatalytic under conditions where the evolved acetic acid is prevented from leaving the plastic, for example, by the use of sealed enclosures for storage (8,14,31,78,82). Residual sulphuric acid from the manufacturing process may also catalyse the reaction. This occurs by water first hydrolysing the aceto-sulphate ester group remaining from the CA synthesis and liberating sulphuric acid (30,83–86).

Reduction in DS makes CA more hydrophilic, resulting in increased moisture content at constant relative humidity (RH) (37). This could promote hydrolysis reactions including deacetylation, chain scission, and plasticiser degradation.

In CTA films, plasticiser loss is high in film regions corresponding to those with a high moisture regain (12). This observation implies a correlation between plasticiser loss and deacetylation. Changes in DS are associated with changes to the compatibility with plasticiser, influencing the loss of plasticiser by diffusion (32,44).

Thermal oxidation of the hydroxyl groups formed following deacetylation has been proposed, producing ketones and aldehydes (56,87). The carbonyl groups in these products are chromophores and are blamed for yellowing of CTA films.

2.3.2 Chain degradation

Chain scission refers to reactions that decrease the degree of polymerisation (DP) of the polymer backbone. The DP is the number-average (DP_n) or weight-average (DP_w) number of monomers per molecule. CA is a linear chain polymer, so cross-linking does not take place (88).

Chain degradation reactions can be initiated by several reactants (agents). These include water (hydrolysis), acetic acid or acetic anhydride (acetolysis), oxygen/peroxides (oxidative degradation) and UV light (photo-degradation). Hydrolysis causes cleavage of the β-1,4 glycosidic bond which joins monomers (30,89–91). Acetolysis is similar in that it causes cleavage of the glycosidic bond. While oxidative degradation is associated with attack of oxygen on the glycosidic ring structure, as well as acetyl groups, it leads to the production of small molecules such as formic acid, oxalic acid, carbon dioxide and various aldehydes (30). Photo-degradation is associated with photo-initiated radical generation (92).

A range of experimental techniques has been used to study chain degradation in cultural heritage artefacts. One approach is to measure the DP by measuring the molecular weight, for example, via viscometry (4,10,12,26,93). In viscometry, the specific viscosity η_{sp} of a polymer in solution is measured to obtain the molecular weight by applying the intrinsic viscosity $[\eta]$ relationship:

$$[\eta] = \lim_{c \to 0} \frac{\eta_{sp}}{c} = K_m M_v{}^a \qquad (2.2)$$

where $[\eta]$ is intrinsic viscosity, c is concentration, K_m is an experimentally determined constant for a specific solution, M_v is viscosity-average molecular weight, and the value for a depends on the shape and solution properties of the molecules (37,94). M_v is usually somewhere between the number-average molecular weight M_n and the weight-average molecular weight M_w, two types of statistical quantities representing the molecular weight distribution (MWD).

Size exclusion chromatography (SEC) was used to measure DP in naturally aged sample locations which appeared to differ in visible appearance of degradation (17). SEC (also known as gel permeation chromatography (GPC)) can be used to obtain the MWD, rather than just the average as reported in this study, but this does not appear to have been done yet by any researchers in the field.

There is a lack of data on quantities relevant to chain degradation, like DP or MWD, for CA artefacts subjected to empirical procedure (not cross-sectional studies). For example, a study (95) which used SEC to measure M_n and M_w of CA films presents

only the arithmetic difference in these quantities in samples that had undergone accelerated ageing, and not the values before or after ageing.

Tensile strength generally increases with DP in secondary cellulose acetate (CA manufactured via deacetylation of CTA), though this is not considered a reliable way to measure DP (96). Tensile break stress tends to decrease in badly degraded CTA film, with this effect promoted by the onset of the vinegar syndrome (8). In naturally aged objects, FTIR analysis indicated that loss of acetyl groups does not necessarily lead to loss of mechanical integrity, but if this is followed by chain scission then loss of integrity of the artefact will often occur (30). Crazing, the formation of fine cracks in the surface of an object, is generally caused by loss in molecular weight (97).

The moulding process for the object may affect the orientation of the chains and their structural characteristics. This could affect both the chemical mechanisms by which chain degradation takes place and the physically observable manifestation of the change in the degree of polymerisation. For example, Tsang et al. (98) hypothesised that crizzling-type patterns of small cracks are due to chain degradation, and that cracks appeared to run parallel to where they believed the polymer chains ran due to the injection-moulding process.

A less-common approach to detecting chain degradation is by measuring low molecular weight degradation products or functional groups. In CA artefacts, ion chromatography was used to detect oxalate (product of chain scission) and formate (product of oxidative degradation) (30).

Chain scission by hydrolysis is acid-catalysed so the presence of acetic acid and sulphuric acid promotes it (63). Oxidation appears to be initiated by the presence of oxygen and ultraviolet light; that is, photo-chemical oxidation (99). One study (93) measured hydroperoxide concentration in CTA films subjected to different stabilisation regimes and artificial ageing, under the hypothesis that it acted as an initiator in oxidative mechanisms of chain degradation. The same study also used viscometry to monitor changes in weight-average molecular weight (M_w).

As noted earlier, reduction in DS appears to promote chain degradation. In conservation studies, chain degradation tends to follow deacetylation, although

whether this is a relationship of cause and effect or simply because the chain degradation occurs more slowly than deacetylation at room temperature is not conclusive (73). A study (17) which compared non-degraded and degraded samples from the same (naturally aged) CA and CN objects found a correlation between low DP and low DS.

Mechanisms for chain scission in CTA, following deacetylation steps, have been proposed by workers in the field (100). A study (101) which used ^{1}H and ^{13}C Nuclear Magnetic Resonance (NMR) spectroscopy to measure hydrolysis of the acetyl groups in CA found that the rates of deacetylation are in the following order: C6 > C3 > C2. The author of the study proposes that deacetylation precedes chain degradation since oxidative chain-scission would take place through the C2 acetyl group which is less accessible.

Hydrolysis of the glycosidic bond in cellulose acetate is not necessarily identical to that in cellulose. It is known that substitution of cellulose affects the rate of hydrolysis (102,103). One explanation attributes difference in degradation rates between different cellulose derivatives, including cellulose acetate, in terms of steric effects (104). Another explanation is proposed in terms of the impact of the electronegativity of substituents (105). For example, a study (106) which investigated the kinetics of nitrocellulose degradation in aqueous sulphuric acid solutions found that chain degradation by acid hydrolysis is much slower than denitration, and that the dependence of the chain scission rate on the acidity of the medium is significantly weaker compared with the denitration rate. The authors of the study propose that water probably takes part in the kinetically determining stage of heterolysis of the protonated acetal bond and that the much slower rate of degradation of nitrocellulose compared with cellulose is due to inhibiting effect of electronegative substituents on protonation of the acetal bond. A similar effect is found in cellulose triacetate (107).

Under reaction conditions which vary the proportion of water and acetic anhydride, water appears to inhibit chain scission unless CA is sufficiently deacetylated, suggesting that acetolysis of CA and hydrolysis of cellulose is in fact taking place (108).

Biodegradation studies (59,66) have shown that reduction in DS increases the rate of reduction in DP. Indeed, the biodegradability of CA cigarette filters has been increased by adding a controlled-release acid catalyst whose main effect is accelerating the deacetylation reaction under ambient conditions (109). However, these studies used enzymes to degrade CA, which may be subject to different mechanisms than non-bio chain degradation. For example, acetyl groups may inhibit the binding between the polymer and the catalytic domain of the enzyme (110).

2.3.3 Plasticiser loss

Plasticiser loss describes the mass transport processes that result in the reduction of plasticiser concentration in the CA plastic. Loss of additives from polymer material involves three processes (111):

1. Diffusion of additives up to the interface.
2. Transport through the interface.
3. Loss of additives from the surface into the surrounding medium:
   a. Evaporation (into gas medium).
   b. Extraction (into liquid medium).
   c. Migration (into another material in direct contact).

The mechanism of the loss of additives from the matrix depends on which one of these processes governs its loss. During natural degradation, evaporation is the step that occurs more slowly and controls the kinetics of the process (112). Accelerated ageing experiments speed up evaporation relative to diffusion, so diffusion may appear to become the rate-controlling step (113). This difference could also affect the sequence of other events, such as deacetylation, compared with the sequence that would occur during natural ageing. For example, in a study (113) on thermal degradation of cellulose diacetate, a significant amount of plasticiser was lost before noticeable deacetylation. However, in archival conditions, acetic acid release is a precursor to plasticiser loss (12).

Cellulose acetate may contain significant levels of plasticiser, in addition to pigments and fillers (30). Mouldable CA may contain 20-40% by weight of plasticiser (29,30).

Once plasticiser has diffused to the surface of the object, it is often seen as an oily exudate, in the case of phthalate plasticisers, or solid triphenyl phosphate crystals (12,13,114). The formation of an exudate is also known as leaching of the plasticiser and can make the surface of the artefact sticky and unpleasant to touch (30). Over time, loss of plasticiser leads to embrittlement and cracking of the material (27,30,114).

Lower DS is associated with reduced miscibility between the polymer matrix and the plasticiser, promoting phase separation (32,44). Thus, deacetylation may enhance the rate of plasticiser loss at a given temperature. This is consistent with anecdotal evidence that acetic acid release (vinegar syndrome) precedes plasticiser loss (as observed by surface crystalline deposits) on archival CTA films, although these observations only indicate the sequence of when the processes become noticeable (12). For this reason, it is still considered an open question whether deacetylation precedes or follows plasticiser loss (30).

As reduction in DS increases moisture regain, and the plasticisers are hydrophobic, it is also possible that the compatibility of the polymer and the plasticiser are mediated through changes in moisture content as the material degrades. For example, a study (12) found that plasticiser loss was higher in regions of CTA films which had higher moisture regain. An alternative explanation is that plasticiser loss happens first, making the plastic more hydrophilic in these regions, which increases moisture regain, promoting deacetylation with the reduction in DS further increasing moisture regain.

2.3.4   Reaction of plasticisers and additives

Triphenyl phosphate reacts with water to form diphenyl phosphate, a strong acid (29,30). This accelerates degradation processes such as deacetylation (27). Phthalate plasticiser is thought to have little effect on degradation (27,29).

As noted in Section 2.3.1, some AGUs may have aceto-sulphate rather than acetate substitutions, due to the CA manufacturing process (30). It is not known if or to what extent the presence of aceto-sulphate groups affects polymer properties at these levels. Hydrolysis of these groups results in the release of sulphuric acid, which is a much stronger acid than acetic acid (30,83–86).

2.4 FACTORS IN CELLULOSE ACETATE DEGRADATION

Based on the evidence and theories presented in Section 2.3, CA polymer degradation processes are affected by other processes that are going on in the plastic. Appreciation of the interactions between different processes will be important for proposing relationships between the components of the polymer degradation model. This section reviews how degradation processes are affected by factors or variables other than the processes themselves. These factors are either a function of the environmental conditions (temperature, moisture, radiation, microenvironment), or based on the material characteristics of the object (internal diffusion, crystallinity, chemical composition).

2.4.1 Temperature

Increasing temperature increases degradation rate (115). The effect of the temperature on the reaction rate is described by the Arrhenius equation:

$$r \propto e^{-\frac{E_a}{R_G T}} \qquad (2.3)$$

where r is the instantaneous reaction rate, E_a is the apparent activation energy, R_G is the ideal gas constant, and T is the temperature (116,117). According to classical thermodynamics, reactant molecules must possess a certain amount of energy to undergo chemical change (118). The apparent activation energy depends on the reaction mechanism. As temperature increases, the average energy of the molecules (reactants) increases. Since a higher proportion of the molecules exceeds the activation energy, this speeds up the reaction rate. The apparent activation energy must be measured empirically.

Plasticiser loss is accelerated with increasing temperature (12,113). It appears that under artificial ageing conditions the evaporation rate may be accelerated relative to the diffusion rate, though both increase with temperature. As noted in Section 2.3.3, the fact that increasing temperature may alter the rates of processes relative to one another may mean that accelerated ageing experiments produce a sequence of events different from what occurs under natural ageing conditions.

Temperature change, as opposed to temperature magnitude, may also enhance deterioration, though this has more to do with physical properties than with

34

degradation reactions. Examples of physical changes induced by temperature change (for example, cooling) include crystallization, dimensional changes, increased brittleness, and cracking (119). Periodic temperature cycling does not appear to increase the deacetylation rate of CA films (120). The average deacetylation rate of a cycling temperature regime is somewhere between the values at the temperature extremes.

2.4.2 Moisture

In a museum setting, a plastic object is most likely to encounter moisture via the water vapour present in its immediate environment, measured by the relative humidity which is typically in the 40-60% range. Water is a reactant in hydrolysis reactions including deacetylation, chain scission, and triphenyl phosphate degradation.

Increasing the relative humidity has been shown experimentally to increase the rate of deacetylation and chain degradation (4,11). Independently from environmental conditions, the moisture regain of CA also tends to increase as it degrades. This correlation holds when comparing between less degraded and more degraded films, and between less degraded and more degraded samples in the same films (12). Reduction in DS makes CA more hydrophilic, resulting in increased moisture content at constant relative humidity (37,121). While the relative humidity is an environmental factor, the effect it has on moisture-related degradation may depend on the extent of degradation present in the sample already (4). There is a correlation between plasticiser loss and higher moisture regain as discussed earlier, but it is not clear why (12).

As with temperature variations, moisture variation may play a role in deterioration. Periodic RH cycling does not appear to increase the deacetylation rate of CA films, with the average deacetylation rate for the cycling condition somewhere between the values at the RH extremes (120). Moisture is slower to equilibrate than temperature, so moisture change in a material may lag changing relative humidity (119). If plastic which contains some moisture is cooled rapidly, then it is possible for condensation to form. A study (122) concluded that "The risk of introducing either irreversible physical changes or damage due to the formation of condensation into degraded plastics materials during the cooling process is not

significant for plastics thinner than 1 cm (thin-walled), regardless of their polymer type or extent of degradation." Thus, CA objects thicker than 1 cm may be at risk for condensation-related degradation.

2.4.3 Radiation

Photo-degradation of the CA polymer is initiated by exposure to high-frequency radiation such as UV radiation. Theoretically, exposure to lower-frequency radiation does not initiate photo-degradation, regardless of dosage (123). In practice, plastic objects will often have slight impurities, e.g., C=O groups, that will absorb in the visible range. Additives such as titanium oxide, a whitening agent used in many consumer products, can significantly increase photodegradability by acting as a photocatalyst (59). While a study (124) comparing the impact of different environmental factors on plastic degradation found a correlation between visible light intensity and discolouration in CA, this is most likely due to concurrent correlation of visible light intensity and UV light intensity in the absence of any filtering. UV radiation is normally filtered out of indoor heritage environments, so much of the photo-degradation research in the literature is not that relevant. There is also a lack of studies on CA photo-degradation in the spectral range typically found in a museum setting, which is usually represented by CIE light source D65 to represent UV-filtered daylight (125). Nevertheless, exposure to UV radiation prior to acquisition may contribute to CA degradation or in the case of improper storage or display conditions.

UV radiation can be subdivided into different frequencies, from lowest to highest: UVA, UVB, and UVC (123). UVC rays are not transmitted through the atmosphere, but they have been used in experiments to study the effect of UV radiation frequency on photo-degradation. A study (113) on ageing of CDA found that UVC induced higher levels of discolouration, deacetylation, and photo-degradation of plasticiser, compared with UVB and UVA. However, samples degraded under UVB radiation were extremely brittle and fragile and were also prone to crazing. This is believed to be due to the ability for the lower frequencies to penetrate more deeply into the samples and induce degradation at a deeper level (based on fluorescent microscopic imaging). The study also found that yellowing induced after 32 days' exposure to UVC radiation could be reversed following 25 days' exposure to UVA

radiation. While this result seems unexpected, reversible yellowing or "bleaching" following exposure to visible light has been observed in other polymers, for example, several aromatic thermoplastics (126), poly(vinylbutyral) (127) and polyvinyl chloride (PVC) (128).

2.4.4 Microenvironment

Aspects of the microenvironment include storage containers and other nearby substances. The material of the storage can in which CA films are stored was shown to have a significant effect on archival life (as measured by 10% loss of intrinsic viscosity), in order from least to most severe detrimental impact: glass, polyethylene, aluminium, iron (26).

Inserts that reduce the amount of moisture or acid in the microenvironment have a beneficial effect, providing additional evidence that moisture and acid are important factors in the degradation process (4). Acid or moisture adsorbents, such as molecular sieves, can aid in the removal of acid from the film, or protect it from relative humidity fluctuations (31,129). Acid-neutralising inserts contain a base such as calcium carbonate which reacts with acetic acid to neutralise it (31). However, buffered cardboard disks were shown to be ineffective at mitigating deacetylation in CA film rolls stored in sealed metal cans, due to inefficient acid adsorption by the disks, and the introduction of additional moisture into the enclosure via the disks (31).

Storage systems that permit acetic acid (produced by deacetylation) to escape also appear to mitigate the degradation rate. Tightly sealed storage containers have been found to prevent acetic acid from escaping from the film, increasing the potential for autocatalysis (12,93); ventilated containers facilitate the escape of acetic acid (129). In ventilated or open enclosure designs, which permit acetic acid to escape, the acid can diffuse faster out of the film if the reel is wound less tightly (89). One of the difficulties in assessing the impact of open vs. closed environments is that most of these studies, which were on CA films, measured the degree of degradation by the free acidity in the films. Obviously, if acid is lost then the free acidity will be lower, but this does not necessarily prove that degradation is reduced, and it might even give observers a false sense of security if the degree of degradation can be made to appear lower simply by ventilating acid which has

already been generated through a degradation process. Furthermore, by ventilating acid, it may expose other nearby artefacts or storage materials to acid.

Emissions of acetic acid from degraded CTA films have been shown to induce degradation in undegraded films stored nearby (8). A study (8) investigated the uptake of acetic acid from the environment in CA films. One of the experiments established that undegraded CTA film will absorb acetic acid from adjacent degraded film and that physical contact is not necessary for absorption to occur. However, it is not clear whether exposure to acidic vapour increased the rate of deacetylation in the (initially) undegraded film. Another experiment in the same study (8) found that decreasing the volume of film in a storage can resulted in lower free acidity, showing that a larger air/film volume ratio allows more acid to escape from the film. In the last set of experiments in this study (8), acetic acid was introduced directly into a closed vessel containing undegraded film and the resulting take-up of acetic acid by the film was determined. Acid take-up by the film after two weeks at 70 °C, 80% relative humidity, is directly proportional to the acetic acid vapour concentration in the vessel. This was also associated with decrease in tensile break stress, compared to a control, showing that the acidic microenvironment led to deterioration of physical properties which are associated with chain degradation.

A study (84) that measured unsaturation (indicating double bond formation) in severely degraded CTA film samples and a CTA sculpture found more unsaturation in the film samples. The authors of the study suggest as possible explanation that different degradation pathways have been promoted, due to the CTA film being stored in a closed storage container, while the CTA sculpture had not been.

A study (64) that measured degradation via viscosity retention in CA films stored in open and closed containers found that the degradation rate is faster in the closed environment, but the rate of increase of moisture regain is slower. In this case, the change of moisture regain was in response to relative humidity fluctuations, suggesting that the closed container offers some protection against macro-environment fluctuations, but at the cost of accumulating acetic acid.

There are many storage options for cultural heritage artefacts and thus many studies have been done to understand the effects of different microenvironments on CA degradation. In general, the "openness" of enclosures incurs a trade-off between facilitating ventilation of acetic acid (preventing its accumulation in the object) and exposing the object to unfavourable shifts in macroenvironmental conditions, mainly relative humidity (and temperature to a lesser extent).

2.4.5 Internal diffusion

In 35 mm CA film reels, variation in degree of degradation appears to be related to the diffusion of volatile components like water and plasticiser over the film width. A study (12) which analysed cross-sections of naturally and artificially aged films found variability in various properties across axial (width) and radial (reel diameter) dimensions in film. Moisture regain was highest at the edges (near the spool and outer circumference), the effect being more evident in severely degraded films and in older film stock. The increase in moisture regain is consistent with an observed decrease in intrinsic viscosity, and more plasticiser loss.

A different study (13) that compared the IR spectra in naturally and artificially aged CTA films and in samples from a naturally aged CA sculpture, in 30 μm thick samples taken through the cross-sections, found little difference between surface and bulk layers in the film, compared with the sculpture. CTA film base is 150 μm thick and the sculpture is most likely several millimetres thick in the narrowest dimension (13). The difference in variation may be due to longer diffusion length in the sculpture, or that the film was stored in a microenvironment (enclosed space, low air/CA volume ratio) that permitted it to approach an equilibrium with the microenvironment, thus reducing the concentration gradient. The difference in storage conditions may also have promoted different degradation pathways altogether in the sculpture than in the films.

2.4.6 Crystallinity

The crystallinity of the plastic affects the accessibility of degradative reactants to the polymer (95,130). Amorphous regions are more easily penetrated by chemical species due to local chain disorder, giving this fraction a faster rate of degradation.

This can cause an increase in the crystalline fraction over time as the amorphous fraction is destroyed.

The distribution of acetyl groups at the three possible sites of the AGU and the distribution along the chains may result in differences in degree of crystallinity (37). The crystalline structure and crystalline fraction may in turn affect the distribution of acetyl groups and the distribution along the chains as certain sites are more accessible to degradative reactants.

2.4.7 Other components

In CA films, plasticiser and the emulsion layer appear to confer some stability to the film base (12,26). The emulsion layer, based on gelatine, may act as an acid-scavenger; or possibly impair the rate of diffusion of oxygen into the film and inhibit oxidation (26). The emulsion layer may also operate as a diffusion barrier for the migration of plasticiser (12). Positive films are generally less stable than negative films; negative film has a thicker emulsion layer (12). However, a different study (10) found no consistent difference between the stability of uncoated base and emulsion-coated base.

Triphenyl phosphate plasticiser may operate as an antioxidant (26). However, the decomposition of triphenyl phosphate to diphenyl phosphate, a strong acid, accelerates hydrolytic degradation (29,30).

Residual manufacturing impurities such as sulphuric acid increase susceptibility to degradation (13,30,83–86). In films, the redox nature of processing reagents may help to catalyse degradation reactions (13). The extreme pHs used in photographic processing could also contribute to instability (13).

2.5 CONSERVATION IMPACTS OF CELLULOSE ACETATE DEGRADATION

Degradation may lead to signs of damage, perceived as a loss in value(s) of an artefact or collection. Identifying and managing degradation processes is a key part of any conservation policy that aims to minimise damage over time. This section reviews practical implications of cellulose acetate degradation in the context of conserving cultural heritage.

2.5.1 Monitoring degradation

Degradation monitoring refers to the detection and measurement of degradation in artefacts or collections. These techniques may be used to study degradation processes or to detect degradation or susceptibility to degradation before it is advanced (30). Many of the analytical techniques that provide information about the chemical characteristics of the plastic material are covered in detail in Section 2.3.

A disadvantage of some analytical methods such as NMR spectroscopy or SEC is that they are labour-intensive and destructive (7). They require access to expensive equipment and specialised knowledge that a conservator may not have. The need for destructive sampling precludes their use for long-term monitoring of valuable cultural heritage.

The extent to which a measurement reflects a qualitative change in condition is also an important characteristic for degradation monitoring. For example, free acidity is considered a more sensitive indicator for deacetylation in CTA film than pH (76). This is mainly due to pH being based on a logscale. As a destructive and labour-intensive technique, free acidity is not suited for large-scale monitoring of a collection. Therefore, non-destructive methods such as A-D strips are preferred for the detection of increasing quantities of acetic acid, even if these do not provide sufficient quantitative information for scientific research on deacetylation (70–72). According to the vinegar syndrome narrative, detecting deacetylation is important when monitoring degradation, as it is believed to be the first sign of degradation and can lead to more severe forms of degradation.

There is a discrepancy between qualities that can be measured and changes that are perceptible. Referring to Figure 2.1, qualities that correspond to degree of degradation (e.g., DS) are useful to a physical scientist studying the underlying phenomena, while qualities that correspond to damage (e.g., tensile stress at break) are linked to values and tend to be prioritised by conservators. A key role for the physical scientist studying heritage artefacts is to bridge this gap between systems of evidence to improve understanding, while remaining aware of what kinds of knowledge will be considered relevant to other stakeholders (131).

Chapter 7 will address this point by exploring the consequences for heritage conservation of the analytical outputs of the model.

2.5.2 Managing degradation

Conservation strategies for preserving cellulose acetate artefacts illustrate conventional beliefs amongst conservation professionals about what and how factors affect cellulose acetate degradation. While the focus of this thesis is not to develop new conservation guidelines, awareness of the current recommendations provides the context for a model that considers factors and scenarios that are realistic and relevant to conservators.

Photo-degradation is effectively inhibited by minimising exposure to UV radiation. Most museums and archives have storage and display systems that prevent UV radiation exposure, for example: dark storage, artificial lighting, natural lighting with UV filters (132).

Storage below room temperature is widely recommended as this broadly inhibits the rates of various degradation processes (11,120,133). For example, it is believed that "reducing the temperature by 5 to 10 °C halves the rate of the most common chemical degradation reactions of plastics, such as hydrolysis and oxidation" (6). The advice to store new CA films at <0 °C, and older films which already contained acetic acid at -18 °C to freeze the acid (melting point -17 °C), illustrates how temperature might be used to control physical phenomena as well as chemical (4). Research (134) on cooling rolls of CA-based movie films concluded that to avoid formation of condensation, the temperature difference between film and its storage container or between any two areas in the mass of materials should not exceed 10 °C. Cool storage is suitable for constructed objects or those made from mixed materials, but temperatures close to or below 0°C is not, due to differential thermal expansion.

Moisture content is usually controlled by the relative humidity, as moisture promotes hydrolysis reactions. A study (11) that used a model to extrapolate film lifespans from artificial ageing experiments concluded that decreasing relative humidity from 50% to 20% appears to increase lifespan of films by a factor of about 3. Some disadvantages of very low relative humidity are increased

dehumidification costs and possible increase in film brittleness and curl (mostly reversible, though one can imagine that even a reversible change in brittleness could lead to irreversible mechanical damage) (11).

Ventilation has been recommended to prevent build-up of acetic acid, for example by storing CA films in aerated cans (4). However, this strategy requires careful control of relative humidity as there is less buffer from the storage container. Ventilation of acetic acid also comes at the cost of increasing plasticiser loss rates. Microenvironment conditions to avoid include low air volume (e.g., a vacuum-sealed bag), no air movement and/or absence of acid-absorbing materials (11). Desiccants such as zeolite crystals inhibit degradation of CA by absorbing water and acetic acid (135,136). However, their effectiveness at absorbing acid in a moisture-permeable container is limited as the absorption of water from the outside environment reduces the uptake of acetic acid (136). Patented designs (135,137–139) for film enclosures attempt to either absorb acetic acid or allow its release. While it would seem like a good idea to use a sealed container (to limit moisture ingress and plasticiser loss) with acid-absorbing desiccants, in practice, many conservators are reluctant to do this (136). First, the use of sealed containers limits access to the collection. Second, there is the risk that reaction products will eventually accumulate as degradation proceeds, resulting in rapid and severe deterioration.

It is advised not to store degraded CA film in the same microclimate or confined storage area with undegraded film unless steps are taken to continually remove acetic acid vapours from the area as they are produced (8). For similar reasons, it is recommended to separate degrading plastics from cellulose, iron, and silver, as the degradation products can corrode other organic materials and metals (140).

2.6 CONCLUSIONS

I have presented approaches in preventive conservation that aim to mitigate or inhibit degradation, rather than interventions to reduce or reverse damage that has already occurred. Intervention deals with addressing the effects of degradation, while prevention focuses on understanding its causes. However, preventive conservation benefits from awareness of both causes and effects of

degradation that were reviewed in this chapter, as the effect is what we are trying to prevent! This motivates the field of study within heritage science concerned with lifetime prediction, which will be discussed next in Chapter 3.

3 MODELLING POLYMER DEGRADATION

This chapter is a literature review of mathematical models of polymer degradation. The review discusses:

- *applications and motivations for the development of mathematical models of polymer degradation*
- *definitions and models of degradation in the context of cultural heritage conservation*
- *how modelling approaches in heritage science attempt to predict the effect of environmental factors on the longevity of collections to inform conservation decisions*
- *mathematical models of mechanisms and phenomena relevant to cellulose acetate (CA) degradation.*

The aims and original contribution of this thesis are argued in light of the modelling state-of -the-art.

3.1 INTRODUCTION

Mathematical models are a form of knowledge representation (141). Formalising knowledge in a rules-based system of logic (mathematics) enables us to make deductions and reveals new insights which were not obvious based on earlier empirical observations. Such models may yield novel hypotheses based on their underlying assumptions, which can then be tested empirically. Furthermore, a model which is represented in a mathematical framework has the benefit that a computer can perform calculations on the model. Even complex models can be solved in an efficient and scalable way using readily available software programs. Finally, mathematical models are versatile and inspire cross-pollination of ideas by recognising the similarities between abstract representations of different systems.

Mathematical modelling has been used to study polymer degradation and to predict object lifetimes across a range of disciplines:

- In heritage conservation, being based on extrapolation from accelerated ageing experiments via the Arrhenius equation (26,142).

- In industrial applications, which may expose materials to harsher conditions than those encountered in a heritage context, and where the definitions and/or threshold for damage may be different. For example: EVA polymer degradation in solar panels (143); cellulosic insulation in power transformers (144); nylon 6.6 degradation in parachutes (145).
- To predict the behaviour of bioresorbable medical implants (146).
- In pharmaceutical applications, to simulate and design the drug delivery properties of controlled-release formulations (147–149).
- In environmental sciences, to assess the biodegradability of plastic waste and its ecological impact (150,151).

These applications involve the interactions of the object with its immediate environment. In the last four examples, the environmental conditions are a constraint that engineers and scientists use to design an object, or to manage its usage—for example, to plan the frequency of replacements. The heritage sector is distinct in that there is no option to "engineer" the object. Instead, conservators can control the environment to minimise damage and extend lifetime of the object. For this reason, degradation models created in the context of heritage conservation have tended to focus on the effects of environmental factors.

3.2 MODELLING POLYMER DEGRADATION IN CULTURAL HERITAGE ARTEFACTS

Modelling is used in preventive conservation to inform decision-making and risk management (3). Mathematical models of degradation can support a holistic risk management strategy which incorporates objectively measurable variables as well as subjective values (152). The main purpose of these models is to predict object condition (output) as a function of tuneable environmental conditions and, although less frequently, the independent variable time (inputs). These models have tended to be highly empirical and do not seek to explain underlying phenomena. An advantage of this approach for heritage is that the phenomena may be complex, and a simpler approach may be sufficient for achieving the desired objectives. A disadvantage is that it can be hard or impossible to predict new types of behaviour, particularly when considering unique or modern artefacts. An

empirical model can be used for a small class of systems and is not easy to extend or generalise. Finally, it does not offer much insight, as it can tell you what will happen, but not why it happens.

3.2.1 Damage and dose-response functions

A dose-response function f_C attempts to predict an objectively measurable change as a function of parameters p (2). A values-based function f_V can be applied to the output, to get a damage function f_D.

$$f_D = f_V(f_C(p)) \tag{3.1}$$

For example, Strlic et al. (153– 155) developed a model of paper degradation that links the change in degree of polymerisation over time t (years) to temperature T (°C), relative humidity RH (expressed as a ratio) and pH:

$$kt = \frac{1}{DP_n} - \frac{1}{DP_0} \tag{3.2}$$

$$\ln k = 36.981 + 36.72 \left(\frac{\ln(1 - RH)}{1.67T - 285.655} \right)^{\frac{1}{2.491 - 0.012T}} \tag{3.3}$$

$$+ 0.244 \ln(10^{-pH}) - \frac{14300}{T + 273.15}$$

DP_n is the number-average degree of polymerisation at time t, DP_0 is the number-average degree of polymerisation at $t = 0$ and k (year^{-1}) is the rate constant. In this example, the parameters p are t, T, RH and pH, and the dose-response function is $f_C = DP_n$. The dose-response function was developed by fitting empirical data to a form of the Ekenstam equation (Equation 3.2), which is covered in more detail in Section 3.3.2 (156). This dose-response function provides the input, DP_n, to a wear-out function (f_V) linking degradation to accumulation of mechanical damage due to use. The wear-out function (Equation 3.4) considers the "number of handlings" ($no_{handling} until\ unfit$) before the paper in question becomes unfit for use (154). A fitness-for-use threshold, based on psychosocial factors, is defined as the state of an object where its use is no longer satisfactory. In

this case, this is defined by the "threshold number of large missing pieces per 100 sheets" ($threshold_{LMP}/100sheets$).

$$\ln(no_{handling} \, until \, unfit) = (0.01050 \pm 0.00097) \times DP_n \qquad (3.4)$$
$$+ \ln(threshold_{LMP}/100sheets) -$$
$$(0.02 \pm 0.51)$$

Combining these three elements (dose-response function, wear-out function, and fitness-for-use threshold) establishes the damage function f_D.

Relative humidity and temperature are the most common inputs found in dose-response functions, but other factors may be considered as well. A study (124) on degradation in historic plastics used principal component analysis (PCA) to map correlations between colour change and yellowing, and environmental factors: light intensity, relative humidity, temperature, SO_2, O_3 and NO_2. This kind of analysis could be useful for exploratory purposes to decide which factors to focus on when developing a dose-response function, with environmental factors as parameters p, and colour change and yellowing as the output of the dose-response function f_C. Researchers can limit the number of required experiments to obtain sufficient data for a model. In another study (157), Design-of-Experiment, a procedure to optimise experiments for efficient data collection, was used to develop a dose-response function for colour photographs. The form of the Equation 3.5 is based on the Arrhenius equation in the sense that it suggests a linear relationship between the logarithm of a rate of reaction and temperature T (K), but the terms in the equation do not represent an activation energy:

$$\ln\left(\frac{\Delta E_{RGB}}{t}\right) = 32 + 0.0002\big(c(AA)\big) + 0.01(RH) - 11\left(\frac{1000}{T}\right) \qquad (3.5)$$

The rate of reaction is represented by the colour change ΔE_{RGB} over time t (years). The term $c(AA)$ stands for concentration of acetic acid (ppb). Relative humidity RH is expressed in percent. In terms of Equation 3.1, ΔE_{RGB} or $\Delta E_{RGB}/t$ could be considered as outputs of f_C, with the remaining variables as parameters p.

3.2.2   Kinetic models of decay rate

According to kinetic theory, for a first-order reaction consisting of a reactant R going to product P:

$$R \rightarrow P \tag{3.6}$$
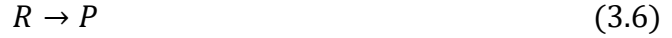
The rate of reaction r in terms of their molar concentrations $[R]$ and $[P]$ is

$$r = -\frac{d[R]}{dt} = \frac{d[P]}{dt} = k[P] \tag{3.7}$$

$$k = A \times e^{\frac{-E_a}{R_G T}} \tag{3.8}$$

where k is the rate constant, A is the pre-exponent factor, R_G is the ideal gas constant, and E_a is the apparent activation energy. Equation 3.8, the Arrhenius equation, has been relied on extensively to extrapolate lifetime predictions for collections from accelerated ageing experiments. As explained in Chapter 2, the equation expresses the dependence of the reaction rate on the temperature. Typically, heritage scientists have utilised the temperature dependency set out by the Arrhenius equation to model macroscopic changes regardless of whether these changes are known to correspond to a simple reaction like Equation 3.6, simply because the relationship between temperature and the macroscopic change has been found empirically to follow the Arrhenius dependence. For example, Equation 3.5 makes an analogy between rate of reaction and rate of colour change. It is also common to define r as the rate of change of a relevant degradation indicator, by measuring the time to reach a threshold level of this indicator, such as the time for cellulose triacetate (CTA) film to lose 10% viscosity (26). It is possible, on theoretical grounds, to model macroscopic changes as following the Arrhenius dependence if a reactant or product can be identified with a degradation indicator and a degradation mechanism (chemical reaction).

Another example of the use of the Arrhenius equation in museum conservation is in the temperature-dependence multiplier $f(T)$ of the object lifetime L (years). Assuming that the rate of decay is constant, the lifetime is the reciprocal of the rate of decay. Therefore, $f(T)$ is derived from the reciprocal of the Arrhenius equation.

For example, for the most rapidly decaying organic materials, including cellulose acetate (CA), the dominant degradation mechanism is acid hydrolysis (158,159). In Chapter 24 "Museums, Galleries, Archives, and Libraries" of the 2019 ASHRAE Handbook—HVAC Applications (159), the lifetime of objects composed of these materials is calculated using the following form of equation:

$$L = f(pH) \times f(T) \times f(RH) \tag{3.9}$$

According to this standard (159), "for our purposes, acidity is a given, and only temperature and relative humidity can be controlled." In general, the equation assumes that all the inputs (which determine the rate of decay) are constants, even though acidity may vary with the degree of decay.

The idea of lifetimes is well-established in heritage conservation literature, with guidelines building upon this concept to provide further reference tools for conservators to understand the potential impacts of the environment on the longevity of collections. For example, isoperms are lines of constant lifetime plotted with respect to temperature and relative humidity as the axis (160). For a given object, isoperms represent relative lifetime L_r, the ratio of the lifetime at storage conditions to the lifetime at room conditions 20°C, 50% relative humidity. Object-specific properties will influence the absolute lifetime. This approach only considers the influence of degradation on lifetime, and in that sense, it defines lifetime by the extent of degradation alone. For example, an object could break due to repeated mechanical stresses, without any change in chemical composition. This is not accounted for in the concept of lifetimes as used in isoperms.

Chapter 24 of the 2019 ASHRAE Handbook (159) provides three advisory tools that are essentially isoperm models. As expressed in Equations 3.10-12, temperature T is in Kelvin, relative humidity RH is expressed as a ratio, and ideal gas constant R_G is 8.134×10^{-3} kJ mol^{-1} K^{-1}.

1. The Preservation Index, derived primarily from acetate film data (14). The model is the basis of a software tool offered by the Image Permanence Institute (161,162).

$$L_r = 4.69 \times 10^{-17} \exp\left(\frac{94.9}{R_G T}\right) \exp\left(RH(0.02087T - 8.79)\right) \tag{3.10}$$

2. Michalski (115) derived the following expression for L_r from a review of data on paper, film and dyes, but it is considered applicable to all organic objects:

$$L_r = 6.17 \times 10^{-19} \exp\left(\frac{100}{R_G T}\right)\left(\frac{1}{RH}\right)^{1.3} \tag{3.11}$$

3. By rearranging the dose-function in Equation 3.3, it is possible to obtain a formula for L_r which is applicable primarily to paper and other cellulosic materials (155):

$$L_r = 9.468 \times 10^{-21} \exp\left(\frac{119}{R_G T}\right)$$

$$\times \exp\left\{-36.72\left(\frac{\ln(1-RH)}{1.67T - 741.82}\right)^{\frac{1}{5.7688 - 0.012T}}\right\} \tag{3.12}$$

These advisory tools assume constant environmental conditions. For fluctuating relative humidity, the 2019 ASHRAE Handbook (159) recommends using a time-weighted average of the relative humidity. For temperature dependence, the Handbook (159) recommends obtaining the decay rate from the time-weighted average of the decay rates at each temperature, calculating lifetime as the reciprocal of the final decay rate.

These models can predict what will happen, but they do not tell conservators what should be done. This can lead to confusion and uncertainty for conservators wishing to use these tools to make decisions about storage conditions (163). It is worth bearing in mind the practical limitations of these kinds of models in heritage conservation, and that knowledge (model-based or otherwise) is not a substitute for judgement.

3.2.3 Deacetylation

Kinetic models of deacetylation in CTA film have been developed with the motivation to predict the time until the onset of the vinegar syndrome under different conditions of temperature and relative humidity (142). This is the basis for the Preservation Index mentioned earlier (161). Outputs from this model are cited as the standard in guidelines for photographic film preservation (164). The model assumes a constant rate of reaction during the so-called induction phase (below a free acidity of 0.5) and does not account for the catalytic effect of acetic acid (10,14). To use a volatile product (acetic acid) as the measure of the extent of degradation, all the product must be retained in the system. Therefore, this model only applies to a storage scenario in which all the acetic acid is retained in the film, which requires a sealed enclosure with minimal air-film volume ratio (e.g., vacuum-sealed). This "no-ventilation" scenario is considered the worst-case scenario for promoting the vinegar syndrome and so the model provides an upper bound on the rate (lower bound on lifetime). Curiously, under the premise that the acid has no effect when the free acidity is less than 0.5, this implies that deacetylation (if measured by degree of substitution) would proceed at the same (constant) rate if the acid was ventilated, for example, by storing the film in an open enclosure.

3.2.4 Chain degradation

The best-known model concerning chain degradation in linear chain polymers is the Ekenstam equation (Equation 3.2) (156). The original equation was obtained by fitting a line of best fit to data from experiments of cellulose degrading in acidic aqueous solutions. While the model was first conceived empirically, numerous phenomenological models of degradation in linear chain polymers have predicted functions consistent with the Ekenstam model under certain assumptions (see Sections 3.3.2.1 and 3.3.2.2). The Ekenstam model has been the basis for dose-response functions in heritage concerning cellulose hydrolysis, particularly paper degradation in archival collections (158,165,166).

When it comes to simulating polymer degradation, heritage science has tended to deploy the Ekenstam model in an empirical spirit without substantial inquiry into the theoretical reasons for the application of this particular equation to this particular polymer system. This approach is not necessarily inaccurate in specific

cases, but it limits our ability to generalise from the specific cases and prevents the transfer of knowledge to describing new situations. In a review on mathematical models of polymer erosion for drug delivery, Sackett and Narasimhan (149) make the following observation about empirical models: "While empirical models are in general reliable within a system that has been studied experimentally and are easy to apply, they are not applicable to all systems and conditions. Additionally, accurate empirical models usually require an input of a large number of parameters and as a result contain little information about the actual underlying mechanisms." With respect to heritage science, models are trained on data that may not be representative of the collections they attempt to simulate. They may only work well for collections that are very similar to the objects/conditions in the training data. One can attempt to define "similarity" as variables being within a range of validity, but without understanding why these or other variables affect the underlying phenomena, one risks comparing two systems that may behave in very different ways. In the absence of an explanation of the underlying causes, it is difficult to study the relationship between cause and effect, which is essential when justifying the course of action in a particular conservation plan.

Mathematical models which represent a causal chain of processes can produce insights that an empirical model alone cannot reveal. For example, to investigate the impact of acetic acid on libraries and archives, Ligterink et al. (167) developed a model by combining existing partial models describing the transfer of acetic acid through air, the pH response of paper, and the kinetics of acid-catalysed hydrolytic depolymerisation. The kinetic model was based on the Ekenstam equation. This model predicts that the impact of acetic acid on archival collections is limited. This conclusion contradicts conventional wisdom, but it is consistent with the lack of direct evidence for acetic acid in typical storage conditions causing significant damage to paper heritage. One limitation of the model is that it does not account for acidic products generated by cellulose degradation during the natural ageing of paper (168). Therefore, the model may only be valid for situations where it is possible to maintain a constant level of acidity.

Variation within a collection has been modelled using a population distribution, simulating cellulose degradation in different segments of an archive that have

similar properties/conditions (169). Note that using a distribution to describe (known) variation in a collection is mathematically similar to using a distribution to describe uncertainty (unknown) in model inputs, but the former is suitable for calculating the probability of outcomes and the latter, the range of outcomes.

In summary, models of polymer degradation in heritage science have tended to focus on the effects of external (exogenous) factors/inputs such as temperature and relative humidity, with minimal representation of the structural characteristics of the system on which these factors act. The models are often descriptive, in comparison with the models presented in the following section, which have a more analytical basis.

3.3 MODELLING POLYMER DEGRADATION IN OTHER CONTEXTS

Outside heritage science, there are many models of polymer degradation which focus on representing underlying mechanisms. Such models can provide greater understanding of how endogenous factors—the internal organisation, qualities, and interactions between parts of the system itself—affect the system's outputs. This section presents a selection of mathematical models of mechanisms/phenomena relevant to cellulose acetate degradation.

3.3.1 Deacetylation

The kinetics of hydrolytic deacetylation have been studied experimentally primarily in aqueous solution systems. Typically, the reaction conditions are either homogeneous or, if heterogeneous, the experiments are designed to limit the role of diffusion, for example, by using very thin fibres of cellulose acetate. One feature of these conditions is that water concentration is effectively constant, therefore the effect of moisture is not studied. Mathematical models based on such experiments treat acetyl groups as a uniform chemical species, and hence, the overall rate is first order in acetyl concentration:

$$r = k_1[ROAc] \tag{3.13}$$

where k_1 stands for the first order rate constant. A study (82) using this approach measured the overall rate in a range of pH from 2-10. Because the reaction can be

acid- or base-catalysed, the authors of this study modelled these mechanisms as separate terms in a cumulative reaction rate constant:

$$k_1 = k_{H^+}[H^+] + k_{OH^-}[OH^-] + k_{H_2O} \qquad (3.14)$$

where $[H^+]$ is hydrogen ion concentration, $[OH^-]$ is hydroxide concentration, k_{H^+} and k_{OH^-} are second order rate constants for the acid- and base-catalysed reactions respectively, and k_{H_2O} is the first order rate constant for the neutral reaction [82]. The model assumes that concentrations of the ions can be calculated accurately based on dissociation constants and pH.
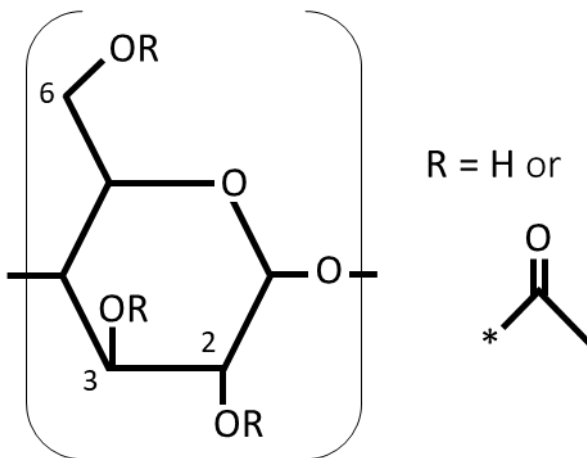
Figure 3.1 Cellulose acetate anhydroglucose unit (AGU). Functional groups bonded to C2 and C3 are secondary (e.g., secondary acetyls, when R = CH3CO), while the one bonded to C6 is primary.

Other models have attempted to account for variation in reaction rates between acetyl groups. The rate is still first order in acetyl group concentration, but the groups are distinguished from each other (see Figure 3.1). For example, one model distinguishes between primary and secondary acetyls (thus combining C2 and C3 acetyls) and considers the reverse reaction (re-acetylation) as well as the forward reaction [63]. The reverse reaction is not expected to play a role in heritage materials and environments as it is not thermodynamically favourable under these conditions.

Spurlin's model for substitution kinetics in cellulose derivatives distinguishes three reactive functional groups, with a rate constant for the substituent at each carbon position (170). The model assumes that the ratio of rate constants $k_2:k_3:k_6$, as well as the ratio of equilibrium constants $K_2:K_3:K_6$, are constants (the subscripts denote the carbon position of the substituents that the rate constant or equilibrium constant refers to). Assuming that these ratios remain the same during the whole reaction, and that all anhydroglucose units (AGU – the general term for a single monomer in a CA molecule) in the chain remain equally accessible for substitution at all times, then the equations of Spurlin's model may be solved to yield a characteristic distribution known as the Spurlin distribution (171).

The Spurlin model was augmented by Salmi and others (172–174) to account for the decrease in reactivity as substitution proceeds, during the carboxymethylation of cellulose. This model defines the 8 types of AGUs (2 substituent types and 3 substituent positions $= 2^3 = 8$ unique AGUs) as the chemical species, with 12 substitution reactions linking them (see Chapter 5, Figure 5.2). For each of the three positions, the model defines a reference rate constant and a parameter which relates to the decline in reactivity as substitution progresses. Therefore, while this model involves 12 substitution reactions, it defines no more than 6 kinetic parameters to describe the reactions.

The Spurlin model assumes that the substitution reactions on neighbouring AGUs are independent of each other. Another model was developed that distinguished between un-, mono- and di-substituted AGUs as a group and tri-substituted AGUs, to model the effect of substitutions in adjacent AGUs on substitution kinetics (175). Like the Spurlin model, this model generates distributions of AGUs as a function of degree of substitution. Recall that the degree of substitution (DS) is the average degree of acetylation of cellulose acetate and can vary between 0 and 3 (36). Using data of the AGU distributions in dimers (polymer molecules comprising exactly two monomers) generated from commercial cellulose acetate (DS = 2.44), it was found that the new model (which assumes dependence on adjacent substitutions) fits better than the Spurlin model (175).

As noted previously, the Arrhenius equation is often applied empirically to describe the temperature-dependence of reactions. The Eyring equation is based

on molecular modelling to predict the Gibbs free energy of activation, or the entropy and enthalpy change of the reaction (176). It models the chemical mechanism(s) of the reaction including intermediate and transition states (176). One such model was developed for deacetylation in cellulose diacetate, considering the reaction in neutral and acidic conditions:

$$\frac{d[ROAc]}{dt} = -\frac{K_B T}{h} \exp\left(\frac{\Delta S^{\ddagger}}{R_G}\right) \exp\left(-\frac{\Delta H^{\ddagger}}{R_G T}\right) \frac{[ROAc]C_B}{C_S} \qquad (3.15)$$

where K_B is Boltzmann's constant, h is Plank's constant, $\Delta S^{\ddagger}$ and $\Delta H^{\ddagger}$ are the maximum changes in entropy and enthalpy that correspond to the transition state, and C_S is the standard concentration (usually 1 mol L^{-1}) (177). In neutral conditions, C_B is the water concentration. In acidic autocatalytic conditions, C_B is the concentration of acetic acid. This study (177) cites a published peer-reviewed paper (172) based on Chapter 4 of this thesis.

3.3.2 Chain degradation

Chain degradation models comprise a far greater breadth and depth than do models relating to deacetylation. While a variety of approaches are presented in this section, all the mathematical models are based on a common conceptual model. In this conceptual model, a scission event occurs when one polymer molecule of length n splits into two polymer molecules of length m and $n - m$. Therefore, chain scission increases the number of chains, but makes the chains smaller.

3.3.2.1 Stochastic models

In a sample of polymer, polymer molecules of different sizes will be present in varying proportions (mole fractions). The molecular weight distribution (MWD) is a population distribution which maps molecular weight to mole fraction. Molecule size can also be expressed in terms of degree of polymerisation (DP), the number of monomers per polymer molecule.

Stochastic models of chain degradation attempt to deal with the polydispersity of the polymer molecules and the large number of possible scission events through

probabilistic approaches. These output MWD as a function of time or extent of reaction (degradation).

In a linear chain polymer, probability of reaction of a bond could depend on its position in the chain and the chain length (thus, the initial chain length or MWD is also required). Most of the stochastic models presented in this review vary by the assumptions they make concerning the effect of these two factors, the initial conditions, and in the analytical and/or numerical methods used to solve the equations.

Kuhn (179) assumed that initial chains are infinitely long compared with the degradation products and that all links are split with the same probability. Since the initial chains are infinitely long, individual fragments of length n are formed when a bond at position n away from the chain end is broken, while the $n - 1$ bonds in between remain intact. If the probability of any particular polymer bond being broken is a, then the (relative) frequency f_n of molecules of size n may be calculated as:

$$f_n = a(1 - a)^{n-1} \tag{3.16}$$

Equation 3.16 is analogous to MWD, where f_n represents mole fraction as a function of DP $= n$ and probability a corresponds to the extent of chain degradation.

Mark and Simha (180) derived MWD as a function of the initial (monodisperse) chain length $b + 1$ ($b =$ initial number of bonds per chain) and number of scissions per chain r. This assumes that r is the same for all chains undergoing degradation. They validated the model against experimental results of acetolysis of cellulose acetate, which was fractionated initially to a DP of 350. They noted that the model only holds for homogeneous reactions and that the reaction conditions were considered sufficiently homogeneous to make the comparison valid. They observed that there is no complete quantitative agreement between the experimental and theoretical curves, but that their results show good qualitative agreement. As this study was published in 1940, all the plots were hand-drawn, and the best-fit curves were obtained manually. Therefore, this limited the ability

of the researchers to make quantitative comparisons. The authors of the study did not demonstrate the relevance or advantage of including b as a parameter in their model compared with the model of Kuhn (179), for example, by showing how different b results in different MWDs.

Montroll and Simha (181) extended the previous model. Formally, the assumption that r is the same for all (initially monodisperse) chains undergoing degradation, is defined as all bonds connecting monomeric elements in the system having the same probability of being broken regardless of (1) their position in a polymer chain and (2) the size of the polymer in which they are found. In terms of a kinetic expression, the concentration term corresponds to the moles of bonds per unit volume. The model also assumes that all chains are equally accessible to reaction. Building on the work of Mark and Simha (180), the model predicts the average molecular weight of the degraded product as a function of the average number of bonds split per molecule (181). Experiments of acetolytic degradation of cellulose acetate are briefly discussed and compared with the model. The authors of the study predicted that at high degrees of depolymerisation, the chain length in which monomeric elements are most likely to be found (the mode length) tends to a limit, suggesting that the distribution functions tend to become independent of the initial chain length as the degradation process nears completion. It can be shown that the statistical model due to Montroll and Simha (181) simplifies to the Ekenstam equation (156), a result which went unremarked by the authors of the study despite publishing several years after Ekenstam. It requires the additional assumption that the rate of bond cleavage is constant, as Montroll and Simha's model is based on extent of reaction whereas Ekenstam's model is a function of time.

Researchers have benefited from gains in computational power, allowing stochastic models to be simulated via Monte Carlo methods (MC) (182). Early models assumed that all the bonds in the chain had the same probability of being broken. This is termed "random" scission, after the definition of random: "of or characterising a process of selection in which each item of a set has an equal probability of being chosen" (183). It was often possible to solve the equations analytically. Models with non-random scission events are usually too complex to

solve analytically. In this context, the term "non-random" refers to the fact that the probabilities of scission may not be equal and does not imply that the process is deterministic. MC deals with this by running many simulations of a stochastic model, generating a distribution of outputs over all the simulations. In this way, the MWD is obtained from the results of the simulation, rather than by solving model equations analytically. This makes it easier to study the effects of non-random scissions. Another benefit of performing calculations with computers is that it becomes possible to calculate numerical solutions for MWD in fine resolution, which would be extremely time-consuming if done by hand. This makes it easier to characterise statistical properties of the MWD such as the dispersity based on molecular mass, which is defined as:

$$\DJ_M = \frac{M_w}{M_n} \tag{3.17}$$

and the dispersity based on degree of polymerisation, defined as (184):

$$\DJ_X = \frac{DP_w}{DP_n} \tag{3.18}$$

As mentioned in Chapter 2, number-average molecular weight (M_n) and weight-average molecular weight (M_w) are two types of average values of the MWD in terms of molecular weight. Number-average degree of polymerisation (DP_n) and weight-average (DP_w) are the equivalents for MWD expressed in terms of DP.

In large polymers containing identical or uniform distribution of monomers, $\DJ_M$ and $\DJ_X$ are the same. Under these conditions, both types of average molecular weights can be calculated by multiplying the corresponding average degree of polymerisation by the average molecular weight of one monomer. Therefore, $\DJ_M/\DJ_X = 1$.

Guaita et al. (185) found that dispersity tends towards 2 when scission events are random, studied using MC. Favouring centre-scissions causes the dispersity to dip below 2, while favouring end scissions is associated with increasing dispersity above 2. Nishida et al. (186) developed a mathematical model of autocatalytic random hydrolysis in polyesters and found the same result, up until a threshold DP

termed the "critical point". The model's predictions were compared against hydrolysis data of aliphatic polyesters. The model and the data agreed up until the critical point, which depended on the polymer type. The authors of the study attribute this to structural changes such as disintegration of the amorphous regions, which "would result in failure of the most probable distribution and the broadening of distribution" (186).

Using MC, Emsley and Heywood (187) compared the effect of random bond cleavage to non-random bond cleavage, such as favouring centre-scissions or slicing off a fixed number or percentage of units. They found that the non-random processes are needed to cause a shift in molecular weight distribution, otherwise the peak DP does not shift. New peaks only occurred with chopping off a fixed number of units. Breaking the molecule in half resulted in a shift of the peak DP to lower molecular weights. Broadening towards higher molecular weights only occurred if there was recombination.

Similarly, Bose and Git (188) simulated different scission mechanisms using two new mathematical algorithms, an iterative Monte Carlo structured probability scheme and a semi-iterative algebraic exact statistical formulation method. They concluded that "The nature of molecular destruction can be well-characterised if the distinct MWD shift patterns can be simulated to fingerprint the different chain scission dynamics."

3.3.2.2 Deterministic models

Deterministic models are typically based on mass balances in the form of differential equations. The species described by the balances could be molecules, functional groups, or bonds (143). Unlike stochastic models, which consider the probabilities of discrete reaction events taking place in a time interval, deterministic models use reaction rates to describe the frequency of reaction events.

Because the polymer species are a distribution of molecular weights, which can be both reactants and products of scission events, it is computationally expensive to build and run a model as a system of differential equations representing the entire distribution. This approach is used in population balances, described in

Section 3.3.2.2.3. Most other deterministic models of linear chain polymers, including cellulose and its derivatives, characterise the hydrolysis rate by the generation rate of newly formed chain ends (189). The total chain end concentration at any time is equal to $(2 \times volume)/DP_n$, therefore the hydrolysis rate is frequently expressed in terms of $1/DP_n$ or $1/M_n$. Equivalently, the concentration of only reducing chain ends is equal to $1/DP_n$.

3.3.2.2.1 Hydrolysis of cellulose and cellulose derivatives

The Ekenstam model can be derived from kinetic principles (190). The reaction involves the conversion of inter-monomer bonds (concentration C) to two chain ends, resulting in a net gain of one polymer chain. Consider the random hydrolysis of inter-monomer bonds (B), producing chain ends (E) as product:

$$B + H_2O \rightarrow 2E \tag{3.19}$$

Assuming the water concentration is constant, the reaction rate depends on the concentration C of reactant B as:

$$\frac{dC}{dt} = -kC \tag{3.20}$$

$$C(t) = C(0)e^{-kt} \tag{3.21}$$

The initial number-average degree of polymerisation DP_0 is:

$$DP_0 = \frac{M1}{M0} = \frac{\sum_i n_i P_i}{\sum_i n_i} \tag{3.22}$$

where $M0$ is the initial zero-order moment of chain length distribution, $M1$ is the initial first-order moment of chain length distribution, n_i is the concentration of chains of length i, and P_i is the number of monomers in a chain of length i. The units of n_i are "chains per unit volume" and the units of P_i are "monomers per chain". Considering that each chain has one less bond than there are monomeric units, and using $P_1 = 1$:

$$C(0) = \sum_i n_i(P_i - P_1) = M1 - P_1 M0 \tag{3.23}$$

Denoting the number of scissions per unit volume as S:

$$DP_n = \frac{M1}{M0 + S} \tag{3.24}$$

$$C(t) = M1 - P_1 M0 - P_1 S \tag{3.25}$$

Substituting these into Equation 3.21:

$$M1 - P_1 M0 - P_1 S = (M1 - P_1 M0)e^{-kt} \tag{3.26}$$

$$\frac{M1 - P_1 M0 - P_1 S}{M0 + S} = \frac{M1 - P_1 M0}{M0 + S}e^{-kt}$$

$$DP_n - 1 = \left(DP_n - \frac{DP_n}{DP_0}\right)e^{-kt}$$

$$1 - \frac{1}{DP_n} = \left(1 - \frac{1}{DP_0}\right)e^{-kt}$$

$$\frac{1}{DP_n} - \frac{1}{DP_0} = \left(1 - \frac{1}{DP_0}\right)(1 - e^{-kt}) \tag{3.27}$$

Equation 3.27 is the first-order rate law. Expanding the exponential function in a Taylor series around $t = 0$ and retaining only the first two terms:

$$1 - e^{-kt} \sim kt + O(t^2) \tag{3.28}$$

Replacing the exponential function in Equation 3.27 with the linear approximation:

$$\frac{1}{DP_n} - \frac{1}{DP_0} = \left(1 - \frac{1}{DP_0}\right)kt \tag{3.29}$$

Assuming DP_0 is large, this approximates to:

$$\frac{1}{DP_n} - \frac{1}{DP_0} = kt \tag{3.30}$$

Equation 3.30 (the Ekenstam equation) corresponds to a zero-order reaction where the rate of bond cleavage is constant (191). The rate of bond cleavage is approximately constant at the start of the reaction because the concentration of bonds, on which the rate has a first-order dependence, changes very little during this period.

Molecular weight distributions obtained by size exclusion chromatography show that the depolymerisation of cellulose proceeds in a random fashion and follows first-order reaction kinetics (Equation 3.20) (191,192). As this meets the conditions of the first-order law (Equation 3.27), the zero-order law (Equation 3.30) is therefore applicable when the additional conditions are met, such as constant rate of bond cleavage.

Studies (193–195) built on these assumptions have often focused on deriving analytic solutions to their models. Elegant formulas can be satisfying to their authors and other readers, and simple models are probably more likely to diffuse in the scientific community than complex ones. Sometimes there are good reasons for the acceptance and sharing of models: for example, if the equations are better suited to fitting data. Nonetheless, it should be stressed that the human preference for aesthetically pleasing equations is a bias in the development and dissemination of models. The fact that an assumption results in a more tractable function is not sufficient to justify the underlying assertion that is being made about the system under study.

Several cellulose degradation models attempt to account for non-Ekenstam behaviour by incorporating additional explanatory features. Around $DP_n = 250$, experimental data deviate from the Ekenstam model (196). This is called the Levelling Off Degree of Polymerisation (LODP). Below this, the rate constant appears to decrease, possibly due to the breaking off of soluble molecules of very low DP, causing weight loss and leaving behind larger molecules with little change in DP_n in residual polymer. LODP is comparable to the "critical point" mentioned earlier in the context of stochastic models (186). It is simply the point where the data deviate from the model, presumably because something in the physical system has changed so that the model assumptions are no longer valid.

Global deviation may also be due to presence of weak and amorphous links, leading to a model of two parallel first-order reactions (197). Several studies (198–202) found that if there were weak links or acid-sensitive links present in paper during acid-catalysed hydrolysis, a two-stage degradation process could be observed, giving a non-constant slope. The acid-catalysed hydrolytic degradation of cellulose may proceed in several stages, resulting in distinct phases where the dominant mechanism determines the apparent rate of reaction. Proposed stages include (203):

1. Rapid initial stage: very susceptible weak bonds, due to physically induced strains.
2. Accessibility: Reaction of the chains in the amorphous region.
3. Attack on crystallites: Reaction of the crystalline regions of the polymer.
4. Even more weakening of weak bonds by light.

Other phenomena accounted for in cellulose degradation models include considering an oxidised vs. non-oxidised portion, and a model for autocatalytic depolymerisation in sealed vessels based on generation of H^+ ions during degradation (194,196).

Despite such deviations from the Ekenstam model, researchers have continued to apply the formula (or at least, to quantify extent of reaction according to $1/DP_n$) to study the effects of parameters like temperature, relative humidity, and acidity on paper ageing (158). The activation energy of the Arrhenius equation (Equation 3.8) indicates the temperature sensitivity of the reaction rate. A paper ageing study (158) which looked at the performance of fresh paper pulps (as opposed to the deterioration of archival papers) obtained activation energies of 104-113 kJ mol^{-1}, close to those obtained in different study (201) for the hydrolysis of cellulose in a dilute acid solution, 113-117 kJ mol^{-1}. This supports acid-catalysed hydrolysis of cellulose as the dominant mechanism during ageing because any reaction with an activation energy far from the apparent activation energy is weighted very little (158).

The relationships between RH and cellulose degradation resembles the relationship between RH and moisture content (158). Based on this, Zou et al.

(158) suggest that the moisture content in the paper may be the controlling factor of cellulose degradation. The significant effect of moisture may be explained by the fact that cellulose is hydrolysed according to the following mechanism (acid-catalysed hydrolysis) (204):

1. A rapid protonation of the glycosidic oxygen atom.
2. Slow transfer of the positive charge to C1 with consequent formation of a carbonium ion and fission of the glycosidic bond by a water molecule.
3. Reformation of hydronium.

Hence, water reacts in the slowest step (step 2), also known as the rate-controlling step.

It has been speculated that dissociated hydrogen ions can be present in paper if sufficient moisture is present during moist ageing. The true hydrogen ion concentration in paper under ageing conditions is hard to define, but an approximation of the true value may be measured using the cold-water leach method (158). A linear relationship between the degradation rate constant (Ekenstam model) and hydrogen ion concentration was found using this measurement (158).

Zou et al. (165) outline the following fundamental problems when a kinetic analysis approach has previously been applied to determine the validity of accelerated ageing tests for predicting paper permanence:

1. The use of inappropriate parameters for kinetic analysis e.g., physical properties.
2. Lack of critical examination of the Arrhenius equation.
3. No examination of the statistical errors of the predictions.
4. No quantitative comparison of the results of accelerated and natural ageing.

As similar approaches have been used to study fresh paper performance as degradation of archival papers, it is worth keeping these concerns in mind when using accelerated ageing tests in heritage science.

Chain degradation in cellulose acetate is less well studied than either deacetylation in CA or chain degradation in cellulose. Relatively few studies have looked at

modelling chain degradation in cellulose acetate; therefore, this review includes models of chain degradation in other cellulose derivatives.

The pseudo-zero order chain scission rate was measured in cellulose acetate in acetic acid containing varying water or acetic anhydride concentrations at fixed sulphuric acid concentration and temperature (104). The degradation rates in water were 1-3 orders of magnitude less than those in acetic anhydride, dropping sharply with increasing water concentration.

Homogeneous hydrolysis/acetolysis of cellulose acetate in acidic aqueous solution was modelled using the Ekenstam equation (63,156). Deacetylation kinetics were also modelled in this study, treating deacetylation and chain degradation as independent processes. The main findings were that activation energies of deacetylation are significantly lower than those for chain scission, indicating that chain scission is more sensitive to temperature than deacetylation. The CA chain scission activation energies found in this study (63), 95-124 kJ mol^{-1}, agree approximately with the values that have been measured for cellulose chain degradation, 104-117 kJ mol^{-1} (158,201).

Despite awareness that deacetylation precedes chain degradation, and theories positing deacetylation as a condition for chain degradation in CA, a review of the literature did not find any models that attempt to consolidate these two mechanisms into a unified mathematical framework. In a study (205) concerning the biodegradability of CA, a model was proposed that calculates the probability of the occurrence of unsubstituted AGUs adjacent to one another, assuming deacetylation occurs randomly with equal probability for all the reactions. By assuming constant reaction rate, the model obtains the proportion of "reactive" glycosidic bonds as a function of time. The "reactive" glycosidic bonds constitute bonds between adjacent unsubstituted AGUs, as these are believed to be more susceptible to biodegradation than glycosidic bonds between substituted AGUs.

In a study (106) that attempted to model denitration and chain degradation of nitrocellulose in aqueous sulphuric acid solutions, Lure et al. acknowledged that chain degradation was inhibited in nitrocellulose compared with cellulose, but they modelled denitration and chain degradation as two independent processes.

The Ekenstam equation was used to model chain degradation (106,156). The chain degradation rate in nitrocellulose was estimated as a third of that in cellulose under similar reaction conditions.

A study (102) that aimed to investigate how substitution could *increase* the rate of chain degradation produced substituted and unsubstituted cellulose using a proprietary substitution agent. Mu et al. (102) developed and trained a model that accounts for the proportion of substituted cellulose on the first-order chain scission rate constant. Their results show that the apparent scission rate in substituted (more reactive) cellulose converges (decreases) over time to the apparent scission rate in unsubstituted (less reactive) cellulose, as the proportion of substituted (more reactive) cellulose decreases as the reaction progresses. However, the model does not consider kinetics of substitution itself and the interaction of this with the chain scission dynamics.

3.3.2.2.2 Hydrolysis of linear chain polymers

Chain scission in other linear chain polymer molecules share (or may share) common aspects with CA chain degradation. For example, the Ekenstam model, originally applied to cellulose hydrolysis and cellulose acetate acetolysis, can be applied to other degrading polymers if the following conditions are met (206):

1. The polymer chain is linear and of high molecular weight.
2. The polymer is monodisperse and the products of scission are themselves long chain molecules.
3. There is a low degree of chain end-chopping.
4. There is no loss of monomer units during scission.

The first-order model, Equation 3.27, is also valid for linear chain polymers over longer reaction times when the bond scission rate has changed from the initial bond scission rate. The most basic modification to this model is to consider what happens when chain scission is non-random. As noted earlier, "randomness" in the context of chain scission refers to uniform rates (or probabilities) of bond scissions, independent of bond position or molecule size. Since there are many more non-terminal bonds than terminal bonds (bonds at the end of the chain), random scission implies the third condition (above). Therefore, one type of non-

random scission is when end scission is faster, i.e., more probable, than expected in random scission.

Numerous deterministic models have incorporated varying degrees of end scission (207–210). Chain scission is modelled using specific bonds or radicals as reacting species. Reactivity is independent of position in chain other than distinguishing between species in main chain and species in terminal position (or near terminal position) (143). The differential equations are expressed and solved in terms of concentrations of non-terminal bonds and terminal bonds. These models output M_n and fraction residual monomer (sometimes referred to as soluble fraction), enabling comparison with experimental data. These models demonstrate that it is feasible to have deterministic models with non-uniform bond reactivities, without the need to resort to computationally intensive population balances (see Section 3.3.2.2.3).

Some basic patterns emerge, enabling identification with the dominant chain scission mechanism (209). This two-part study also looked at the effect of autocatalysis by chain ends. Since this is not believed to be relevant to CA degradation, it is worth pointing out that the conclusions given here pertain to the noncatalytic cases. Part 1 of the study (209) focused on effects of the kinetic parameters (reaction rate constants). The kinetic parameters determine the chain scission mechanisms – random scission or end scission. The model predicts that random scission will result in deceleration (convexity) in the M_n-time curve. The convexity of the M_n-time curve under random scission is consistent with its inverse being linear, per the Ekenstam model (Equation 3.30 – recall M_n and DP_n are proportional when the monomer masses are uniformly distributed). When the dominant mechanism is end scission, the model predicts the absence of this convexity in the M_n-time curve. End scission is also predicted to result in mass loss due to diffusion of small, soluble molecules. This is because end scission produces low-molecular weight degradation products—single monomers. A linear relationship between mass loss and time is associated with end scission. The upper limit of mass loss is determined by the rate of soluble degradation products, which is essentially linear during end scission. Because mass loss also requires the small

chains to diffuse out of the sample specimen, a lack of mass loss does not necessarily indicate that end scissions do not occur (209).

Part 2 of this study (210) looked at effects of initial conditions (molecular weight and monomer content) on M_n half-life and time to obtain 10% soluble fraction. The M_n half-life time is the (normalised) time for the molecular weight to reach half its initial value. M_n half-life is positively correlated with initial M_n for end scission. This is because the number of end scissions required to reduce M_n by half is directly proportional to the chain length, and so to M_n. M_n half-life is negatively correlated with initial M_n for random scission. This is because with larger initial M_n, there are fewer polymer chains initially. So, for the same rate of random chain scission, the effect of each random scission on molecular weight is greater, resulting in shorter half-life.

3.3.2.2.3 Population balances

Population balance models look at the generation and consumption of all the molecules in the molecular weight distribution. The MWD is a discrete distribution which describes the mole fraction of polymers of each molecular weight or degree of polymerisation. In the population balance, for each (discrete) polymer length j in the MWD, there is a mass balance on polymers of length j, accounting for all the possible reactions that produce it from a larger chain or break the molecule into smaller fragments.

Simha (211) developed a population balance model for depolymerization of linear chain molecules. In the general case, there are independent rate constants $k_i^{(j)}$ for the breakage of bond i in a chain consisting of j monomers. This results in a set of differential equations describing the rates of change of N_j, the number of molecules of size j, from $j = 1$ to the upper limit of the MWD. Three special cases are considered:

a. Equal disintegration probability for all linkages independently of their position in the chain. The results confirm and extend those previously found from statistical considerations.
b. Preferred breaking at the ends.
c. Equal disintegration probability for all chains independently of their size.

Equations for the decrease of number and weight average molecular weight with time are given in each case. For the case of (a), the model simplifies to the result found using identical assumptions for the stochastic model by Montroll and Simha (181). The statistical result involves the trivial assumption that N_j are very large numbers, a condition which is introduced implicitly by describing the rate process by means of differential equations rather than difference equations.

3.3.2.3 Mechanistic models

Mechanistic models invoke detailed explanations of the underlying chemical mechanisms involved in reactions. Stochastic and deterministic models may or may not rely on mechanistic explanations of phenomena to support their assumptions. Mechanistic models could support the assumptions of existing stochastic and deterministic models, or they could be used to predict what assumptions to include in a new model.

According to a review by Laycock et al. (146), "the use of molecular modelling, where polymer chains are modelled atom by atom, is . . . limited in its applicability. Such simulations can assess disrupted bonds and the influence of thermodynamic enthalpy on product formation, but give less insight into kinetic processes". This conclusion would appear to be contradicted by the example given in Section 2.3.1 of a molecular model of deacetylation, Equation 3.15 (177). In that example, the contribution of the Eyring equation is to predict kinetic parameters. The mechanistic model of deacetylation of a cellulose acetate AGU is comparable to a model of the same reaction in cellobiose acetate, a two-monomer molecule of cellulose acetate. It may be the case that molecular modelling of polymer chains, which are more complex and significantly larger, is less useful for understanding kinetics of chain degradation. Molecular modelling has been used to rank relative degradation rates in PLLA/PDLA polymer blends by comparing states of polymer chains before and after an artificially introduced cleavage event and calculating the change in potential energy (146,212). However, the correlation with polymer degradation that occurs over long timescales is less clear cut.

3.4 CONCLUSIONS AND CONTRIBUTION OF THIS THESIS

This chapter has covered a range of mathematical models of polymer degradation in heritage and non-heritage contexts. Following the review of cellulose acetate degradation in Chapter 2, this modelling literature review uncovered opportunities to model phenomena believed to play a role in CA polymer degradation, while also suggesting an assortment of modelling methods to draw upon for this task.

As noted in Chapter 1, and illustrated with several examples in this last chapter, mathematical models of degradation in heritage science have tended to focus on the effects of environmental factors, mainly to establish guidelines for storage conditions. Subject to the environment being constant, the rate of degradation is modelled as constant, also known as a linear model. However, as was shown in Chapter 2, there is substantial evidence that degradation in CA is non-linear, as well as explanations and additional evidence for how the underlying phenomena may cause this. Many of the mathematical models in this chapter are based on differential equations and utilise calculus to deal with systems that have non-constant rates, and so yield non-linear solutions.

This thesis develops mathematical models for deacetylation and chain degradation in cellulose acetate cultural heritage artefacts. Utilising differential equations, the models attempt to simulate the dynamics of these reactions based on descriptions of underlying phenomena. These descriptions are based on causal relationships and interactions that have been hypothesised by other scientists in the field. The research focuses on two dynamical phenomena which have not been adequately modelled using existing approaches and have been identified as suitable for modelling in terms of mass balances:

1. Autocatalysis of the deacetylation reaction by acetic acid: The total amount of acetic acid produced by deacetylation (and retained in the artefact) is a time-varying quantity. Therefore, the rate of the reaction which it impacts is not constant, so deacetylation is a non-linear process which could be modelled using calculus. As deacetylation also produces acetic acid, which increases the rate of deacetylation, the dynamics are characterised by *positive feedback*. In a feedback process, the rate of change of a quantity is a

function of the current value of the quantity. In positive feedback, an increase in the quantity causes an increase in its rate.

2. Linking AGU composition to chain scission: AGU composition changes as deacetylation advances. The impact of AGU composition on the rate of chain scission can be modelled using differential equations, which can be integrated to predict the extent of chain scission as a function of time. The rate of chain scission is mediated by the extent of deacetylation, which describes a *cascade process*. In a cascade, the (time-dependent) value of an output from one process affects the rate of a second process.

The difference between these models and previous degradation models in heritage science is that, in broad terms, positive feedback and cascade models attempt to describe how the degree of degradation in a CA artefact influences its rate of degradation. These models identify causal relationships between inputs and outputs, based on physicochemical processes, offering insight and knowledge to alter these relationships and thus manage degradation in CA artefacts. Non-linear dynamics and variable rates are the mathematical consequences of accounting for the relationship between degree and rate of degradation.

Chapter 4 presents the development of the autocatalysis model of deacetylation. The chain degradation model is based on the theory that glycosidic bonds are more susceptible to cleavage when adjacent AGUs are deacetylated. The model of deacetylation which predicts AGU composition is developed in Chapter 5. Chapter 6 builds on the outputs of this model—AGU composition as a function of time—to develop the chain degradation model. Chapter 7 presents the conclusions that can be drawn from these models in the context of CA artefacts and their consequences for heritage conservation.

4 DEACETYLATION AND AUTOCATALYSIS

This chapter presents a mathematical model of deacetylation that accounts for the autocatalytic effect of acetic acid continuously, including before and after initiation of the vinegar syndrome. The research I carried out for my PhD was published in a paper (178), which I am the lead author of. This research includes:

- *motivation for the development of the model in the context of predicting cellulose acetate (CA) film degradation*
- *model system definition, model assumptions, and model equations*
- *estimation of kinetic parameters from a set of published experimental data*
- *comparison of model predictions with a second set of published experimental data*
- *discussion of model performance and limitations.*

4.1 INTRODUCTION

As discussed in Chapter 2, the vinegar syndrome is typically one of the earliest signs of degradation in cellulose acetate (CA) cultural heritage artefacts. Vinegar syndrome is due to deacetylation, which reduces the degree of substitution (DS) of CA and produces acetic acid. Recall the chemical reaction:

$$ROAc + H_2O \rightarrow HOAc + ROH \tag{4.1}$$

where OAc stands for CH_3COO (Ac is short for acetyl), HOAc is acetic acid, OH is hydroxyl, and R represents the rest of the polymer (61). Vinegar syndrome, recognisable by its odour, is typically a precedent to more rapid degradation and damage, such as reduction in tensile strength, and can also expose nearby storage materials or artefacts to acidic vapours.

While this reaction takes place in all kinds of CA objects, the term "vinegar syndrome" is most associated with CA films, including photographic, motion picture, and microfilms. Technically, vinegar syndrome is considered to begin after the concentration of acetic acid in the film reaches a threshold level, corresponding

to a free acidity[1] of 0.5 (10,14). It was believed that after this point, the rate of reaction increases dramatically due to accumulation of acetic acid which catalyses the reaction producing it, a phenomenon known as autocatalysis. This idea has been central to the development of models of deacetylation in CA films, which assumed that prior to the vinegar syndrome, the deacetylation rate was constant (10). Models with a constant degradation rate are also known as linear models. Such models were developed with the aim of predicting the onset of vinegar syndrome i.e., to predict the time until free acidity of 0.5, under various environmental conditions (temperature and relative humidity) (11).

As discussed in Chapter 2, Section 2.3.1, there is a lack of evidence supporting the theory that the mechanism changes from non-catalytic to autocatalytic at 0.5 free acidity (78). There is also no scientific explanation for why the mechanism would change, or why it would change at a free acidity of 0.5. This chapter presents a model which accounts for autocatalysis. Autocatalysis is an example of *positive feedback*. Positive feedback occurs when an increase in the output of a system (acetic acid) increases the rate of that output (deacetylation rate). When a system has a positive feedback process, this results in non-linear dynamics. Therefore, this model differs from previous research by accounting for the positive feedback effect of autocatalysis in the form of non-linear equations to describe deacetylation rate.

4.2 METHODS

In the model system, it is assumed that the film is stored in an air-tight enclosure made of a material that does not interact with any of the compounds in the film. The film, which can be a roll or strip, occupies most of the enclosed volume.

Two different experimental procedures, carried out by other researchers, were considered to fit this scenario. In both, cellulose triacetate (CTA) film was first moisture-conditioned, so that the initial moisture content was in equilibrium with

---

[1] As mentioned in Chapter 2, free acidity is measured as the mL of 0.1 M NaOH required to neutralise 1 g of CA . For brevity, the units for free acidity are omitted from hereon, except for in the figures and tables, or anywhere the units of free acidity are required for conversion to different units or other calculations.

the temperature and relative humidity (RH) of the environment in which the film was placed.

In the first procedure, referred to as the *bag method*, following moisture-conditioning, strips of film were incubated in two heat-sealed aluminium foil-polyethylene bags (10). Air was removed from the bags prior to sealing to maintain a high film-to-air volume ratio.

In the second procedure, referred to as the *can method*, rolls of film were incubated in taped metal cans (31). Experiments separate from the studies used to train and test the model confirmed that measurements of free acidity using the bag method and the can method agree with one another (8).

To model this scenario, it was assumed that the volume inside the enclosure consists of only the film base, with the chemical species of interest distributed initially uniformly throughout. An assumption of no mass transport across the boundaries of the enclosed volume was made. Given an initially uniform field of chemical species, the field will remain uniform, and the concentrations depend only on time as the independent variable.

Because the system is closed, any volatile compounds present in the system (water and acetic acid) are retained completely in the film base. Assuming that deacetylation is the only reaction taking place, the concentrations of acetyl, water, and acetic acid are related by the following balance equations, which are based on the reaction in Equation 4.1:

$$[ROAc](t) = [ROAc]_0 - ([HOAc](t) - [HOAc]_0) \qquad (4.2)$$

$$[H_2O](t) = [H_2O]_0 - ([HOAc](t) - [HOAc]_0) \qquad (4.3)$$

where the terms in brackets are the concentrations of the chemical species in the film base (mol m^{-3}), t is time (s) and the subscript 0 denotes the initial concentration of the component at time $t = 0$.

These equations were solved to obtain $[HOAc](t)$, the acetic acid concentration as a function of time. It was assumed that the acid-catalysed mechanism dominates the deacetylation reaction kinetics in this system, compared with neutral or base-

catalysed mechanisms. This requires $[HOAc]_0 > 0$. The free acidity in fresh CTA film is about 0.04, meeting the minimum requirement (8). Defining the control volume as the enclosed volume of film base, the mass balance on acetic acid is:

$$\frac{d[HOAc]}{dt} = k\,[ROAc]\,[H_2O]\,[HOAc] \tag{4.4}$$

where k is the deacetylation rate constant (mol^{-2} m^6 s^{-1}).

The temperature dependence of k is given by the Arrhenius equation:

$$k = A\,e^{\frac{-E_a}{R_G T}} \tag{4.5}$$

where A is the pre-exponent factor (mol^{-2} m^6 s^{-1}), E_a is the activation energy (kJ mol^{-1}), R_G is the ideal gas constant (8.3145×10^{-3} kJ mol^{-1} K^{-1}), and T is the temperature (K).

The kinetic model is characterised by the following set of assumptions:

1. **First order dependence on acetyl concentration**: Deacetylation of CTA in solution shows a first-order dependence on degree of substitution (62). As noted earlier, acetyl groups may react at different rates (63–69). The kinetic model considers the reacting acetyl groups as equivalent, independent of acetyl position and degree of substitution. This approach has been successfully applied in other models of this reaction (78,82). Mathematically, this approach is suitable either if reactions of different acetyls have identical rates, or if one reaction is significantly faster than other reactions. In the latter case, the validity range of the model is limited by the concentration of the fast-reacting acetyl in the initially dominating reaction, because as the fast-reacting acetyl becomes depleted, this reaction will cease to dominate the overall deacetylation rate.

2. **First order dependence on water concentration**: Based on consideration of the reaction stoichiometry, this distinguishes Equation 4.4 from the kinetic expression for a typical aqueous ester hydrolysis, which does not depend on water concentration. However, given the relative scarcity of water in CA

film compared to an aqueous reaction phase, this difference in dependency makes sense.

3. **First order dependence on acetic acid concentration**: The rate depends on $[HOAc]$ as the acid catalyses the reaction. In an aqueous solution, the rate of the acid-catalysed reaction is expected to depend on $[H^+]$ (82). As the reaction takes place in solid film base, not solution, this quantity is difficult to measure or even define. Conveniently, free acidity is considered a reliable measurement of acetic acid content in CTA film base, rather than the concentration of hydrogen ions (76). A first-order dependence on the concentration of acidic hydrolysis products, not on $[H^+]$, was proposed by Pitt et al. (213) while working on poly(ε-caprolactone). This type of model is considered generally applicable in the field of polymer degradation kinetics (146,189). In a study modelling cellulose diacetate deacetylation from first principles, Mohtar et al. (177) assumed a first-order dependence on acetic acid concentration for the acid-catalysed reaction. An analysis (78) of free acidity changes in CTA films during accelerated ageing observed a first-order dependence on free acidity, so this result is used for Equation 4.4. A mechanism has been proposed by Mohtar et al. (177) which may be valid here but it is beyond the scope of this thesis to explore this in detail.

To simplify the notation, the following constants were defined:

$$a \equiv [ROAc]_0 + [HOAc]_0 \qquad (4.6)$$

$$b \equiv [H_2O]_0 + [HOAc]_0 \qquad (4.7)$$

Equation 4.2 and 4.3 become:

$$[ROAc](t) = a - [HOAc](t) \qquad (4.8)$$

$$[H_2O](t) = b - [HOAc](t) \qquad (4.9)$$

The expressions for $[ROAc]$ and $[H_2O]$ in Equation 4.8 and 4.9 were substituted into Equation 4.4 to obtain a differential equation with one time-dependent variable, $[HOAc]$:

$$\frac{d[HOAc]}{dt} = k\,(a - [HOAc])\,(b - [HOAc])\,[HOAc] \tag{4.10}$$

This equation describes how the concentration of acetic acid varies in time. Assuming that free acidity provides a direct means to measure acetic acid concentration, this formulation has the advantage that most of the published literature which employed the relevant experimental procedures (the bag method and the can method) measured the extent of deacetylation by measuring free acidity over time.

4.3 RESULTS AND DISCUSSION

This thesis uses the terms training, (cross-)validation, and testing to describe aspects of model development. Sometimes associated with machine learning, these concepts are useful for creating and evaluating quantitative models using real-world data. The definitions are as follows (214):

Training dataset: The sample of data used to fit the model.

Validation dataset: The sample of data used to provide an unbiased evaluation of a model fit on the training dataset while tuning model hyperparameters.

Test dataset: The sample of data used to provide an unbiased evaluation of a final model fit on the training dataset.

4.3.1 Training

The kinetic parameters A and E_a were fit to published data from accelerated ageing experiments. In these studies (10), the free acidity of CTA film was measured to assess the impact of temperature and RH on the rate at which the vinegar syndrome progresses. Fresh CTA film was moisture-conditioned at 21 °C and 50% RH. The film was then incubated using the bag method.

Data from film base pre-conditioned at 50% RH was used to estimate the kinetic parameters, as it was the only RH for which the data were available over a wide range of temperatures. Experimental results had to be estimated from graphical observation. The data used are presented in Table 4.1. Measurements over 5.2 acidity were excluded from the data used in this analysis because Adelstein et al. (10) believed that, at higher acidity, some of the acetic acid may have been lost between removing the film from the bag and making the measurements. The maximum temperature used, 100 °C, is below the glass transition temperature of CTA film, observed at approximately 120 °C (215).

Table 4.1   Experimental data used for estimating kinetic parameters (10).

70 °C		80 °C		90 °C		100 °C	
Time (days)	Free acidity (mL)	Time (days)	Free acidity (mL)	Time (days)	Free acidity (mL)	Time (days)	Free acidity (mL)
0	0.04	0	0.04	0	0.04	0	0.04
30	0.1	25	0.25	5	0.1	2	0.1
60	0.25	50	3.4	10	0.2	4	0.2
75	0.6	60	5.2	20	3.2	8	0.8
90	1.3					15	1.5
114	4.6					20	4.7

Rate constant k at different temperatures was obtained by fitting the model to this data. Equation 4.10 was rearranged to integrate it:

$$\int_{[HOAc]_0}^{[HOAc]} \frac{1}{(a-x)(b-x)}\, dx = \int_0^t k\, d\tau \qquad (4.11)$$

where x and τ are dummy integration variables. Equation 4.11 was solved analytically (see Appendix A), obtaining:

$$\alpha \ln\left(\frac{[HOAc] - a}{[HOAc]_0 - a}\right) + \beta \ln\left(\frac{[HOAc] - b}{[HOAc]_0 - b}\right) + \gamma \ln\left(\frac{[HOAc]}{[HOAc]_0}\right) = kt \qquad (4.12)$$

$$\alpha \equiv \frac{1}{a\,(b - a)} \qquad (4.13)$$

$$\beta \equiv \frac{1}{b\,(b - a)} \qquad (4.14)$$

$$\gamma \equiv \frac{1}{a\,b} \qquad (4.15)$$

The free acidity data in Table 4.1 were processed according to Equation 4.12, using the initial conditions in Table 4.2. The procedure for converting between free acidity and acetic acid concentration is explained in Appendix B.

Table 4.2   Initial conditions used to process data in Table 4.1.

Quantity	Value (mol m^{-3})	Description
$[ROAc]_0$	13403.6	Based on density of cellulose triacetate (37).
$[H_2O]_0$	2137.2	Based on the moisture isotherm for fresh CTA film base at 20 °C, as this was the nearest temperature to 21 °C for which the data were available (121).
$[HOAc]_0$	5.2	Calculated by converting the measured free acidity at $t = 0$ (see Table 4.1) to acetic acid concentration.

By plotting the left-hand side of Equation 4.12 against time (Figure 4.1), it is possible to visualise how the rate constant k was found from the gradient of the best-fit line at each temperature.

The rate constant k was estimated at each temperature by calculating the slope of the best-fit line, where the y-intercept was set to zero. This was done using linear least squares regression in Microsoft Excel™. The results are reported in Table 4.3. The errors in k refer to the standard error in the gradient. The r^2 values are close

to 1, suggesting that Equation 4.12 is a good fit for the data and supporting the validity of the kinetic model for this reaction system.
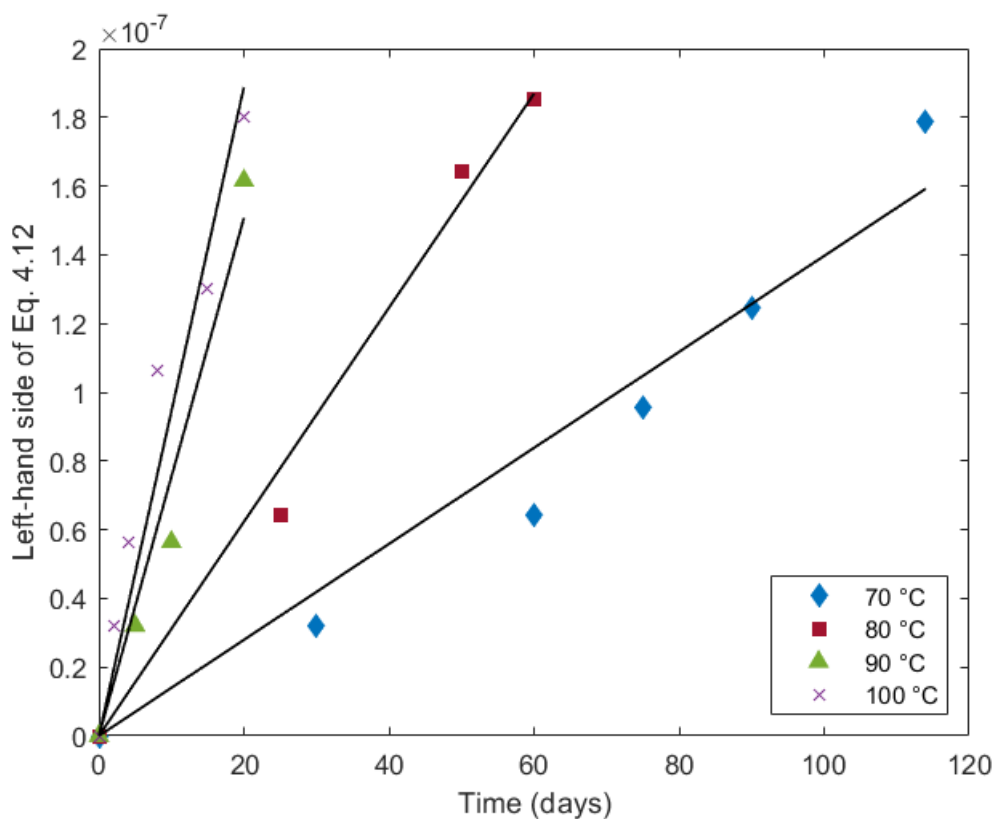
Figure 4.1 Data in Table 4.1 processed using Equation 4.12.

Table 4.3 Values of k fitted at each temperature.

Temperature °C	$k \times 10^{-14}$ (mol^{-2} m^6 s^{-1})	r^2
70	1.62 ± 0.09	0.985
80	3.6 ± 0.1	0.996
90	8.7 ± 0.7	0.983
100	10.9 ± 0.8	0.974

The data in Table 4.3 were linearised by rearranging Equation 4.5:

$$\ln(k) = \ln(A) - \left(\frac{E_a}{R_G}\right)\left(\frac{1}{T}\right) \tag{4.16}$$

Plotting $\ln(k)$ against $1/T$ (Figure 4.2) shows how $\ln(A)$ was found from the y-intercept of the best-fit line, and E_a/R_G from the gradient. This was done using linear least squares regression in Microsoft Excel™. The results are reported in Table 4.4.
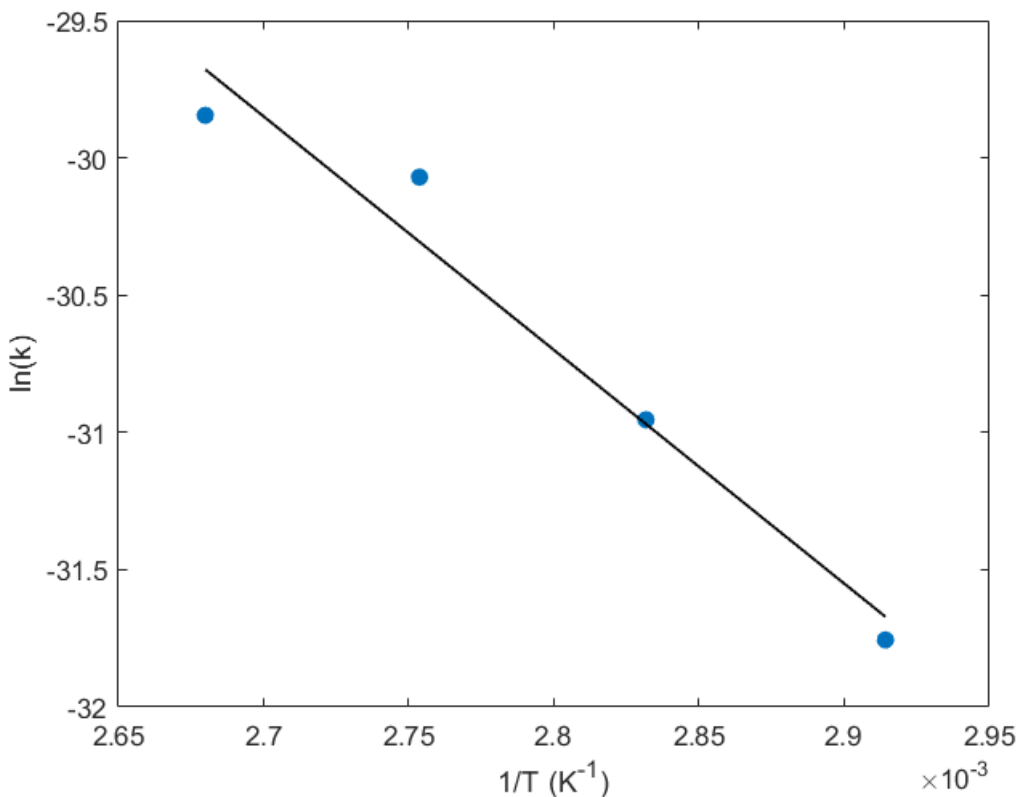
Figure 4.2 Estimated rate constants at different (reciprocal) temperatures.

Table 4.4 Estimated kinetic parameters.

Quantity	Value
$\ln(A)$	-6.9 $\pm$ 3.4
A	$0.00103^{+0.030159}_{-0.000996}$ mol^{-2} m^6 s^{-1}
E_a	70.734 $\pm$ 10.141 kJ mol^{-1}
r^2	0.961

The relatively large error in $\ln(A)$ is due in part to the small size of the training dataset. The precision could be improved by taking measurements at more

temperatures. As these errors are magnified exponentially when calculating A, this causes the asymmetry in the final reported standard errors.

Other studies have estimated the apparent activation energy of the deacetylation of cellulose acetate, under various conditions and with different models. These are summarised in Table 4.5.

Table 4.5 Deacetylation activation energies reported in the literature.

E_a (kJ mol^{-1})	Reaction system	Model description
92.048	CTA film at 20% RH.	Zero-order kinetics. Based on time taken to reach free acidity of 0.5 (142).
87.864	CTA film at 50% RH.	
87.864	CTA film at 60% RH.	
83.68	CTA film at 80% RH.	
68.6	CA reverse osmosis (RO) membranes in aqueous solution (acid-catalysed).	Models acid-catalysed, base-catalysed, and neutral reactions separately, with first-order dependence on DS. For the acid- and base-catalysed reactions, there is also first-order dependence on the activity of H$^+$ and OH$^-$ in solution, respectively (82).
34.0	CA reverse osmosis (RO) membranes in aqueous solution (neutral).	
48.1	CA reverse osmosis (RO) membranes in aqueous solution (base-catalysed).	
59.8	Uncatalysed C6 deacetylation, CA dissolved in aqueous solution.	The original study modelled both the forward and backward reactions, for the primary and secondary acetyls (63). A subsequent analysis calculated the activation energies of the reactions listed (100).
67.4	Acid-catalysed C6 deacetylation, CA dissolved in aqueous solution with sulphuric acid.	
86.2	Uncatalysed C2/C3 deacetylation, CA dissolved in aqueous solution.	
35.6	Acid-catalysed C2/C3 deacetylation, CA dissolved in aqueous solution with sulphuric acid.	

While it is not possible to directly compare the fitted activation energy with other published values due to differences in the experimental conditions and the models, the values in Table 4.5 suggest that the fitted parameter is within the range reasonably expected for the reaction.

4.3.2 Testing

Model performance was evaluated by comparing the model predictions to experimental data from Bigourdan and Reilly (31) for the free acidity change in 35 mm CTA film incubated using the can method, under different conditions of temperature and RH. The conditions describing each experiment are summarised in Table 4.6.

Table 4.6 Experimental conditions for each test case (31).

Case	Temperature (°C)	RH (%)	Initial free acidity (mL 0.1 M NaOH /g CTA film base)
A	35	50	0.4
B	35	35	0.46
C	35	20	0.4
D	21	50	0.4
E	21	35	0.4
F	21	20	0.4
G	21	50	0.58

The model was used to predict free acidity (acetic acid concentration) as a function of time for each case. The rate constant k was calculated from the temperature using Equation 4.5 and the estimated parameters A and E_a. The initial conditions $[ROAc]_0$, $[H_2O]_0$, and $[HOAc]_0$ were required to integrate Equation 4.10.

According to Bigourdan and Reilly (31), the samples were prepared by moisture-conditioning fresh CTA film at 21 °C and 50% RH. They were then incubated using the bag method at 90 °C until the samples reached a free acidity of approximately 0.4 (the precise value is indicated as the initial free acidity in Table 4.6). In cases A-F, the samples were then moisture-conditioned again at 21 °C and their respective RH, before being incubated using the can method at either 21 °C or 35 °C. In case G, the sample was not re-conditioned before the second incubation as it was found that the difference in moisture content before and after the first incubation was insignificant compared with the total water content inside the roll.

The initial acetic acid concentration was determined from the measured free acidity at $t = 0$. The initial water concentration was based on the moisture isotherm for fresh CTA film at 20 °C, as this was the nearest temperature to 21 °C for which the data were available (121). The reported moisture content at 21% RH was used for the moisture content at 20% RH as this was the lowest value reported. The initial acetyl concentration was calculated from the following mass balance, where 13403.6 mol m^{-3} is the concentration of acetyl in fresh CTA, and 5.2 mol m^{-3} is the concentration of acetic acid in fresh CTA film (8):

$$[ROAc]_0 = 13403.6 - ([HOAc]_0 - 5.2) \qquad (4.17)$$

The model inputs for each case are summarised in Table 4.7.

Table 4.7 Model inputs used to simulate each test case.

Case	Temperature (°C)	$[HOAc]_0$ (mol m^{-3})	$[H_2O]_0$ (mol m^{-3})	$[ROAc]_0$ (mol m^{-3})
A	35	52	2137.2	13356.8
B	35	59.8	1605.2	13349.0
C	35	52	1010.0	13356.8
D	21	52	2137.2	13356.8
E	21	52	1605.2	13356.8
F	21	52	1010.0	13356.8
G	21	75	2137.2	13333.8

Using these inputs for each case, numerical integration of Equation 4.10 was carried out in MATLAB® R2018a using the solver ode15s. The predicted free acidity values are shown with the experimental measurements of free acidity in Figures 4.3 and 4.4. For cases D-G, the reported experimental values are the mean of three measurements taken at three different locations in the film roll, with the error bars indicating the minimum and maximum values. In cases A-C, only the mean values were reported in the original report (31). In case G, the authors reported a sharp reduction in the free acidity after 15 months, but they did not

explain the reason for this. This surprising behaviour cannot be predicted with the model but as a decrease in free acidity after exposure to high humidity is unlikely and may be due to experimental error, these data points were excluded from the analysis.
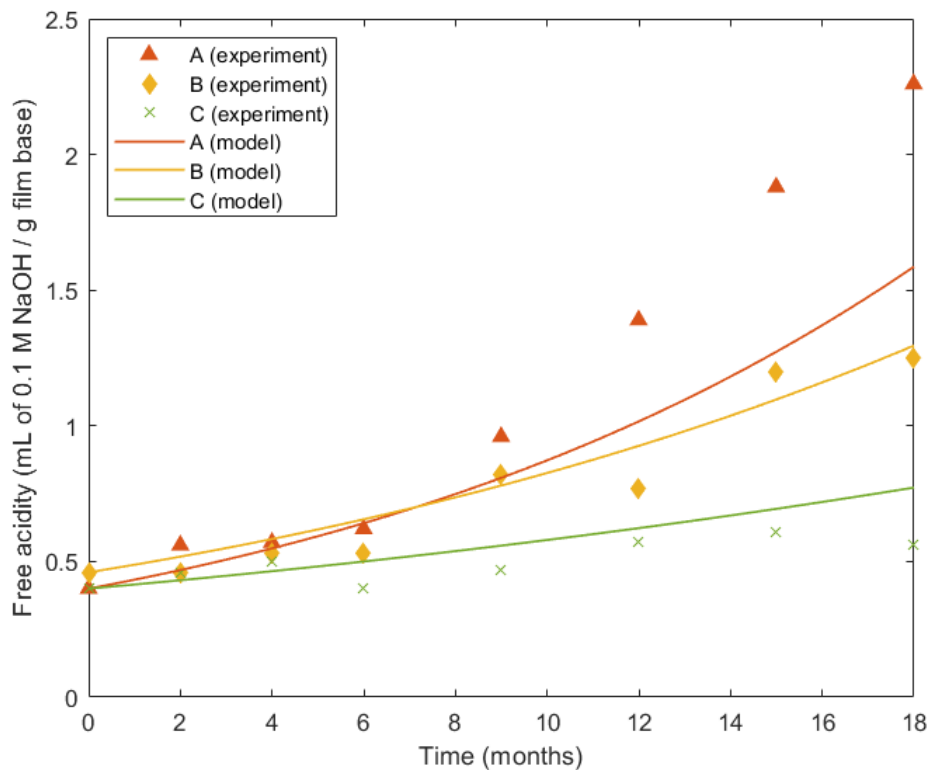
Figure 4.3   Model and experimental free acidity for cases A-C (T = 35 °C).
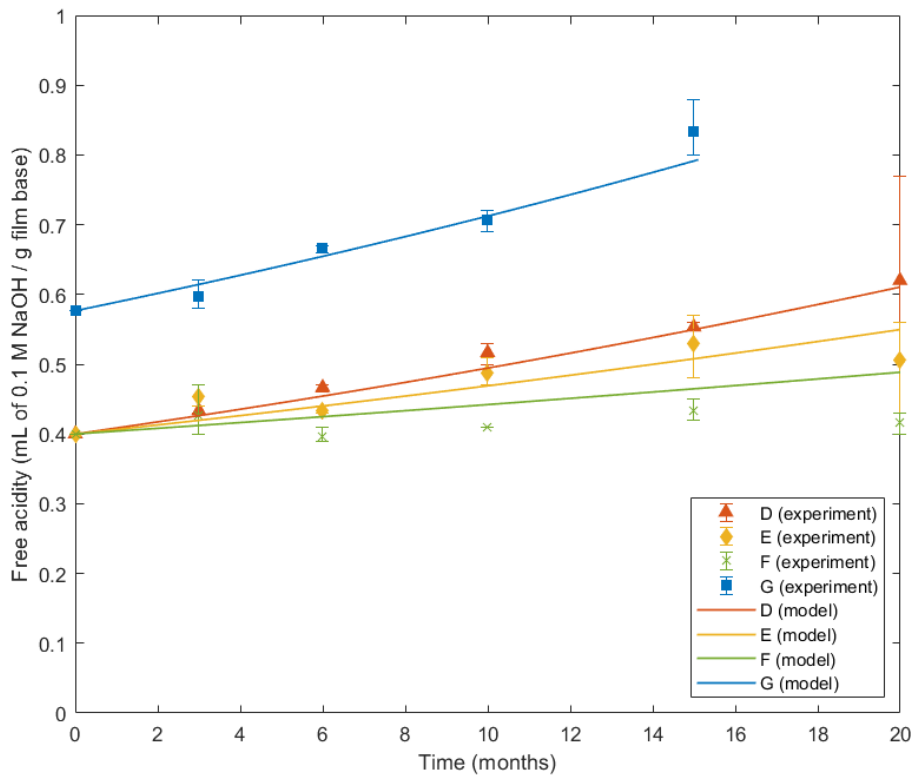
Figure 4.4 Model and experimental free acidity for cases D-G (T = 21 °C).

The accuracy of the model predictions was evaluated using the normalised-root-mean-square-error (NRMSE). The function $(1 - \text{NRMSE})$ represents the accuracy score of the model. Using this statistic, the worst score is -∞, a perfect score is 1, and a score of 0 indicates the model is no better than a horizontal straight line (through the mean value) at fitting the data (216). The results are reported in Table 4.8.

Table 4.8 Model performance on test dataset.

Case	Accuracy
A	0.4551
B	0.7105
C	-0.3202
D	0.8450
E	0.4278
F	-1.7857
G	0.7684

The model performed best at RH of 50 and 35% (cases A, B, D, E and G), and poorly at 20% RH (cases C and F). The best fit was found with 21 °C and 50% RH (case D).

To investigate whether an error in $[H_2O]_0$ could explain the poor accuracy of the model at 20% RH, for cases C and F, the model was run with varying $[H_2O]_0$ to obtain the value that maximised the accuracy ($= 1 - \text{NRMSE}$). For case C, the optimal fit was obtained using $[H_2O]_0 = 636$ mol m^{-3} (accuracy $= 0.4042$). For case G, the optimal fit was obtained using $[H_2O]_0 = 317$ mol m^{-3} (accuracy $= 0.0591$). Note that the accuracy scores obtained this way are biased and do not reflect test performance, which measures how well the model performs on data not used for fitting parameters (in this case, $[H_2O]_0$). A high accuracy score obtained this way would not indicate whether the model would generalise well on an unseen dataset, but a low accuracy, as for case G, indicates that the model does not fit well even on the data it was trained on. Given that neither of the fitted values for $[H_2O]_0$ are particularly close to the reference used originally (1010 mol m^{-3}), that the values are not close to each other, and the low accuracy score for G, it seems unlikely that an error in $[H_2O]_0$ could account for the poor performance of the model at 20% RH.

One possible explanation is that different mechanisms are responsible for the observed behaviour at high (50 and 35%) RH and low (20%) RH. In the model (Equation 4.4), the first-order dependence of the reaction rate on $[HOAc]$ is based on empirical observation, where the experimental conditions consisted of solid CTA films prepared by equilibrating with a gas (50% RH) before being placed in a vacuum-sealed bag (10). In a mechanistic model of acid-catalysed hydrolysis in aqueous solution, the rate dependence on $[HOAc]$ is expected to be of order ½, since the acid-catalysed mechanism depends on $[H^+]$:

$$[H^+] = \sqrt{K_a[HOAc]} \tag{4.18}$$

where K_a is the acid dissociation constant (mol m^{-3}) of acetic acid. While Equation 4.4 is not based on a mechanistic model for acid-catalysed hydrolysis of solid films, the difference in the dependence on $[HOAc]$ between this model and the mechanistic model of acid-catalysed hydrolysis in solution acknowledges that the rate-determining mechanisms in the two conditions differ as well. Hence, it is

not an unlikely possibility that yet another set of mechanisms determines the rate of generation of acetic acid at low RH conditions, compared to high RH conditions.

For example, in solution, $[H_2O]$ is essentially constant, therefore it does not feature as a variable in the rate expression for the aqueous system. In the solid CTA model system, $[H_2O]$ is rate-limiting. By analogy, it is possible that some unknown variable which is rate-limiting at low RH is not rate-limiting at high RH, therefore exclusion of the unknown variable(s) from the model only has a noticeable effect on the accuracy of the model at low RH (217).

4.4 CONCLUSIONS

A mathematical model was proposed which accounts for the autocatalytic effect of acetic acid on the vinegar syndrome. This model is based on an understanding of the reaction chemistry which has been established by other researchers in the field. The good agreement between the predictions and previously published experimental data attest to the validity of the model. Later chapters in this thesis, particularly Chapter 6, build upon the autocatalytic model of deacetylation. In Chapter 7, the implications of the model for film conservation are investigated.

5 DEACETYLATION AND AGU COMPOSITION

This chapter presents a mathematical model of deacetylation that distinguishes acetyl groups by their position in the cellulose acetate anhydroglucose unit (CA AGU) and the substitutions on the two remaining positions on the AGU:

- *premises, justification, and motivations for the model*
- *chemical species, reaction pathways, and mass balances*
- *simulations and discussion of cases when some parameters are assumed to be equal*
- *estimation of kinetic parameters for deacetylation of CA in aqueous solution, using published data*
- *how these results compare with qualitative explanations of CA deacetylation*
- *implications for the chain scission model.*

5.1 INTRODUCTION

In the previous chapter, a model was developed under the assumption that, in the time frame investigated, acetyl groups react uniformly and may be treated as a single chemical species. This chapter presents a mathematical model that distinguishes acetyl groups by the position of the carbon to which they are bonded and the substitutions on the two remaining positions on the monomer. The reader is reminded that cellulose acetate (CA) may be acetylated at carbon positions C2, C3 or C6 (see Figure 5.1). The degree of substitution (DS) is the average number of acetyls per CA anhydroglucose unit (AGU).
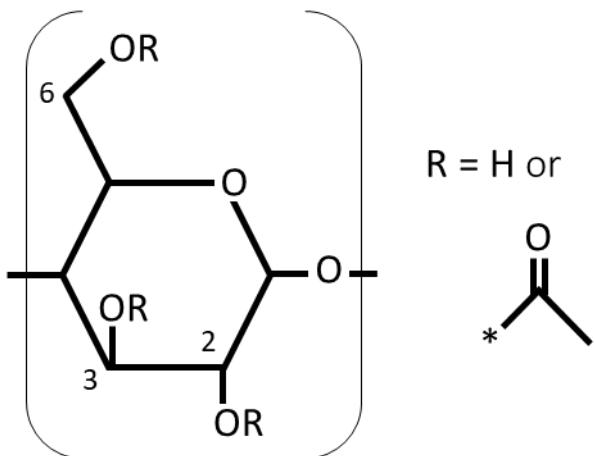
Figure 5.1 Cellulose acetate anhydroglucose unit.

Several reasons motivate the development of this model. Studies (63–69) have found evidence of variation in substitution rates of acetyl groups. A model that accounts for this could fit experimental data better than a model that assumes the acetyl groups react identically and independently of other substitutions on the AGU. This idea is tested by fitting the model to experimental data obtained from the literature in Section 5.4.

The additional parameters (rate constants) have physical significance. The values or ratios of the rate constants can be easily interpreted by other scientists and could be used to corroborate or support explanations regarding chemical mechanisms, enhancing our understanding of carbohydrate chemistry.

The model could help predict variations in monomer composition over time, thereby determining the physicochemical properties of cellulose acetate, such as miscibility with solvents. Compatibility (or incompatibility) with plasticisers and hydrophilicity affect the susceptibility of cellulose acetate to degradation, and the dynamic evolution of these properties may depend on how monomer composition varies under particular conditions or from particular initial compositions.

The model can be applied to modelling of other substituted celluloses such as cellulose nitrate, ethyl cellulose or methyl cellulose.

Finally, the outputs of this model (monomer composition vs. time) provide the inputs for the chain scission model presented in Chapter 6. The chain scission

model assumes that the substitutions on adjacent AGUs affect the reactivity of the glycoside bond between them. Specifically, it assumes that only the bonds between two cellulose AGUs are susceptible to hydrolysis leading to chain cleavage.

5.2 MATHEMATICAL MODEL

The model considers eight types of AGUs. Each of the three carbon positions has two possible substituents (acetyl or hydroxyl), so there are $2^3 = 8$ substitution states: cellulose (no acetyl substituents); 2,3,6-tri; 2,3-di; 3,6-di; 2,6-di; 2-mono; 3-mono; and 6-monoacetate. The numbers denote which carbon positions are acetylated, while "tri", "di", or "mono" indicates the degree of substitution (DS) of the AGU in question. Figure 5.2 illustrates the 12 types of deacetylation reactions that connect the 8 substitution states.
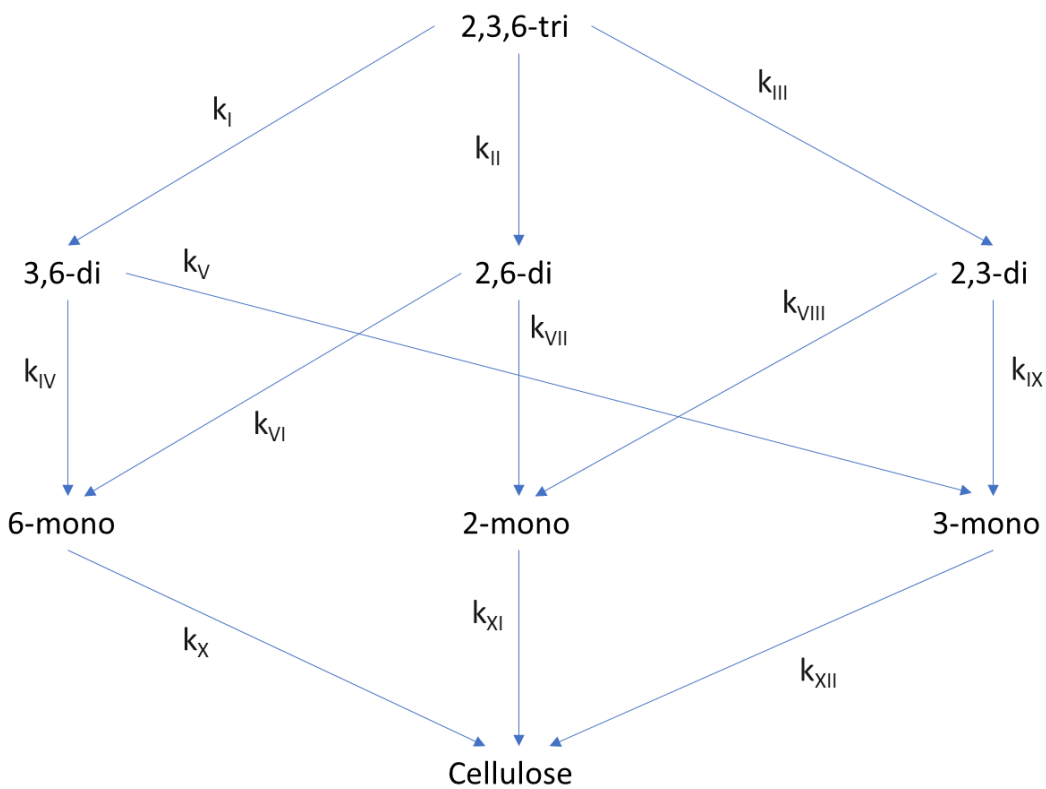
Figure 5.2 Pathways for deacetylation of cellulose acetate. Each arrow represents the conversion of one acetyl to hydroxyl.

93

As in Chapter 4, deacetylation is assumed to depend in the first order on acetyl concentration, where acetyl is one of the reactants. In the model presented in Figure 5.2, there are 12 different types of deacetylation reactions, depending on the acetyl position and AGU substitution state of the reactant. Although the reactant is the acetyl at a particular carbon position on the particular AGU, the concentration of the particular acetyl on the particular AGU is the same as the concentration of the particular AGU. Therefore, rate of reaction depends in the first order on the concentration of the reactant AGU from which the acetyl is lost.

To focus on the effects of AGU composition on deacetylation, in the following equations, it is assumed that the concentrations of other reactants (water) and catalysts (acetic acid) are constant and therefore included in the first-order rate constant k. Later, in Section 5.4, it is verified that the experimental system to which the model is fitted adheres reasonably to these conditions. There is no reason why it should not be possible to replace k with variable terms representing concentrations of water and acid, as in the model in Chapter 4, but there is also no reason to do this if these terms are constant in the system under study.

$$\frac{d[2,3,6 \text{ tri}]}{dt} = -r_I - r_{II} - r_{III} = -(k_I + k_{II} + k_{III})[2,3,6 \text{ tri}] \tag{5.1}$$

$$\frac{d[3,6 \text{ di}]}{dt} = r_I - r_{IV} - r_V = k_I[2,3,6 \text{ tri}] - (k_{IV} + k_V)[3,6 \text{ di}] \tag{5.2}$$

$$\frac{d[2,6 \text{ di}]}{dt} = r_{II} - r_{VI} - r_{VII} = k_{II}[2,3,6 \text{ tri}] - (k_{VI} + k_{VII})[2,6 \text{ di}] \tag{5.3}$$

$$\frac{d[2,3 \text{ di}]}{dt} = r_{III} - r_{VIII} - r_{IX} = k_{III}[2,3,6 \text{ tri}] - (k_{VIII} + k_{IX})[2,3 \text{ di}] \tag{5.4}$$

$$\frac{d[6 \text{ mono}]}{dt} = r_{IV} + r_{VI} - r_X = k_{IV}[3,6 \text{ di}] + k_{VI}[2,6 \text{ di}] - k_X[6 \text{ mono}] \tag{5.5}$$

$$\frac{d[2 \text{ mono}]}{dt} = r_{VII} + r_{VIII} - r_{XI} \tag{5.6}$$

$$= k_{VII}[2,6 \text{ di}] + k_{VIII}[2,3 \text{ di}] - k_{XI}[2 \text{ mono}]$$

$$\frac{d[3 \text{ mono}]}{dt} = r_V + r_{IX} - r_{XII} = k_V[3,6 \text{ di}] + k_{IX}[2,3 \text{ di}] - k_{XII}[3 \text{ mono}] \qquad (5.7)$$

$$\frac{d[\text{Cellulose}]}{dt} = r_X + r_{XI} + r_{XII} \qquad (5.8)$$

$$= k_X[6 \text{ mono}] + k_{XI}[2 \text{ mono}] + k_{XII}[3 \text{ mono}]$$

5.3 DEGENERATE CASES OF INTEREST

The model has 12 parameters, the rate constants k_I - k_{XII}. Degenerate cases are scenarios where the rate constants depend on each other in a way that reduces the effective number of parameters required to specify the model. This results in a simpler model.

From a mathematical perspective, there is no difference between the substitutions at C2, C3, and C6. For example, consider a situation (1) in which k_I is 100 times greater than all the other rate constants, which are all the same. This is not meaningfully different than if (2) it was k_{II} that was the outlier, or (3) k_{III}. The simulation output for (2) would be the same as for (1), only the labels on the variables change. Within the context of the model, the only qualities that distinguish the positions are the magnitudes of the rate constants associated with the reactions involving substituents at those positions. Therefore, for the purpose of investigating theoretical scenarios, it is convenient to redefine the variables in terms which reflect this.

A tri-substitution system was conceptualised based on an AGU substituted at positions A, B, or C. Taking the triacetate species "ABC" as the starting point, the letter O was used in place of the letter A, B or C to indicate a hydroxyl substitution in that position of the named AGU. In this schema, the acetyl at position A is lost via r_I, position B via r_{II} and position C via r_{III} (see Figure 5.3). A, B, and C were defined such that $k_I \geq k_{II} \geq k_{III}$.

ABC

k_I k_{II} k_{III}

OBC k_V AOC   ABO

k_{VIII}

k_{IV} k_{VI} k_{VII} k_{IX}

OOC   AOO   OBO

k_X k_{XI} k_{XII}

OOO
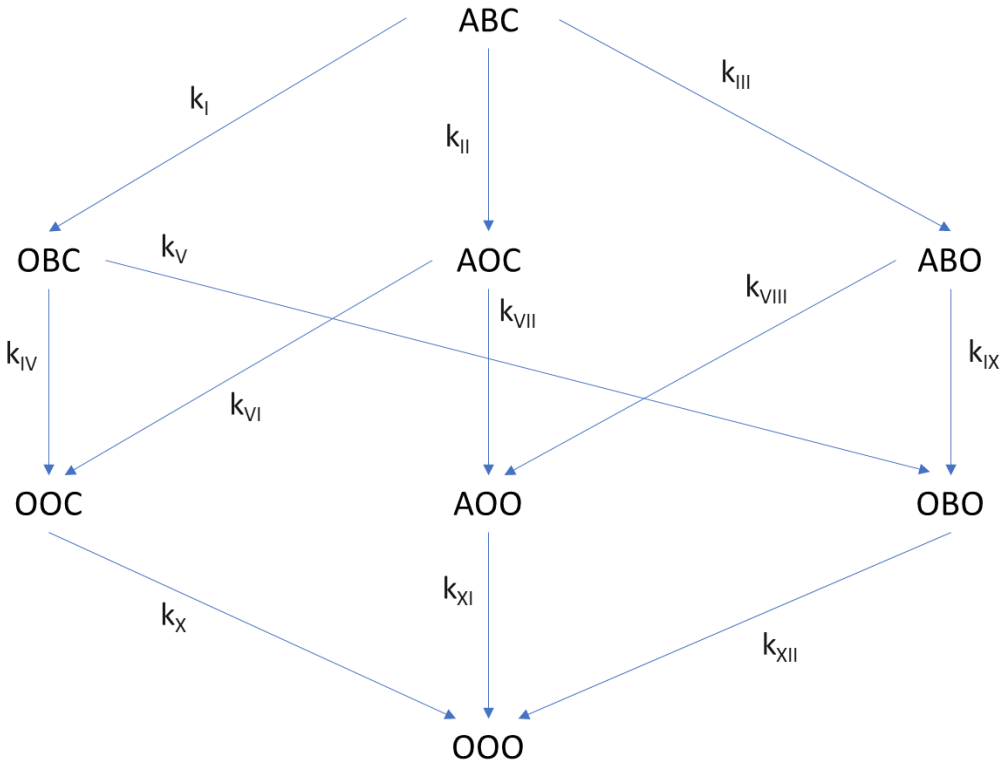
Figure 5.3 As in Figure 5.2, but with A, B, C defined such that $k_I \geq k_{II} \geq k_{III}$.

The rate constants were combined into a 4×3 matrix, $\mathbf{k}$:

$$\mathbf{k} = \begin{bmatrix} k_I & k_{II} & k_{III} \\ k_{VI} & k_{IV} & k_V \\ k_{IX} & k_{VIII} & k_{VII} \\ k_{XI} & k_{XII} & k_X \end{bmatrix} \tag{5.9}$$

In this notation, the columns correspond to which of the positions A, B, or C the acetyl is lost from (in that order, left to right). The first row corresponds to reactions on tri-substituted AGUs, the middle two rows on di-substituted AGUs and the fourth row on mono-substituted AGUs. Note that the row number of the rate constants in the middle two rows is interchangeable but for clarity the definition in Equation 5.9 will be used.

Equations 5.1-8 (in terms of the notation in Figure 5.3) were solved in MATLAB R2021a using the ordinary differential equation solver ode15s. The system was modelled as having a constant volume, so the concentrations in Equations 5.1-8 were replaced with the number of moles. As deacetylation does not change the

total number of moles, the mole fractions were used in place of the number of moles. The mole fraction of an AGU is the proportion (by number, or moles) of the AGU out of all the AGUs and varies between 0 and 1. All the concentrations are normalised as mole fractions, denoted using angle brackets, e.g., the mole fraction of ABC is $\langle ABC \rangle$. The simulations used an initial degree of substitution (DS) of 3, so at $t = 0$, $\langle ABC \rangle = 1$, and for the remaining AGUs is 0. The time scale is normalised so that normalised time $t = 1$ corresponds to when $\langle OOO \rangle = 0.1$.

The formula to calculate DS from the mole fractions is:

$$DS = 3\langle ABC \rangle + 2(\langle OBC \rangle + \langle AOC \rangle + \langle ABO \rangle) + \langle OOC \rangle + \langle AOO \rangle + \langle OBO \rangle \quad (5.10)$$

Using the methods described above, the degenerate cases were simulated by specifying the rate constants in $\boldsymbol{k}$ (Equation 5.9) as the inputs for each case. The results of the simulations are presented in the following sections.

5.3.1   Identical rate constants

In Chapter 4 it was assumed that all deacetylation rate constants are the same. This is the same as assuming identical rate constants, i.e., $\boldsymbol{k} = p\boldsymbol{J}$, where $\boldsymbol{J}$ is a matrix of ones. However, the model in this chapter can predict how AGU composition varies with time under this assumption (see Figure 5.4). After time normalisation, solutions for all (positive) values of p correspond to a single solution. The curves in Figures 5.5 and 5.6 form the benchmark case for comparison in the discussions of the following cases in which the rate constants are not identical.
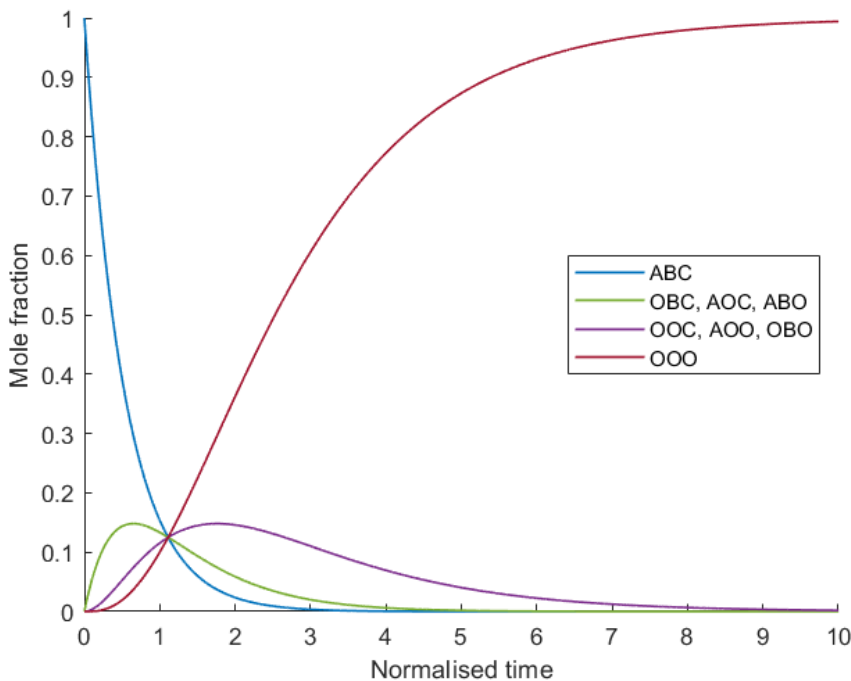
Figure 5.4 Simulated results from the model, predicting mole fraction of each AGU against normalised time. Time is normalised so that $t = 1$ when $\langle OOO \rangle = 0.1$.

In Figure 5.4, the results for the di-substituted AGUs ($\langle OBC \rangle$, $\langle AOC \rangle$, $\langle ABO \rangle$) are identical, so they are indicated by a single-colour trendline. Similarly, mono-substituted AGUs ($\langle OOC \rangle$, $\langle AOO \rangle$, $\langle OBO \rangle$) follow identical paths. $\langle ABC \rangle$ decreases monotonically, while $\langle OOO \rangle$ increases monotonically. Mole fractions of di-substituted AGUs and mono-substituted AGUs each feature a maximum, with the maximum of the di-substituted AGUs occurring earlier than the maximum of the mono-substituted AGUs.

Figure 5.5 shows the simulation results for DS (left axis) and cellulose mole fraction $\langle OOO \rangle$ (right axis) against normalised time. DS is of interest in a museums context as it may be easier to track as an indicator of "degradation elapsed" than time using, for example, proton nuclear magnetic resonance spectroscopy (^{1}H NMR) (218). According to the hypothesis that glycosidic bond cleavage occurs between adjacent cellulose AGUs (see Chapter 6), the mole fraction of cellulose is relevant because it tracks susceptibility to degradation via chain scission. As discussed in Chapter 2, chain scission is linked to brittleness, cracking, and loss of mechanical strength. Figure 5.6 shows how simulated cellulose mole fraction varies with DS.
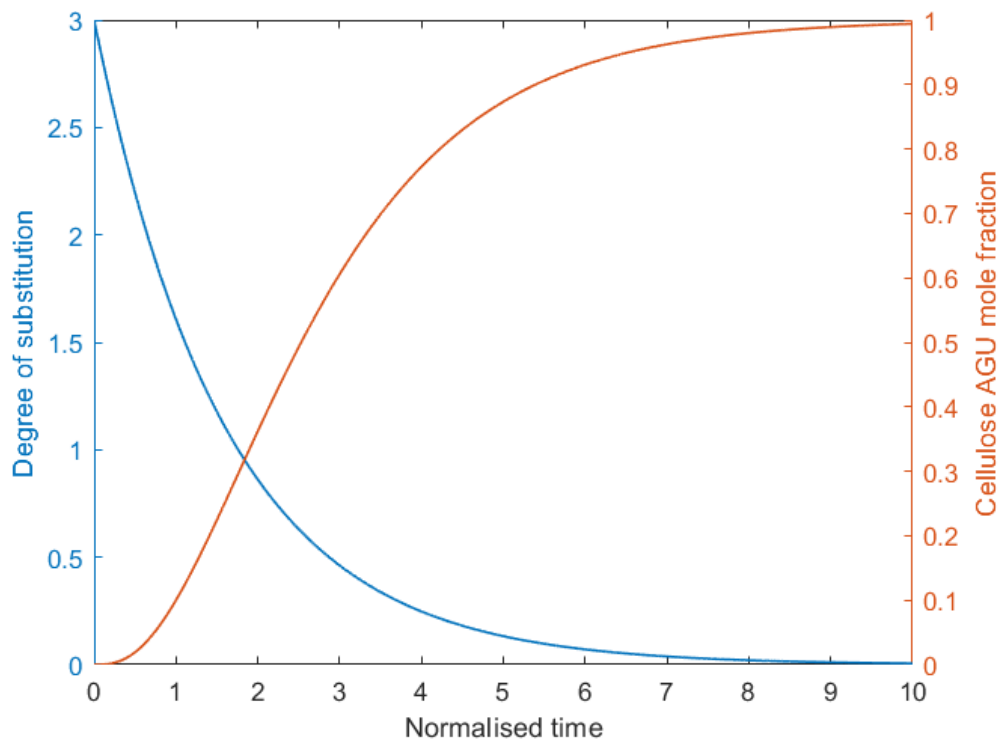
Figure 5.5 Simulated DS, $\langle OOO \rangle$ vs. normalised time, identical deacetylation rate constants.
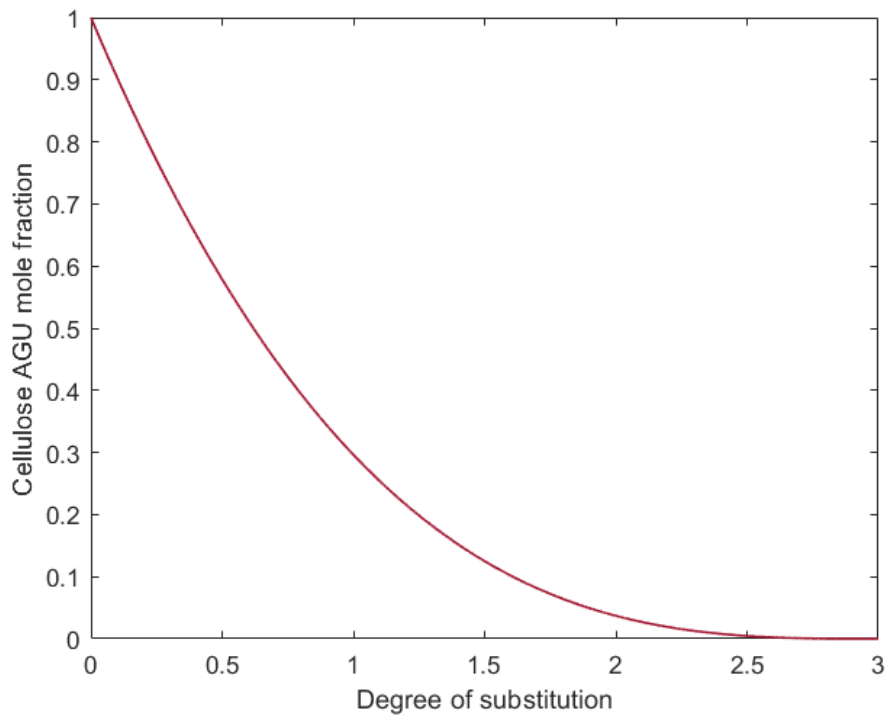
Figure 5.6 Simulated $\langle OOO \rangle$ vs. DS, identical deacetylation rate constants.

5.3.2   Substituent-dependent rate constants

This case corresponds to assuming identical rate constants in each column of the matrix $\boldsymbol{k}$ (Equation 5.9). Physically, this means that deacetylation at a given position on the AGU i.e., whether it occurs at C2, C3 or C6, has the same rate constant, regardless of the other substitutions on the AGU, but that deacetylation rate constants may vary between the positions. As noted previously, the reactivity of acetyl groups varies with the carbon position, and this appears to affect the order in which they react, although this may depend on the reaction conditions (63–69).

This case can be viewed as modelling deacetylation as three *parallel* reactions:

1. Acetyl → hydroxyl at position A
2. Acetyl → hydroxyl at position B
3. Acetyl → hydroxyl at position C

To model three parallel reactions, three rate constants, k_A, k_B, and k_C, were defined:

$$k_A = k_I = k_{VI} = k_{IX} = k_{XI} \tag{5.11}$$

$$k_B = k_{II} = k_{IV} = k_{VIII} = k_{XII} \tag{5.12}$$

$$k_C = k_{III} = k_V = k_{VII} = k_X \tag{5.13}$$

According to the definitions of A, B, and C, $k_A \geq k_B \geq k_C$.

Under time normalisation, only the ratios of the rate constants to each other are relevant. Various scenarios were simulated, varying the ratios of the rate constants, $k_A : k_B : k_C$. The benchmark case corresponds to $k_A : k_B : k_C = 1 : 1 : 1$. This is the case discussed above in Section 5.3.1. Figure 5.7 shows the simulation results for DS (left axis) and cellulose mole fraction $\langle OOO \rangle$ (right axis) over normalised time. Figure 5.8 shows how $\langle OOO \rangle$ varies with DS. The rate constant ratios for each scenario are indicated in the legends of Figures 5.7 and 5.8.
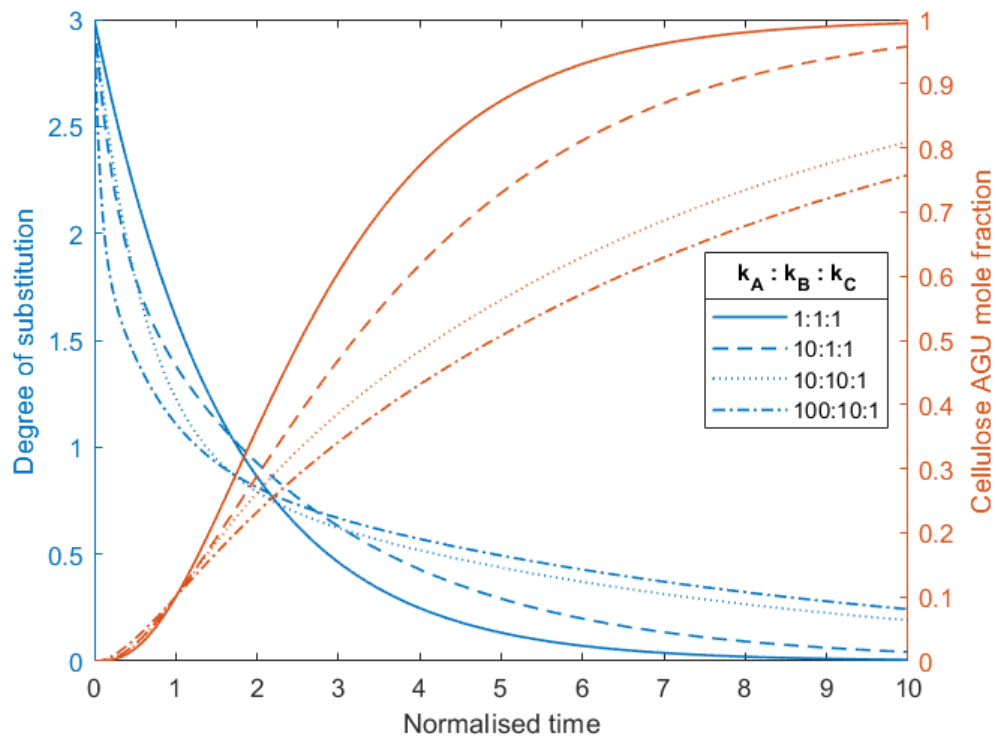
Figure 5.7 Simulated DS, $\langle OOO \rangle$ vs. normalised time. Model assumes that the deacetylation rate constant depends on the position of the substituent on the AGU.
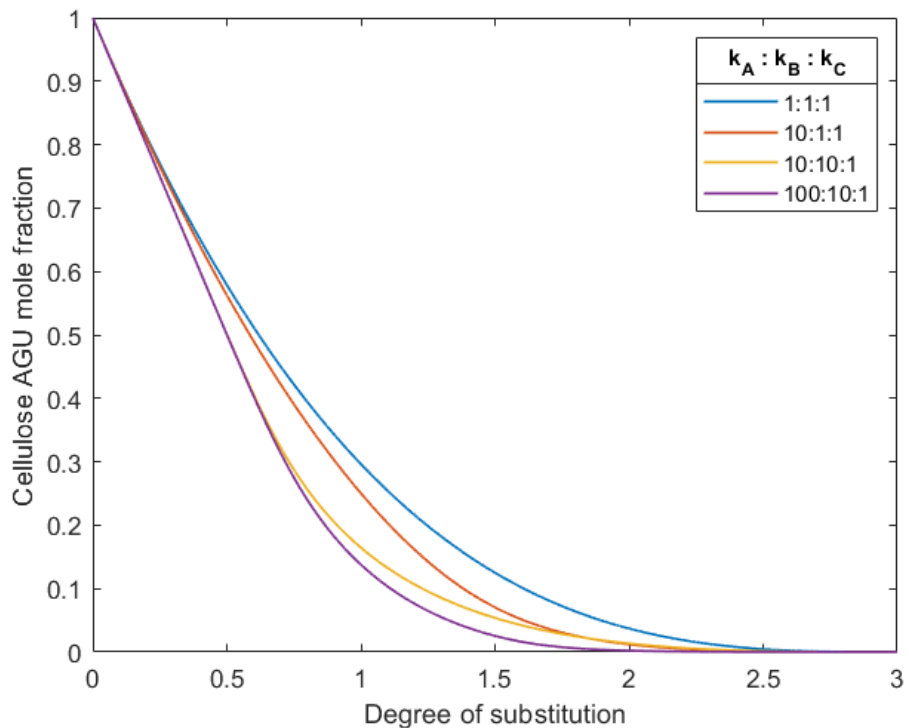
Figure 5.8 Simulated $\langle OOO \rangle$ vs. DS. Model assumes that deacetylation rate constants depend on the position of the substituent on the AGU.

In Figure 5.7, comparing to the benchmark DS-time curve, as k_A and k_B deviate from k_C, DS decreases more rapidly initially, followed by a more gradual decline. The curves develop a sharper inflection around normalised time $t = $ 1-3. The trend in $\langle OOO \rangle$ compared with the benchmark $\langle OOO \rangle$-time curve is an initially faster increase, followed by a slower ascent. The curves have a less sharp inflection compared with the curve when $k_A: k_B: k_C = 1:1:1$. The most likely explanation is that when the substituent rate constants are dissimilar, and independent of the other substitutions on the AGU, the fastest-reacting substituent (largest rate constant) is consumed rapidly initially, causing the initial sharp decline in DS. The remaining substituents react more slowly (due to having smaller rate constants), leading to slower decrease in DS and slower increase in $\langle OOO \rangle$. For example, the convergence of the DS-time curves for $k_A: k_B: k_C = 100:10:1$ and $k_A: k_B: k_C = 10:10:1$ below DS $= 0.7$ (approximately) may be attributed to the faster-reacting A and B acetyls having been consumed, with the slow-reacting C acetyl comprising the majority of the remaining substitutions.

In Figure 5.8, at a given DS, $\langle OOO \rangle$ tends to be lower as k_A and k_B deviate from k_C. Assuming unsubstituted cellulose monomers increase susceptibility to chain scission, setting k_A and k_B closer to k_C confers increased susceptibility to chain degradation at the same DS (all other factors being equal). Conversely, high variation in substituent rate constants confers protection against chain scission. In practice, it would not be feasible to vary the rate constants of cellulose acetate in this way, and certainly not to do so in a museum artefact. However, what may be deduced from the model is that if (1) substituents react at very different rates, and (2) chain scission is attributed to cleavage of cellulose-cellulose bonds, then chain scission will only begin after substantial deacetylation. Chemically, this would result in a large reduction in DS before any decrease in DP begins. Physically, it might manifest as a long period of vinegar odour, increased moisture absorption, loss of plasticiser (due to decreased miscibility with the lower-DS polymer)—all associated with deacetylation—followed by signs of chain scission such as brittleness and cracking. This is generally consistent with the observed progression of deterioration in CA artefacts.

Aside from speculation on chain scission (which depends additionally on the validity of the second condition above), the ratios of the substituent rate constants also impact the DS dynamics, AGU composition dynamics, and the ways these result in changes in material properties. For example, if two substituent rate constants are bigger than the third one (for instance, $k_A: k_B: k_C = 10: 10: 1$), then this predicts a more rapid descent in DS from 3 to 1 followed by a slower decline. If two substituent rate constants are smaller than the third one (for instance, $k_A: k_B: k_C = 10: 1: 1$) then the more rapid descent period is from DS = 3 to 2, with a slower rate of decline thereafter. This should also be considered in the context of the range of starting DS of artefacts, for example, there are cellulose triacetate (CTA) and cellulose diacetate (CDA) photographic films. If the first substituent lost from hydrolysis of CTA is much more reactive than the other two (for example, $k_A: k_B: k_C = 10: 1: 1$) this could imply that CDA is comparatively more stable than CTA.

5.3.3   DS-dependent rate constants

This case corresponds to assuming identical rate constants in each row of the matrix $\boldsymbol{k}$ (Equation 5.9). The two middle rows (corresponding to DS = 2) are also the same. Physically, this means that the deacetylation rate is independent of substituent position (it has the same rate constant whether it is position A, B, or C), but dependent on the number of substitutions on the AGU i.e., the rate varies depending on whether the AGU is tri-, di- or mono-substituted. A possible reason this might be the case is that having fewer acetyls and more hydroxyls could reduce steric hindrance. Another reason could be if changes in DS alter solvent or sorbent interactions (e.g., reduction in DS increases hydrophilicity). These factors, as well as the apparently accelerating degradation of CA experienced in museums, would lead me to expect that lower DS would be associated with larger deacetylation rate constants.

The DS-dependent case can be viewed as modelling deacetylation as three *sequential* reactions:

1. Cellulose triacetate AGU → cellulose diacetate AGU
2. Cellulose diacetate AGU → cellulose monoacetate AGU
3. Cellulose monoacetate AGU → cellulose AGU

To model three sequential reactions, three rate constants, k_3, k_2 and k_1, were defined:

$$k_3 = k_I = k_{II} = k_{III} \tag{5.14}$$

$$k_2 = k_{IV} = k_V = k_{VI} = k_{VII} = k_{VIII} = k_{IX} \tag{5.15}$$

$$k_1 = k_X = k_{XI} = k_{XII} \tag{5.16}$$

There are six possible inequalities expressing the relationship between DS and rate constants:

a. $k_1 \leq k_2 \leq k_3$
b. $k_2 \leq k_1 \leq k_3$
c. $k_1 \leq k_3 \leq k_2$
d. $k_2 \leq k_3 \leq k_1$
e. $k_3 \leq k_1 \leq k_2$
f. $k_3 \leq k_2 \leq k_1$

The physical reasons suggested above for why deacetylation rate constants could be DS-dependent both imply $k_3 \leq k_2 \leq k_1$, corresponding to sub-case (f). All six cases were simulated to compare the effects of assuming different relationship between DS and rate constants, and to understand whether the predicted effects were consistent with the observed progression of deterioration in CA artefacts.

Under time normalisation, only the ratios of the rate constants to each other are relevant. Various scenarios were simulated, varying the ratios of the rate constants, $k_3 : k_2 : k_1$. The benchmark case again corresponds to $k_3 : k_2 : k_1 = 1 : 1 : 1$. Figures 5.9-10 show the results of the simulations. The rate constant ratios for each scenario are indicated in the legends of Figures 5.9-10.
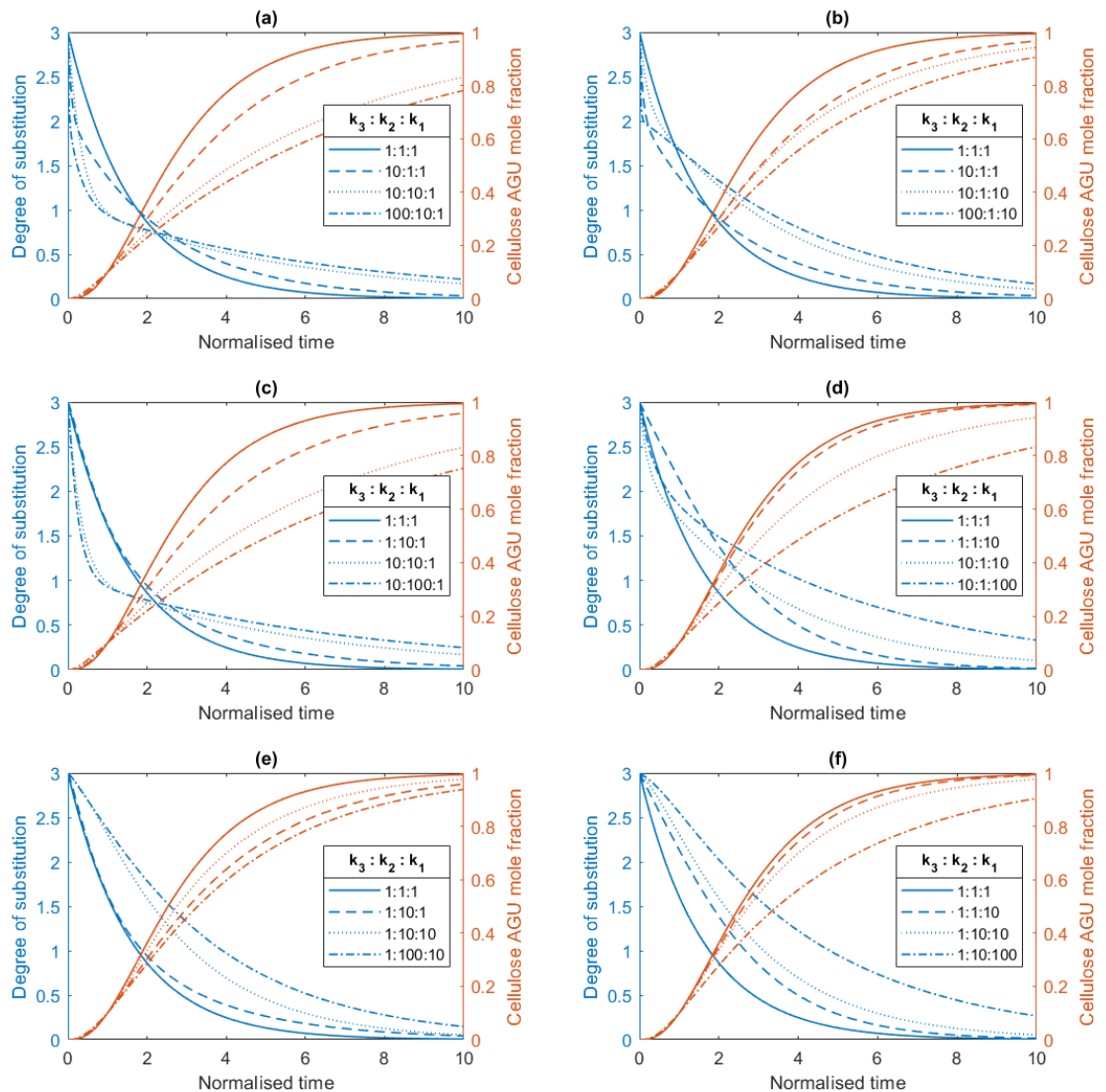
Figure 5.9 Simulated DS, $\langle OOO \rangle$ vs. normalised time. Sub-cases: (a) $k_1 \leq k_2 \leq k_3$; (b) $k_2 \leq k_1 \leq k_3$; (c) $k_1 \leq k_3 \leq k_2$; (d) $k_2 \leq k_3 \leq k_1$; (e) $k_3 \leq k_1 \leq k_2$; (f) $k_3 \leq k_2 \leq k_1$.
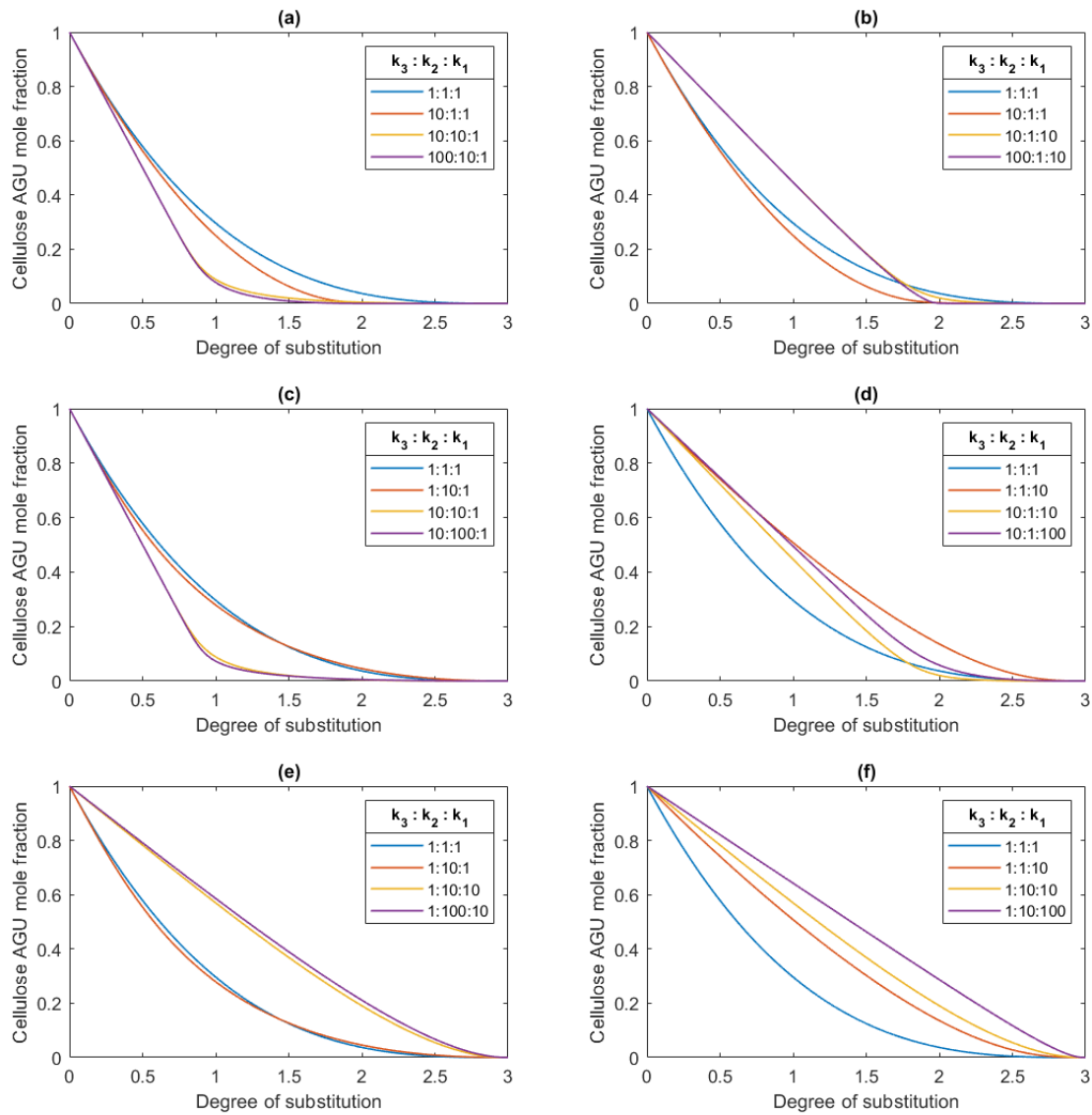
Figure 5.10 Simulated $\langle OOO \rangle$ vs. DS. Sub-cases: (a) $k_1 \leq k_2 \leq k_3$; (b) $k_2 \leq k_1 \leq k_3$; (c) $k_1 \leq k_3 \leq k_2$; (d) $k_2 \leq k_3 \leq k_1$; (e) $k_3 \leq k_1 \leq k_2$; (f) $k_3 \leq k_2 \leq k_1$.

Sub-case (a) ($k_1 \leq k_2 \leq k_3$) simulates the effect of k *increasing with DS*. In Figure 5.10(a), increasing variation in k in this order lowers $\langle OOO \rangle$ at the same DS, thereby *decreasing susceptibility to chain scission*. Sub-case (f) ($k_3 \leq k_2 \leq k_1$) illustrates the opposite effect, with k *decreasing with DS*. In Figure 5.10(f), increasing variation in k increases $\langle OOO \rangle$ at the same DS, thereby *increasing susceptibility to chain scission*.

As might be expected, sub-cases (b)-(e) indicate trends somewhere between these two extremes, or perhaps combining elements of both.

Sub-cases (b) ($k_2 \leq k_1 \leq k_3$) and (d) ($k_2 \leq k_3 \leq k_1$) both characterise "bottleneck" cases in which k_2 limits the rate of deacetylation. In sub-case (b), $k_1 \leq k_3$, whereas in sub-case (d), $k_3 \leq k_1$. The effect of $k_1 \leq k_3$ is rapid initial decline in DS, illustrated in Figure 5.9(b), with little associated change in $\langle OOO \rangle$, illustrated in Figure 5.10(b). There are visible inflections in the DS-time and $\langle OOO \rangle$-DS curves around DS $= 2$ in both Figures 5.9(b) and 5.10(b), where the bottleneck occurs. In comparison, when $k_3 \leq k_1$, the above effects of the bottleneck are diminished, most likely because k3 and k2 are more similar. There are still inflections in the DS-time and $\langle OOO \rangle$-DS curves around DS $= 2$ in Figures 5.9(d) and 5.10(d), but the inflections are more rounded than in Figures 5.9(b) and 5.10(b).

Sub-cases (a) ($k_1 \leq k_2 \leq k_3$) and (c) ($k_1 \leq k_3 \leq k_2$) are both characterised by k_1 as the limiting rate of deacetylation. Similar to the bottleneck cases presenting inflections around DS $= 2$ due to having k_2 as the limiting rate, there are evident inflections in the DS-time and $\langle OOO \rangle$-DS curves around DS $= 1$ in Figures 5.9(a), 5.10(a), 5.9(c), and 5.10(c). The inflections are sharper in sub-case (c) compared with sub-case (a). This is most likely due to k_2 and k_1 being more similar in sub-case (a) than sub-case (c).

Sub-cases (e) ($k_3 \leq k_1 \leq k_2$) and (f) ($k_3 \leq k_2 \leq k_1$) both have k_3 as the limiting rate of deacetylation. As seen in Figures 5.9(e) and 5.9(f), the DS-time curve moves right from the benchmark curve as the initial deacetylation rate is impeded, creating a "lag" (relative to the benchmark) from the start. There are no evident inflections.

As discussed in Section 5.3.2, the observed progression of degradation in CA artefacts appears to be more consistent with an $\langle OOO \rangle$-DS trendline below or coincident with the benchmark curve. Based on this, sub-case (f) does not appear to be a suitable model of DS-dependence of deacetylation rate constants. This is a surprising result, as it directly contradicts the prediction made at the start of this section. Sub-cases (a) and (c) are more consistent with chain scission occurring after advanced deacetylation, but these lack explanations of why the deacetylation rate constant would be smaller when DS $= 1$. These findings suggest that variation

in deacetylation rate constants may not be sufficiently described in terms of dependence on DS alone.

The presence of sharp inflections in the DS-time curve or $\langle OOO \rangle$-DS curve illustrate how highly non-linear behaviour could arise from the deacetylation kinetics (even when autocatalysis is excluded), by considering (1) the complete sequence of reactions required to yield cellulose AGUs from triacetate and (2) the distribution of deacetylation rate constants. By comparing the curves with how degradation in CA artefact appears to progress, the initial hypothesis about how DS affects reactivity was tested. Next, the model will be used to analyse real data on CA deacetylation, to find out whether DS or substituent position affects reactivity.

5.4 FITTING THE MODEL TO EXPERIMENTAL DATA

As a proof-of-concept, the model was fitted to published experimental data (65) comprising the mole fractions of monomers in cellulose acetate in progressive stages of deacetylation. This was done by estimating the rate constants in Equations 5.1-8 using experimental AGU mole fractions for the dependent variables and experiment time for the independent (time) variable.

The experimental system did not resemble the conditions expected in a museum setting, but data was not available for such conditions. Therefore, the results for the rates or the rate ratios cannot be generalised to the simulation of a museum setting. Nevertheless, this work demonstrates that this mathematical model could be used to simulate and analyse such data were it available.

5.4.1 Methods

In this experiment, 1.0 g of commercial cellulose triacetate (DS = 2.92) was reacted in a solution of pure acetic acid (15 mL), water (1.5 mL) and concentrated sulphuric acid (0.40 g) at 358 K (85 °C) for 10, 40 and 70 minutes, for a total of four grades of CA corresponding to four degrees of deacetylation (65). The mole fraction of each AGU was measured using NMR (219,220). The data used for fitting the model consist of mole fractions for 2,3,6-triacetate, 3,6-diacetate, 2,6-diacetate, 2,3-diacetate, 6-monoacetate, 3-monoacetate and 2-monoacetate in each of the four grades of CA, corresponding to reaction time = 0, 10, 40, 70 minutes.

Tabulated data and details of data processing are included in Appendix C. As the initial monomer composition (DS = 2.92) was not reported in Kono et al. (2017) (65), it was assumed to be the same as that reported in Kono et al. (2015) (220), as the CA had the same DS.

Several assumptions and approximations were made to apply the model to the experimental set-up. It was assumed that the reaction system had constant volume, so the concentrations in Equations 5.1-8 were replaced with the number of moles. As the total number of moles is also a constant, the mole fractions were used in place of the number of moles. In the case of completed deacetylation, the number of moles of water would decrease by 12.3%. In the experiment, CTA (DS = 2.92) was converted to DS = 1.28, so the number of moles of water decreased by 6.9%. Due to this relatively small change, the water concentration was approximated as constant. It was further assumed that in the presence of sulphuric acid (a strong acid) and a large quantity of acetic acid, the small quantities of acetic acid being generated by the reaction had negligible impact on acid-catalysed deacetylation. Calculations show that the change in number of moles of acetic acid under complete and experimentally realised deacetylation are 3.9 and 2.2%, respectively, supporting the approximation of acetic acid concentration as constant. Subject to these assumptions, deacetylation is approximately first-order in the concentration (mole fraction) of acetyl, consistent with the model Equations 5.1-8.

As the experimental data were insufficient to estimate time derivatives, Equations 5.1-7 were integrated analytically to produce algebraic expressions for the mole fractions. The integrated equations (see Appendix D) were fitted to the experimental data using lsqcurvefit in MATLAB R2021a. Equation 5.8 was not included as the mole fraction of cellulose AGU was not reported.

5.4.2 Results

The model was fit according to four different scenarios: (1) identical rate constants, (2) substituent-dependent rate constants, (3) DS-dependent rate constants, and (4) independent rate constants. This was done to identify the set(s) of assumptions that best describes the experimental data.

Table 5.1 shows the results for (1) identical rate constants and (2) substituent-dependent rate constants. Table 5.2 show the results for (3) DS-dependent rate constants and (4) independent rate constants. The rows and columns for each scenario correspond to the rows and columns of matrix k in Equation 5.9, with the columns (corresponding to carbon positions A, B, C in Equation 5.9) corresponding to carbon positions 2, 3, 6. Simulations for the different scenarios are shown in Figures 5.11-14.

Table 5.1 Fitted rate constants under different model assumptions. The rows and columns for each scenario correspond to the rows and columns of matrix k in Equation 5.9.

	Identical rate constants			Substituent-dependent rate constants		
Estimated rate constants (10^{-3} min^{-1})	16.5	-	-	28.4	26.8	6.26
	-	-	-	-	-	-
	-	-	-	-	-	-
	-	-	-	-	-	-

Table 5.2 Fitted rate constants under different model assumptions. The rows and columns for each scenario correspond to the rows and columns of matrix k in Equation 5.9.

	DS-dependent rate constants			Independent rate constants		
Estimated rate constants (10^{-3} min^{-1})	11.8	-	-	10.0	28.9	7.41
	19.6	-	-	102	2.69×10^{-8}	22.3
	-	-	-	10.4	2.22×10^{-11}	9.53
	15.6	-	-	2.66×10^{-3}	38.9	1.24
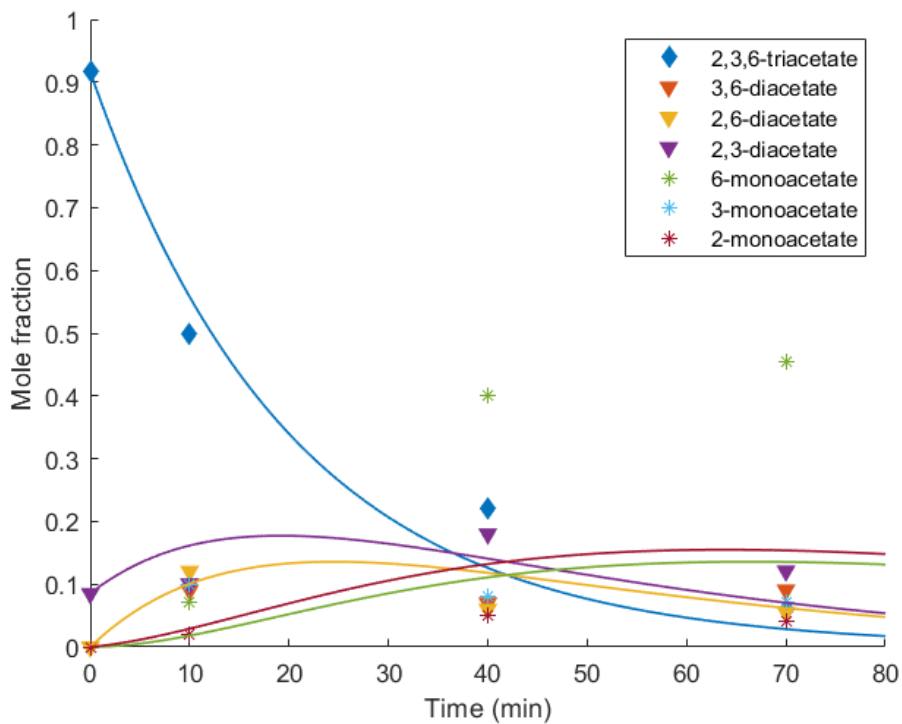
Figure 5.11 Identical rate constants: Experiment (markers) and simulated (lines) AGU mole fractions vs. time, in cellulose acetate undergoing deacetylation. The predictions for 3,6-diacetate and 2,6-diacetate (yellow) coincide, as do the predictions for 3-monoacetate and 2-monoacetate (magenta).
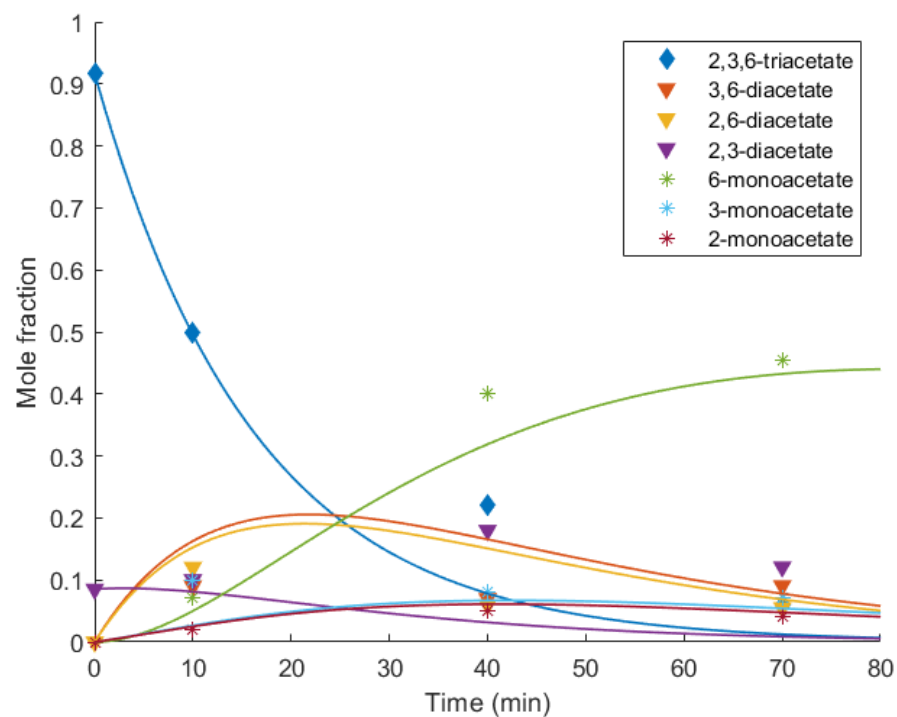
Figure 5.12 Substituent-dependent rate constants: Experiment (markers) and simulated (lines) AGU mole fractions vs. time, in cellulose acetate undergoing deacetylation.
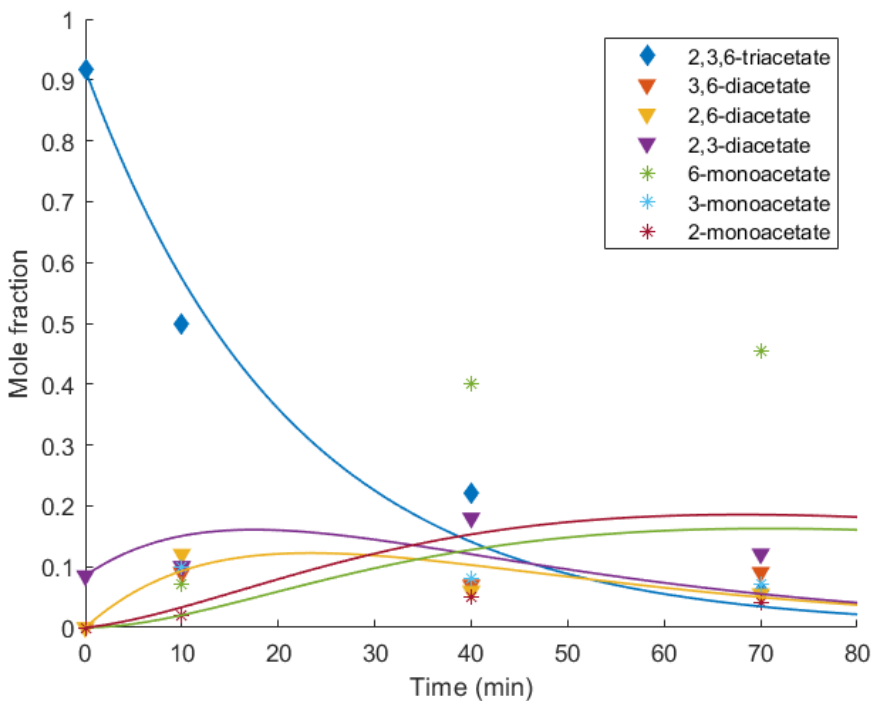
Figure 5.13 DS-dependent rate constants: Experiment (markers) and simulated (lines) AGU mole fractions vs. time, in cellulose acetate undergoing deacetylation. The predictions for 3,6-diacetate and 2,6-diacetate (yellow) coincide, as do the predictions for 3- monoacetate and 2-monoacetate (magenta).
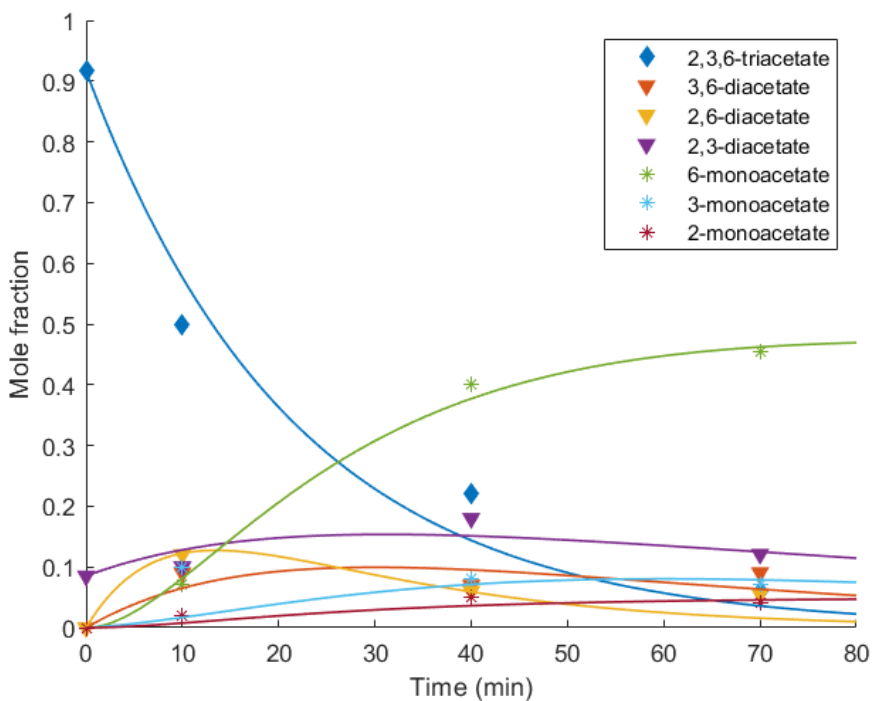
Figure 5.14 Independent rate constants: Experiment (markers) and simulated (lines) AGU mole fractions vs. time, in cellulose acetate undergoing deacetylation.

5.4.3 Discussion

Due to insufficient data for a validation or test set, it was not possible to estimate the unbiased error of the models. However, analysis of the results in Table 5.1 provides some interesting insights.

The DS-dependent case does not suggest that reactivity increases or decreases monotonically with DS. k_2 is larger than k_3 and k_1, and the rate constants vary by less than a factor of two, which is closer to the benchmark than the ratios explored in scenarios in Section 5.3.3. In Figures 5.11 and 5.13, the identical rate constants and DS-dependent cases are not able to simulate the progression of 6-monoacetate, unlike the substituent-dependent case in Figure 5.12.

In the substituent-dependent case, the estimated rate constants suggest that the acetyls react in the order C2, C3, C6. This is the same conclusion that was reached by the authors of the study where the data came from (65). C2 and C3 are both secondary alcohols, while C6 is primary, so it makes sense that the rate constants of C2 and C3 would be similar to each other yet different from that of C6. However, typically it would be expected that the primary alcohol is more reactive than the secondary (63). As noted earlier, the reaction conditions seem to affect the reaction order of the substituents. For example, a study (64) using NMR spectroscopy to measure hydrolysis of the acetyl groups in CA suggested that acetyls are lost in the order C2, C6, C3. The context of the study –which was published in the journal Polymers in Conservation and cited in the book Conservation of Plastics (56)—implies that this is the reaction order believed to take place under conditions found in a museum/archive setting. This shows how the results based on the lab data may not be applicable to modelling deacetylation in a museums environment.

Although there is a risk that the scenario with 12 independent rate constants could be over-fitted, the data comprise 28 data points and were fitted to seven equations, leaving 21 degrees of freedom. Therefore, based on the number of degrees of freedom, 12 rate constants is acceptable, but it would be better to verify this using the error on a separate validation dataset. Based on some of the values of the estimated rate constants for this scenario in Table 5.1, the estimates themselves may be unreliable. For example, $k_{VIII} = 2.22 \times 10^{-14}$ min^{-1}, is so close to zero that

it is likely due to the optimisation algorithm hitting the lower bound for the parameter, even though this was not the reason that the algorithm stopped. Repeated runs of the optimisation algorithm using random initial guesses converged to the same local minimum.

The mean[2] of the DS-dependent rate constants is 16.7×10^{-3} min^{-1}, similar to the result obtained for fitting identical rate constants, 16.5×10^{-3} min^{-1}. The mean substituent-dependent rate constant is 20.5×10^{-3} min^{-1}, close to the mean of the case with 12 independent rate constants, 19.6×10^{-3} min^{-1}.

By row (DS = 3, 2, 1), the means of the case with 12 independent rate constants are: 15.4, 24.0, 13.4 ($\times 10^{-3}$ min^{-1}). This roughly resembles the relationship in the DS-dependent case, where the rate constant for DS = 2 is larger than the other two, and the rate constants vary from each other by less than a factor of two.

By column (substituent positions = C2, C3, C6), the means of the case with 12 independent rate constants are: 30.6, 17.0, 10.1 ($\times 10^{-3}$ min^{-1}). This order agrees with the result obtained by the substituent-dependent case, although the magnitude of the mean C3 and C6 rate constants are more similar. Another similarity between the means-by-substituents of the 12 independent rate constants case and the substituent-dependent case are that the rate constants vary by more than a factor of three, although this is still closer to the benchmark than the ratios explored in the scenarios in Section 5.3.2.

It is interesting to consider how a mathematical model can affect the interpretation of the data. The authors of the study where the data came from did not use any mathematical kinetic models to interpret the data (65). The following passage illustrates their qualitative interpretation:

> "Notably, the accumulation of the . . . [2,6-diacetate] and . . . [3,6-diacetate] of CA chains was not observed before the increase of . . . [6-monoacetate], indicating that the rate of the hydrolysis of the acetyl groups at the 2- and 3-positions was greater than that at the 6-position . . . This could be explained by the mechanism of the acid-catalyzed ester hydrolysis and the order of

---

[2] This is a weighted mean of all the rate constants in Equation 5.9, so the rate constant for DS = 2 is counted twice because it is the rate constants for the two middle rows.

electron charge density of the cellulose hydroxyl groups at the 2-, 3- and 6-positions (221)*. The hydrolysis of the acetyl groups begins with the abstraction of a proton from a hydroxonium ion in the solvent by the ester to make the ester carbonyl more electrophilic. The oxygen of water functions as a nucleophile and attacks the electrophilic carbonyl atom, which results in the formation of a cationic tetrahedral intermediate. Next, a proton (a hydrogen ion) from water binds to the carbonyl carbon and is transferred to the oxygen atom of the ester derived from the cellulose hydroxyl by the unpaired electrons of the oxygen atom, which facilitates the dissociation of the hydroxyl group from the ester. Thus, the electronegativity of the oxygen atom in the hydroxyl groups of cellulose promotes the acid-catalyzed ester hydrolysis. Because the electron density of the hydroxyl groups of cellulose ranks as OH(2) > OH(3) > OH(6)* (221)*, the electronegativity of the hydroxyl groups in cellulose reflects the rate of hydrolysis at the 2-, 3-, and 6-positions. Therefore, the very fast hydrolysis at the 2- and 3-positions resulted in a prompt increase of . . . [6-monoacetate] in CA chains, without increasing . . . [2,6-diacetate] and . . . [3,6-diacetate]."* (65)

However, the results of the scenario with 12 independent rate constants tell a slightly different story (in the following description, the units of the rate constants are ($\times 10^{-3}$ min^{-1})). Considering deacetylation of 2,3,6-triacetate, hydrolysis at C3 ($k_{II} = 28.9$) is faster (though not by a large degree) than at either C2 or C6 ($k_I = 10.0$, $k_{III} = 7.41$) (disagrees with quoted passage). On 3,6-diacetate, hydrolysis at C6 ($k_V = 22.3$) is much faster than at C3 ($k_{IV} = 2.69 \times 10^{-8}$) (disagrees with quoted passage). On 2,6-diacetate, hydrolysis at C2 ($k_{VI} = 102$) is much faster than at C6 ($k_{VII} = 9.53$) (agrees with quoted passage). Based on this, increase in 6-monoacetate could not be attributed to "very fast hydrolysis at the . . . [3-position]" of 3,6-diacetate, as C6 reacts significantly faster than C3 in this AGU. Furthermore, the order of preference of reaction in 2,3,6-triacetate is C3 > C2 > C6, disagreeing with the order of electron density, OH(2) > OH(3) > OH(6). Thus, assuming the estimated rate constants are unique, the mathematical model raises some doubts about the original interpretation of the data.

To investigate the effect of the various model assumptions and estimated rate constants on the $\langle OOO \rangle$ vs. DS curve, simulated $\langle OOO \rangle$ vs. DS was plotted for each of the four scenarios, as well as the experimental data, in Figure 5.15. Experimental $\langle OOO \rangle$ was estimated as:

$$\langle OOO \rangle = \max\big(0, (1 - \langle 2,3,6 \text{ triacetate} \rangle - \langle 3,6 \text{ diacetate} \rangle \qquad (5.17)$$

$$- \langle 2,6 \text{ diacetate} \rangle - \langle 2,3 \text{ diacetate} \rangle - \langle 6 \text{ monoacetate} \rangle$$

$$- \langle 3 \text{ monoacetate} \rangle - \langle 2 \text{ monoacetate} \rangle)\big)$$
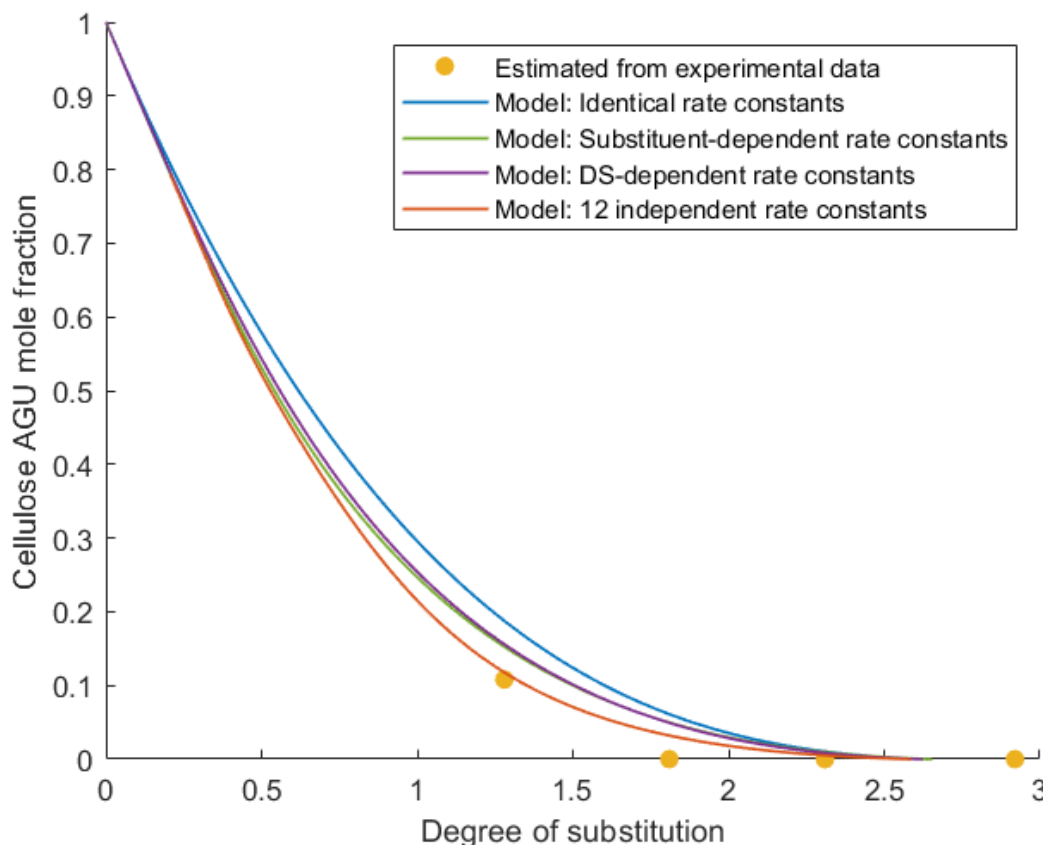
Figure 5.15 $\langle OOO \rangle$ vs. DS, simulated (lines) and estimated from experimental data (markers).

There are likely errors in the data as three out of four of the $\langle OOO \rangle$ values were estimated as 0. For example, the mole fractions of the other seven AGUs may be overestimated. There are limits on the accuracy of NMR, which was used to detect the other seven AGUs. Figure 5.15 is not intended to show which of the cases gives the best fit to the experimental data. It demonstrates that the estimated

experimental $\langle OOO \rangle$ lies below the benchmark (the case with identical rate constants), and that the more complex (non-benchmark) cases are consistent with each other and the data by simulating this trend.

Figure 5.16 plots rate constant vs. AGU DS for the model with 12 independent rate constants. As is apparent from this graph, there is no discernible consistent effect of DS on the rate constant for a particular substituent. The correlation coefficients between the AGU DS and the rate constants support this, which for C2, C3 and C6 are 0.0856, -0.2046 and 0.2748, respectively. This agrees with the conclusion drawn earlier based on the fitted rate constants for the DS-dependent case. However, as noted earlier, the estimated rate constants may be unreliable.
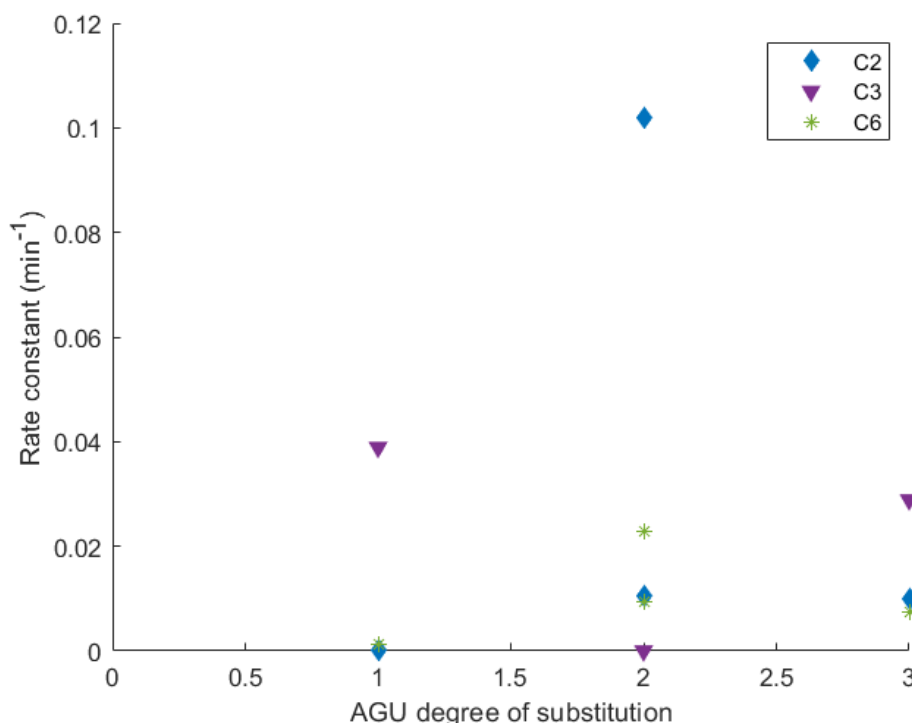
Figure 5.16 Fitted rate constants vs. DS, for the model assuming independent rate constants.

As mentioned in Chapter 3, Section 3.3.1, several models of substitution kinetics in cellulose derivatives have been developed which are basically consistent with the diagram in Figure 5.2, with initial credit being due to Spurlin (170). For comparison, the model due to Salmi et al. (172,173) has a similar structure as the model presented in this chapter: using Equation 5.9 as reference, in their model,

the first row are three free parameters, then the terms in subsequent rows are declining functions of the term in the same column in the first row. The functions are described in terms of rate decline parameters which quantify the extent to which the presence of other substitutions in the AGU affect the rate constant. While the Salmi et al. applied their data to carboxymethylation of cellulose, and therefore the effect of substituting carboxymethyl for hydroxyl is not necessarily comparable to substituting hydroxyl for acetyl, the implication of their model is that substitution is expected to have a consistent effect on reactivity of other substituents in the AGU. For example, deacetylation of one substituent could increase reactivity of other substituents due to diminished steric hindrance or increase/decrease reactivity of other substituents by being electron withdrawing or donating. What the results in Figure 5.16 suggest, as well as the correlation coefficients calculated above, is that other substitutions on the AGU may not have a consistent positive or negative effect on the reactivity of an acetyl substituent in cellulose acetate (at least under the reaction conditions of this experiment). This is also consistent with the results of the DS-dependent case, which suggested that deacetylation rate constants do not seem to correspond strongly with the total substitutions on the AGU. This suggests that a model which attempts to capture variation in the rate constants by presuming this correlation exists, such as the one due to Salmi et al., may not be suitable for modelling deacetylation kinetics in cellulose acetate.

5.5 CONCLUSIONS

Variation in rate constants for the 12 reactions identified in Figure 5.2 could explain deviations from the benchmark case, conferring increased or decreased susceptibility to chain scission (assuming chain scission depends on $\langle OOO \rangle$) relative to progression of deacetylation (as measured by DS). Fitting the model to lab data from the literature verified the existence of such deviations and the capability of the model to simulate the trends. An interesting result was that the rate constants do not appear to increase or decrease monotonically with decreasing DS. While the findings cannot necessarily be generalised to deacetylation in a museum setting, this is surprising as I expected the rate constants to increase as DS decreases due to the observed tendency for CA to

become more unstable as degradation progresses. Another thought-provoking finding was that although the model agreed with the original interpretation (by the authors of the study where the data came from) that generally, deacetylation proceeded in the order C2 > C3 > C6, there were some inconsistencies that were not explained by or disagreed with the original interpretation. This shows how the mathematical model can be used to interpret complex data and test assumptions.

The outputs of this model provide a link between deacetylation and chain scission under the assumption that glycosidic bonds cleave primarily between adjacent cellulose AGUs. Having demonstrated the validity and relevance of this model for predicting AGU composition, Chapter 6 presents a model of chain scission that builds further on these concepts. The mathematical model of chain scission will be used to explore the consequences of the assumption that glycosidic bonds cleave primarily between adjacent cellulose AGUs and whether implementing this assumption results in a more accurate model compared to not implementing this assumption.

6 CHAIN SCISSION

This chapter presents a mathematical model of chain scission in cellulose acetate (CA) based on the hypothesis that bond cleavage is more likely to occur between adjacent cellulose anhydroglucose units (AGUs):

- *premises, justification, and motivations for the model*
- *chemical species, reactions, and mass balances*
- *pre-processing data, model assumptions, and framing the problem in modelling terms*
- *fitting models to experimental data and estimating the out-of-sample errors of the models*
- *what the results indicate about the hypothesis being tested.*

6.1 INTRODUCTION

As discussed in Chapter 2, chain scission in cellulose acetate (CA) artefacts—associated with reduction in the degree of polymerisation (DP) and/or tensile strength—tends to occur only after advanced deacetylation—evidenced by development of the vinegar syndrome or reduction in degree of substitution (DS). The observation can be restated as "the rate of chain scission increases after deacetylation has advanced to some extent." The model in this chapter assumed that chain scission in CA artefacts occurs via hydrolysis (see Figure 6.1), as oxidative chain scission appears to require UV light, an unlikely factor in museums and archives (99).
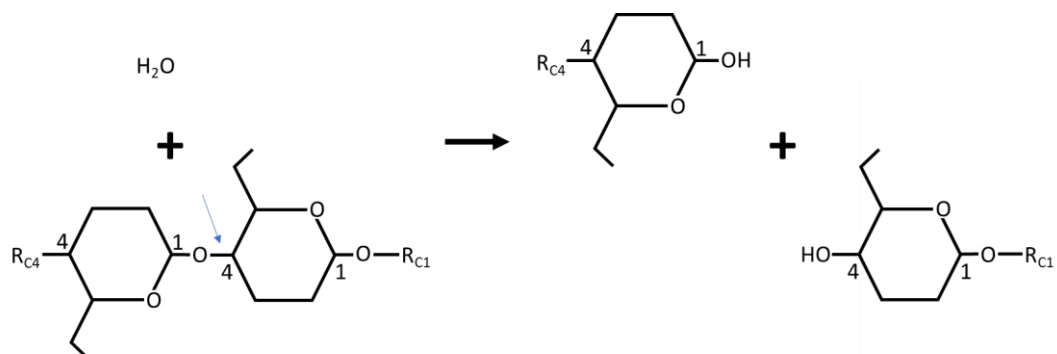
Figure 6.1 Schematic of chain scission via hydrolysis. The small arrow points to the β-1,4 glycosidic bond. R_{C4} and R_{C1} represent the rest of the CA polymer on each side of the anhydroglucose units (AGUs) involved in the bond.

The rate of chain scission r is the sum of all the rates of reactions which result in cleavage of a glycosidic bond in the polymer (Equation 6.1). The rate r_i of reaction i is determined by a rate constant k_i, the concentration of the type of glycosidic bond involved in the reaction $[B_i]$, the concentration of water $[H_2O]$ and the concentrations of any catalysts $[catalyst]$ (e.g., acetic acid)(Equation 6.2).

$$r = \sum_i r_i \tag{6.1}$$

$$r_i = f_i(k_i, [B_i], [H_2O], [catalyst]) \tag{6.2}$$

Function f_i expresses the dependence of r_i on the aforementioned factors. Basing k_i on the Arrhenius equation, k_i is constant when the temperature is constant. As deacetylation does not cause temperature changes, it is assumed that k_i is constant at a given temperature, so the development of chain scission is not attributable to this factor. The link between deacetylation and chain scission is observed even in cellulose acetate degrading in acidic aqueous solutions, systems which maintain constant $[H_2O]$ and $[catalyst]$ (108). It is reasonable to infer that the increase in the rate of chain scission may be attributed to a change in $[B_i]$. Specifically, if some bonds are more susceptible to chain scission and have larger rate constants k_i, then an increase in the concentration of such bonds will cause an increase in their respective r_i leading to increase in r. Additionally, the features which distinguish different bonds B_i are affected by deacetylation.

In this chapter, a mathematical model of CA chain scission is developed based on the hypothesis that bond cleavage is more likely to occur between adjacent cellulose anhydroglucose units (AGUs). This could be due to steric hindrance (with hydroxyls being less obstructive than acetyls to the reacting water molecule), as well as the effects of the electronegativity of the moieties on the glycosidic bond. The influence of acetic acid on the chain scission reaction is also modelled. Using experimental data from the literature, this chapter attempts to establish whether the proposed model is better at simulating empirical trends than the benchmark, which assumes that bond cleavage is equally likely to occur regardless of AGU substitution states.

Using the deacetylation models from Chapters 4-5 to simulate the AGU composition over time, the chain scission model in this chapter predicts (1) the proportion of types of glycosidic bonds present for a given AGU composition and (2) the chain scission rate as a function of the composition at a particular time. By solving these equations, the deacetylation and chain scission model predicts DS and DP as a function of time, and correlates DP with DS.

6.2 MATHEMATICAL MODEL

6.2.1 Chemical species

The substitution states comprise the 8 AGUs that were presented in the previous chapter. These can combine into $8 \times 8 = 64$ pairs of AGUs in a bond. While it is not strictly necessary for the assumptions used in the model, the model distinguishes between whether an AGU is on the C4 side or the C1 side of a glycosidic bond (see Figure 6.2). The β-1,4 glycosidic bond is not symmetrical; as suggested by the name, it involves the C1 of one AGU and the C4 of a second AGU, which are linked via the oxygen atom between them.
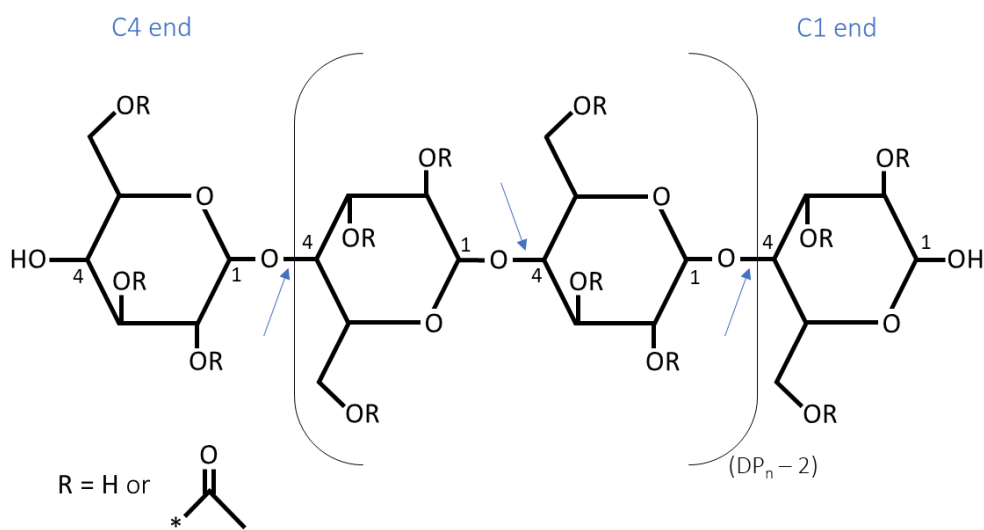
Figure 6.2 Structure of CA polymer molecule. The arrows point to glycosidic bonds, also known as chain bonds. The left-most arrow points to the "C4 end bond" of the molecule. The middle arrow points to a "non-end chain bond". The right-most arrow points to the "C1 end bond" of the molecule. The middle two AGUs have "both ends bonded". The left-most AGU "terminates at the C4 end". The right-most AGU "terminates at the C1 end".
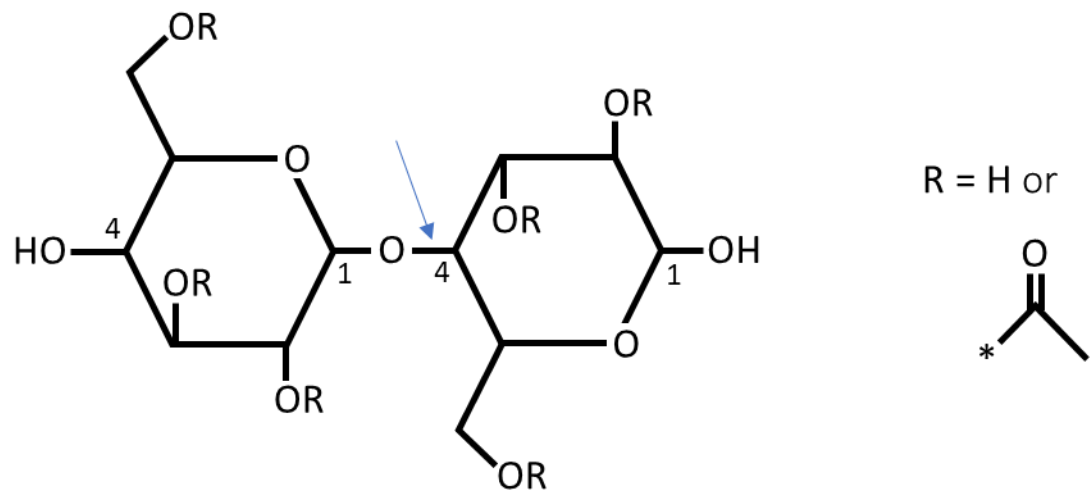
Figure 6.3 Structure of CA dimer molecule. The arrow points to a "dimer bond".
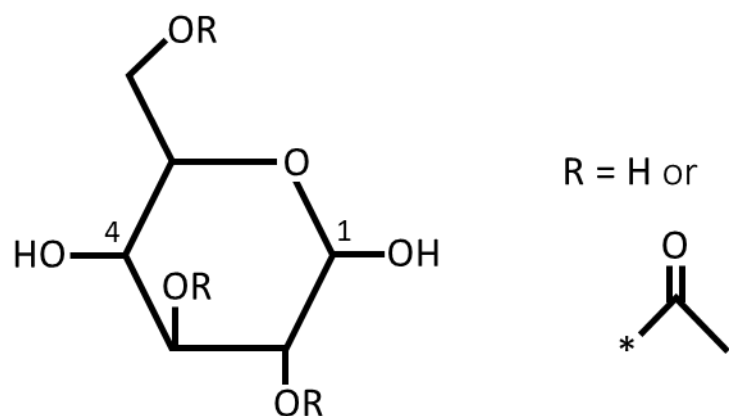
Figure 6.4 Structure of CA monomer, an AGU having "no glycosidic bonds".

Similarly, while this chapter will not consider scenarios in which the rate constants depend on the bond position in the chain, it will be useful for accounting purposes to define four types of bonds (see Figures 6.2-3). The four types of bonds and their notations are defined in Table 6.1.

Table 6.1 Types of bonds in the model.

Description of bond	Symbol
Non-end chain bond	xBx
C1 end bond	xB
C4 end bond	Bx
Dimer bond	B

Chain bonds are defined by two AGUs joined together, which may or may not be joined to other AGUs (see Figures 6.2-4). The chain bonding states that an AGU may take are defined in Table 6.2.

Table 6.2 Types of AGUs in the model.

Description of AGU	Symbol
Both ends bonded	xAx
Terminates at C1 end	xA
Terminates at C4 end	Ax
No glycosidic bonds	A

Finally, an AGU is also characterised by its substitution state, defined in Table 6.3. The substitution state of an AGU or of the AGUs involved in a chain bond is expressed using these symbols as indices. For example, xA(236) refers to a 2,3,6-triacetate AGU at the C1 end of a CA molecule; xBx(000,000) refers to a non-end chain bond between two cellulose AGUs.

Table 6.3 Substitution states of AGUs.

Chemical name	Symbol
2,3,6-triacetate	236
3,6-diacetate	036
2,6-diacetate	206
2,3-diacetate	230
6-monoacetate	006
3-monoacetate	030
2-monoacetate	200
Cellulose	000

There are thus (8 substitution states)×(8 substitution states)×(4 bond types) = 256 distinct species of glycosidic bonds, and (8 substitution states)×(4 chain bonding states) = 32 distinct species of AGUs.

The model consists of mass balances on the 32 species of AGUs in the form of differential equations, and algebraic expressions calculating the expected concentrations of each of the 256 bond types as a function of the concentrations of the AGU species.

6.2.2 Chemical reactions

Molar balances on the species of AGUs are expressed as differential equations that sum the rates of production and consumption (by chemical reactions) of each AGU. It was assumed that that AGUs cannot diffuse, so there are no mass transport terms for these species.

6.2.2.1 Deacetylation

The deacetylation term includes any reactions that produce or consume the AGU via deacetylation. The effect of deacetylation reactions is to alter the substitution states, which are denoted by the symbols in parentheses (as defined in Table 6.3). As shown in Chapter 5, for eight substitution states, there are 12 types of substitution reactions. It was assumed that deacetylation depends only on the

substitution state of the AGU on which it takes place, and not on the properties of any adjacent AGUs.

For example, the sum of the deacetylation reaction terms for xAx(036), $R_{D,xAx(036)}$, is:

$$R_{D,xAx(036)} = (k_I[xAx(236)] - k_{IV}[xAx(036)] - k_V[xAx(036)])[H_2O][HOAc] \qquad (6.3)$$

where the deacetylation rate constants k have dimensions (concentration)$^{-2}$ (time)$^{-1}$. The index in the subscript of the rate constant k refers to the substitution reaction as defined in Figure 5.2. For a given AGU, the deacetylation reaction terms involve only AGUs of the same AGU type—in this case, both ends bonded (xAx). This is because deacetylation may only alter substitution states, not AGU type. The first term in Equation 6.3 is the rate of the reaction that produces 3,6-diacetate by deacetylation of 2,3,6-triacetate. The second and third terms are consumption (hence the minus signs) of 3,6-diacetate by deacetylation to 6-monoacetate and 3-monoacetate, respectively. The dependence of the deacetylation rate on $[H_2O]$ and $[HOAc]$ are taken from the model developed in Chapter 4.

6.2.2.2 Chain scission

The chain scission terms include reactions that produce or consume the AGU via hydrolysis of glycosidic bonds. The effect of chain scission reactions is to alter the AGU type, which are denoted by the symbols defined in Table 6.2.

The reactants are chain bonds, and the products are AGU types. Each type of chain bond (as defined in Table 6.1) may undergo a chain scission reaction. There are therefore four possible chain scission reactions:

$$xBx(i,j) \rightarrow xA(i) + Ax(j) \qquad (6.4)$$

$$xB(i,j) \rightarrow xA(i) + A(j) \qquad (6.5)$$

$$Bx(i,j) \rightarrow A(i) + Ax(j) \qquad (6.6)$$

$$B(i,j) \rightarrow A(i) + A(j) \qquad\qquad (6.7)$$

Index i denotes the substitution state of the AGU on the C4 side of the bond and index j denotes the substitution state of the AGU on the C1 side. Figure 6.5 illustrates these chemical reactions.
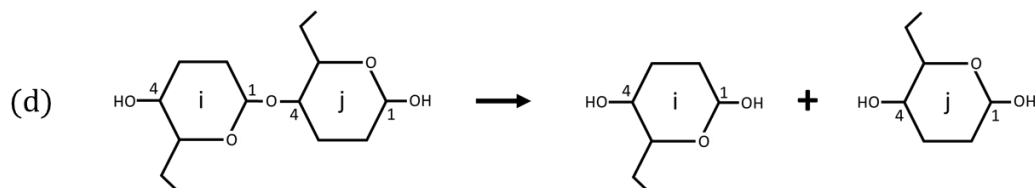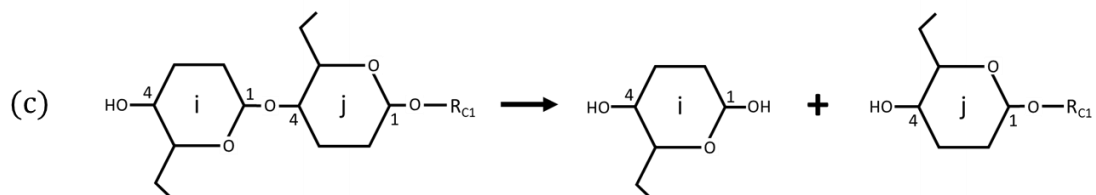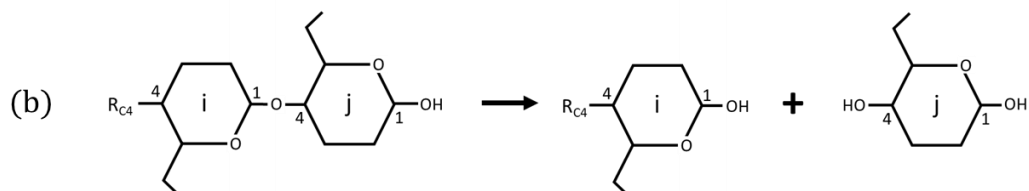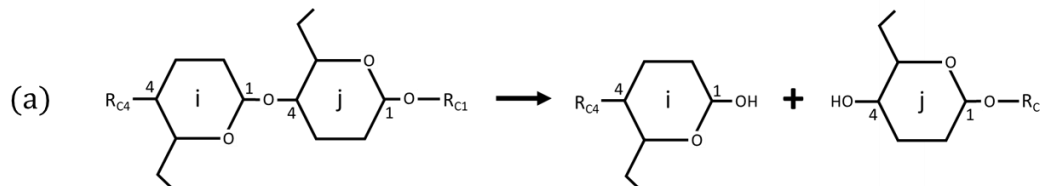
Figure 6.5 The four types of chain scission reactions: (a) Equation 6.4, middle of chain bond goes to C1 end AGU and C4 end AGU; (b) Equation 6.5, C1 end bond goes to C1 end AGU and AGU monomer; (c) Equation 6.6, C4 end bond goes to AGU monomer and C4 end AGU; (d) Equation 6.7, dimer bond goes to AGU monomer and AGU monomer. R_{C4} and R_{C1} represent the rest of the CA polymer on each side of the AGUs involved in the bond. Index i denotes the substitution state of the AGU on the C4 side of the bond and index j denotes the substitution state of the AGU on the C1 side.

Chain scission reactions depend on the concentration or mole fraction of chain bonds. The mole fraction of each type of chain bond is estimated using a probability model that has the mole fraction of the AGU species as inputs. The model assumes that AGU species are initially randomly distributed and that all chemical reactions are independent of chain length or position in the chain (other than as reflected by the AGU type or chain bond type). As mentioned at the start of Section 6.2.2, the model assumes that AGUs cannot diffuse nor evaporate, so the total number of AGUs in the system is conserved.

Consider the chain bond species xBx(i,j), which is made up of xAx(i) and xAx(j) being bonded to one another. The frequency (concentration) of xBx(i,j) is equal to the product of the frequency (concentration) of xAx(i) and the probability that xAx(i) is bonded to xAx(j). Since deacetylation does not depend on the substitution state of adjacent AGUs, the substitution state of xAx(j) is independent of xAx(i). Therefore, the probability that xAx(i) is bonded to xAx(j) is simply equal to the frequency of xAx(j) divided by the sum of the frequencies of all AGUs that may bond to the C1 side of xAx(i) (Equation 6.8).

$$[xBx(i,j)] = [xAx(i)] \times \frac{[xAx(j)]}{\sum_{n \in S}([xAx(n)] + [xA(n)])} \tag{6.8}$$

The denominator in the second term of Equation 6.8 denotes the sum of all AGUs that may bond to the C1 side of xAx(i). S is the set of all substitution states: $S \ni \{236, 036, 206, 230, 006, 030, 200, 000\}$.

Similarly, formulas were derived for the remaining three types of chain bonds:

$$[xB(i,j)] = [xAx(i)] \times \frac{[xA(j)]}{\sum_{n \in S}([xAx(n)] + [xA(n)])} \tag{6.9}$$

$$[Bx(i,j)] = [Ax(i)] \times \frac{[xAx(j)]}{\sum_{n \in S}([xAx(n)] + [xA(n)])} \tag{6.10}$$

$$[B(i,j)] = [Ax(i)] \times \frac{[xA(j)]}{\sum_{n \in S}([xAx(n)] + [xA(n)])} \tag{6.11}$$

As it turns out, the sum in the denominator of the second term is the same for all types of chain bonds, as the species included in the sum account for all AGUs that are chain bonded on their C4 end (and so are bonded to the C1 end of another AGU). Hopefully, by now, it will be apparent to the reader why it was necessary to distinguish between the species defined in Tables 6.1-2, even if these qualities will not later be modelled as having any direct effect on rate constants.

The chain bond concentrations calculated using Equations 6.8-11 are used in the calculation of the chain scission rates. The model assumes that the rates of chain scission depend in the first order on the concentration of the chain bonds. This assumption is made in previous models of cellulose degradation discussed in Chapter 3, Section 3.3.2.2.1, and the reasons for doing so are elaborated there. Dependence on other variables, such as water concentration, was accounted for in the function for the rate constant, as will be shown in the implementation of the model in Section 6.3.2.

For example, the sum of the chain scission reaction terms for xAx(036), $R_{C,xAx(036)}$, is equal to:

$$
\begin{aligned}
R_{C,xAx(036)} = &-\sum_{n \in S} k_{xBx(036,n)}[xBx(036,n)] \\
&-\sum_{n \in S} k_{xBx(n,036)}[xBx(n,036)] \\
&-\sum_{n \in S} k_{xB(036,n)}[xB(036,n)] \\
&-\sum_{n \in S} k_{Bx(n,036)}[Bx(n,036)]
\end{aligned}
\tag{6.12}
$$

The terms are all negative because xAx(036), being bonded on both sides, can only be consumed by chain scission, not produced. In the first summation term, xBx(036,n) represents all possible non-end chain bonds in which xAx(036) is on the C4 side of the bond (see Equation 6.8). In the second summation term, xBx(n,036) represents all possible non-end chain bonds in which xAx(036) is on the C1 side of the bond (Equation 6.8). In the third summation, xB(036,n) represents all possible C1 end chain bonds in which xAx(036) is on the C4 side of the bond (see Equation 6.9). In the fourth summation, Bx(n,036) represents all

possible C4 end chain bonds in which xAx(036) is on the C1 side of the bond (see Equation 6.10). The chain scission rate constants k are defined for each bond type, as indicated by the subscripts. The rate constants in Equation 6.12 are functions of $[H_2O]$ and $[HOAc]$, and have dimensions (time)$^{-1}$.

6.2.2.3 Mass balances

The deacetylation and chain scission reaction model combines the deacetylation and chain scission reaction terms into a single mass balance for each AGU species. For example, the mass balance for xAx(036) is simply the sum of Equation 6.3 and Equation 6.12:

$$
\begin{aligned}
\frac{d[xAx(036)]}{dt} &= R_{D,xAx(036)} + R_{C,xAx(036)} \\
&= (k_I[xAx(236)] - k_{IV}[xAx(036)] \\
&\quad - k_V[xAx(036)])[H_2O][HOAc] \\
&\quad - \sum_{n\in S} k_{xBx(036,n)}[xBx(036,n)] \\
&\quad - \sum_{n\in S} k_{xBx(n,036)}[xBx(n,036)] \\
&\quad - \sum_{n\in S} k_{xB(036,n)}[xB(036,n)] \\
&\quad - \sum_{n\in S} k_{Bx(n,036)}[Bx(n,036)]
\end{aligned}
$$

(6.13)

The model consists of solving the system of differential equations, which are the mass balances for each species of AGU. To solve the model, one needs a procedure to specify or calculate $[H_2O]$ and $[HOAc]$; the values for the rate constants; and initial values for the AGU species. These aspects depend on the features of the physical system being modelled and are explained in Section 6.3.2.

6.2.2.4 Degree of substitution and degree of polymerisation

The model outputs mole fractions of AGUs as a function of time. It is helpful for interpretability to convert these results into more meaningful quantities. The following equations were used to calculate DS and DP_n from AGU mole fractions.

The degree of substitution is calculated as:

$$X_{tr} = \frac{\sum_{m \in G}[m(236)]}{\sum_{m \in G}\sum_{n \in S}[m(n)]} \tag{6.14}$$

$$X_{di} = \frac{\sum_{m \in G}([m(036)] + [m(206)] + [m(230)])}{\sum_{m \in G}\sum_{n \in S}[m(n)]} \tag{6.15}$$

$$X_{mo} = \frac{\sum_{m \in G}([m(200)] + [m(030)] + [m(006)])}{\sum_{m \in G}\sum_{n \in S}[m(n)]} \tag{6.16}$$

$$DS = (3 \times X_{tr}) + (2 \times X_{di}) + X_{mo} \tag{6.17}$$

where X_{tr}, X_{di} and X_{mo} are the mole fractions of triacetate, diacetate and monoacetate, respectively. Recall that mole fractions represent the proportion of chemical species in each state (in this case, the proportion of AGUs of each DS) and can vary between 0 and 1. G is the set of all AGU types (see Table 6.2), $G \ni \{xAx, xA, Ax, A\}$. The denominator in Equations 6.14-17 is equal to the total concentration of AGUs in the system.

Recall that the degree of polymerisation (DP) is the number of monomers per polymer molecule. The number-average degree of polymerisation is calculated as:

$$DP_n = \frac{\sum_{m \in G}\sum_{n \in S}[m(n)]}{\sum_{n \in S}([xA(n)] + [A(n)])} \tag{6.18}$$

The numerator in Equation 6.18 is the same as the denominator in Equations 6.14-17 and is equal to the total concentration of AGUs in the system. The denominator represents the concentration of cellulose acetate or cellulose molecules (including dimers and monomers) in the system.

6.3 METHODS

I compared predictions under different model assumptions about the effect of AGU composition on chain scission. Due to a lack of published data, several assumptions were made in terms of the quantities used for physical or chemical properties. Where possible, I tried to represent or compare the models in terms that reduce the dependence on such approximated quantities. When this is the case, the

absolute numerical values of the predictions are less important than the shape of the curves or functions they output. Chapter 7 discusses the implications of these results for heritage conservation.

The mathematical model in Section 6.2 describes chain scission in cellulose acetate as a function of AGU composition. As discussed earlier in this thesis, the dependence on AGU composition is based on the hypothesis that hydrolysis of the glycosidic bond is significantly more likely between two cellulose AGUs. I model chain scission (and deacetylation) in the absence and presence of the assumption that the chain scission reaction rate may vary depending on the substitution states of bonded AGUs.

6.3.1 Data from analysis of plastic samples

The models aimed to simulate the DP_n and DS in naturally aged CA cultural heritage artefacts, measured at a single point in time (cross-sectional study). One set of data was collected by other members of COMPLEX, not including myself. The second set comes from a study (17,222) published by the Getty Conservation Institute (GCI). Both collections included naturally aged historical objects, some in good condition and some in bad condition. Figure 6.6 shows both sets plotted on a single graph of DP_n vs. DS. The direction of degradation is from right to left, in the direction of decreasing DS. Two data points from the GCI dataset were measured from samples taken from a single object (CA sheet), where one sample was taken from an area that appeared less degraded, and another sample taken from an area that appeared more degraded. The arrow shows the direction of degradation between the non-degraded and degraded samples from this object.
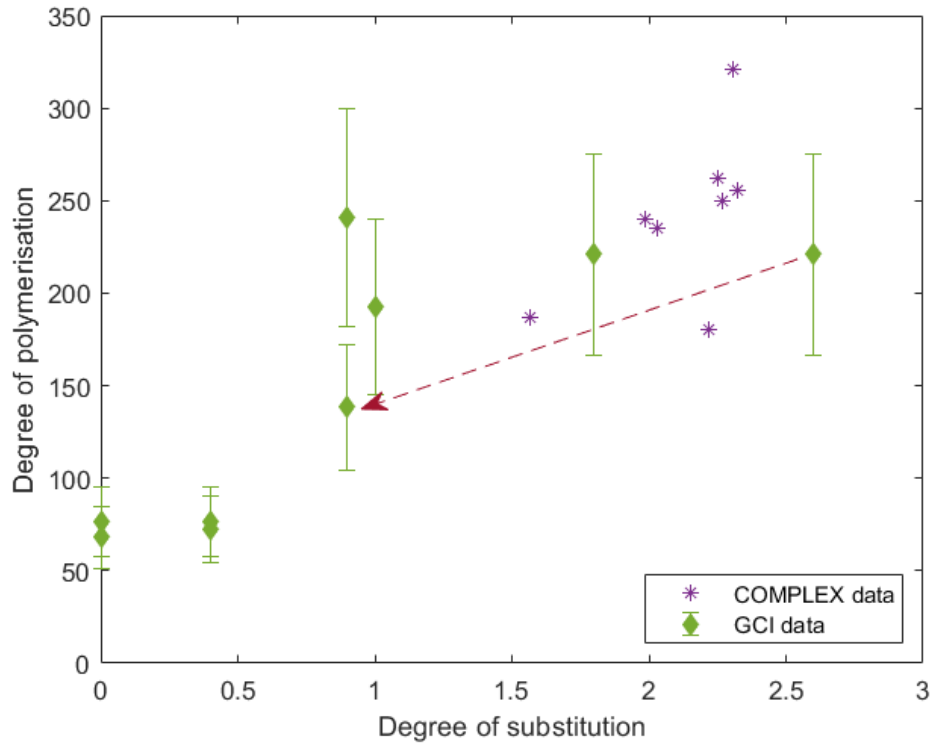
Figure 6.6 DP_n and DS of naturally aged CA objects.

In the COMPLEX study, DS was measured using high-resolution proton nuclear magnetic resonance spectroscopy (^{1}H NMR). DP_n was measured using size exclusion chromatography (SEC) (218).

In the GCI study (17), DS was measured using ion chromatography. Degree of polymerisation was measured using SEC. The authors of the study only provided the weight-average degree of polymerisation DP_w. To estimate DP_n from DP_w, the dispersities Đ$_X$ of the samples in the COMPLEX study were calculated, since both DP_n and DP_w were available for these. As explained in Chapter 3 (Equation 3.18), the dispersity Đ$_X = DP_w/DP_n$. The dispersities were in the range 2.2-3.0. Based on these calculated values, as well as reference values found in the literature (185), and adding some margin for errors, the dispersities of the GCI samples were estimated to be in the range 2-3.3. Re-arranging Equation 3.18, the formula for DP_n is:

$$DP_n = \frac{DP_w}{Đ_X} \tag{6.19}$$

133

Upper and lower bounds for DP_n were calculated using the estimated range of $Đ_X$. The mean of the upper and lower values was used as the final estimate for DP_n.

As can be seen in Figure 6.6, the GCI samples feature more advanced stages of degradation than the COMPLEX samples. The DP_n in the range where DS = 1.6-2.6 are reasonably consistent between the two datasets considering that the GCI DP_n had to be estimated, which gives some confidence in the accuracy (if not precision) of the estimates. These data suggest that DP_n does not change much above DS = 1, while at lower DS, it decreases significantly. The models aimed to simulate this relationship between DP_n and DS, testing the hypothesis that the pattern could be caused by increased susceptibility to chain scission between adjacent AGUs that have certain substitution states.

6.3.2 Model system

To provide a meaningful comparison between model simulations and the data, the model system should ideally resemble the real physical system from which the data were collected. The systems modelled in Chapters 4 and 5 consisted of controlled experiments on lab-prepared samples, while the systems modelled in this chapter are observational studies of naturally aged artefacts. Due to uncertainty in the environments which the objects were exposed to and uncertainty in the initial conditions of the objects, it was necessary to make some assumptions (approximations) when defining the model system. Convenience is another reason for simplifying assumptions, although in defence of this, sometimes one simplifying assumption can preclude the need to make several more speculative assumptions.

As in Chapter 4, the system was modelled as a CA object in a storage container at constant temperature and relative humidity. It was assumed that all the acetic acid was retained in the object. It was assumed that water concentration was constant. The sample was modelled as having initially uniform composition and reacting at a uniform rate throughout.

The assumptions about $[HOAc]$ and $[H_2O]$ may appear to imply conflicting conditions. For example, retention of acid could imply low ventilation (sealed enclosure), whereas constant moisture could imply an open (or very permeable)

enclosure that permits water to enter and replace the reacted water. Acid still tends to accumulate in museum objects over time, whether they are stored in perfectly sealed containers or not. Additionally, moisture levels are typically determined by the relative humidity in the macroenvironment, not by how much water has been consumed by hydrolysis. The assumptions are reasonable in the practical context of considering what kind of exposures to acid and water an object may encounter in a museum collection.

In Chapter 5, a model was developed which outputs AGU composition as a function of time. The model in this chapter is based on that model. While it is possible to specify the model as having different deacetylation rate constants for each acetyl group, insufficient data were available to estimate what these may be in the system that is modelled here. Although the results of Chapter 6 suggest that the deacetylation rate constants may be different in the lab conditions, these may not apply to the conditions found in museums. A pragmatic assumption is that the deacetylation rate constants are the same and equal to the deacetylation rate constant obtained in Chapter 4, using Equation 4.5 and the parameters in Table 4.4. It's important to emphasise that this is distinct from simply copying the deacetylation model in Chapter 4, as that model does not output AGU composition as a function of time.

The mass balance for acetic acid is the sum of the reaction rates for all deacetylation reactions:

$$
\begin{aligned}
\frac{d[HOAc]}{dt} = k_d[H_2O][HOAc] \sum_{m \in G} (3 \times m(236) \\
+ 2 \times (m(036) + m(206) + m(230)) + m(006) \\
+ m(030) + m(200))
\end{aligned}
\tag{6.20}
$$

The expression in the sum corresponds to the term for $[ROAc]$ in Equation 4.4.

For chain scission rate constants, the assumptions were based on literature models/equations for acid-catalysed hydrolysis of cellulose in paper degradation. It was assumed that hydrolysis of the cellulose-cellulose bond in a CA molecule is similar to the hydrolysis of the cellulose-cellulose bond in a cellulose molecule. Referring to Figure 6.5, hydrolysis of a cellulose-cellulose bond in CA is when $i =$

$j = 000$. The chain scission rate constant for a cellulose-cellulose bond is $k_{xBx(000,000)} = k_{xB(000,000)} = k_{Bx(000,000)} = k_{B(000,000)}$. This is abbreviated as k_{cc}. The cellulose chain scission rate constant k_{cc} (s^{-1}) is:

$$k_{cc} = \{(3.992256 \times 10^{14}) + (2.44512 \times 10^{17} \times [H_2O]_F) \quad (6.21)$$
$$+ (8.5104 \times 10^{21} \times [H_3O^+] \times [H_2O]_F)\}$$
$$\times \exp\left(\frac{-13109.6}{T}\right)$$

where T is the temperature (K), $[H_2O]_F$ is the mass fraction of water on a dry-weight basis, and $[H_3O^+]$ is the hydronium ion concentration (mol L^{-1}). The constants in the equation are due to Ligterink et al. (167), whose study on modelling the effects of acid on archival paper degradation is discussed in Chapter 3, Section 3.2.4. The equation draws on Zou et al. (158) and was selected here because it accounts for moisture directly in terms of how much water is in the sample. This was believed to be more reliable than cellulose paper degradation models that use relative humidity, as these models depend implicitly on the moisture adsorption isotherm of the paper and are thus less likely to apply to cellulose-cellulose hydrolysis in cellulose acetate plastic.

When applied to modelling paper degradation, $[H_3O^+]$ is calculated from the pH of the paper as measured using the cold-water leach method. The pH of CA can also be measured using the cold-water leach method, by measuring the pH of aqueous solution (prepared using 100 mL water) which contains acid leached from 1 g of sample (76,223). It was assumed that the definition of pH in CA is comparable to that of paper, and that the pH defined as such may be used to obtain $[H_3O^+]$ in Equation 6.21. Assuming that all the acetic acid is extracted from the CA sample, the concentration (mol L^{-1}) of acetic acid in the extract, $[HOAc]_L$, can be calculated from the concentration (mol m^{-3}) of acetic acid in the sample, $[HOAc]$, as

$$[HOAc]_L = \frac{[HOAc]M}{\rho V} = \frac{[HOAc]}{1.3 \times 10^6 \times 0.1} \quad (6.22)$$

where M is the mass of CA sample (1 g), ρ is the density of CA (1.3×10^6 g m^{-3}) (36), and V is the volume of extract (0.1 L). The formula to calculate $[H_3O^+]$ from

$[HOAc]_L$ depends on the dissociation constant of acetic acid in water, $K_d = 1.8 \times 10^{-5}$ mol L⁻¹ (224,225):

$$[H_3O^+] = \frac{-K_d + \sqrt{K_d{}^2 + 4K_d \times [HOAc]_L}}{2}$$

(6.23)

Equation 6.23 solves the acid-base equilibrium for a weak acid in a dilute solution, using the quadratic formula. The quadratic formula, which gives the precise answer, was used as it was found that this approach is significantly more accurate than approximate strategies for predicting pH from free acidity of CTA films (76).

The initial conditions were based on an initial DP_n of 280, DS of 3, and free acidity of 0.04 (10,37,226). These values are representative of fresh, undegraded cellulose triacetate (CTA). Environmental conditions of 21°C and 50% relative humidity were used for all the simulations, as these are standard set points for room conditions in museums (159). These conditions were used to obtain the initial water concentration (see Chapter 4), which was assumed constant as explained previously. The initial values for all chemical species are summarised in Table 6.4.

Table 6.4 Initial composition for model simulations.

Chemical species	Initial value (mol m⁻³)
$[H_2O]$	2137.2
$[HOAc]$	5.2
$[xAx](236)$	4436.0
$[xA](236)$	16.0
$[Ax](236)$	16.0
$[A](n), n \in S$	0
$[xAx](n), n \in S \backslash 236$	0
$[xA](n), n \in S \backslash 236$	0
$[Ax](n), n \in S \backslash 236$	0

6.3.3   Model hypotheses

As stated previously, this chapter aims to establish whether modelling certain chain bonds as more susceptible to degradation, due to the substitution states of the AGUs involved in the bond, gives a better fit to real-world data than the benchmark model for chain scission. The benchmark model for chain scission (H₀) expresses the hypothesis that the chain scission rate is the same for all chain bonds. The new proposed model (H₁) expresses the hypothesis that cellulose-cellulose bonds are more susceptible to chain scission than other types of bonds. This section explains how the two hypotheses were modelled.

Under the assumption that the chain scission rate does not depend on AGU composition, the logical (extreme) conclusion is that k_{cc} defines the chain scission rate constant for all the chain scission events. This means that the rate constant for any chain scission event in CA is the same as that for the cellulose chain scission event. In H₁, the non-(cellulose-cellulose) chain scission rate constants are some fraction of k_{cc}. The non-(cellulose-cellulose) chain scission rate constants k_{xx} were defined as:

$$k_{xx} = \frac{k_{cc}}{CSRR} \tag{6.24}$$

$CSRR$ stands for "chain scission rate ratio". When $CSRR = 1$, this corresponds to the assumption that chain scission rate does not depend on AGU composition, and $k_{xx} = k_{cc}$. As the ratio is increased, this corresponds to simulating that cellulose-cellulose chain bonds are more reactive than the chain bonds between other AGU pairs.

Because increasing $CSRR$ decreases the overall rate of chain scission, this makes it difficult to compare H₀ and H₁ if they are both based on the same k_{cc}. It would also be unreliable to compare the fit of models based on rate constants which were originally developed for paper degradation. For these reasons, Equation 6.21 was used as an initial guess for k_{cc} for each run of each model. Thereafter, k_{cc} was adjusted by a factor F, until the normalised root-mean square error (NRMSE) between the model and the data was minimised. The fitted cellulose-cellulose chain scission rate constant is:

$$k_{cc}^* = F \times k_{cc} \qquad (6.25)$$

For the GCI datapoints, predictions falling within the uncertainty bars were considered to have error $= 0$. For predictions falling outside the uncertainty bars, the nearest uncertainty limit was used as the reference DP_n. For each run of H1, the optimal $CSRR$ also had to be obtained, and $CSRR$ and F were optimised simultaneously using the same procedure as outlined for optimising factor F alone. The fitted non-(cellulose-cellulose) chain scission rate constant is:

$$k_{xx}^* = \frac{k_{cc}^*}{CSRR} = \frac{F \times k_{cc}}{CSRR} \qquad (6.26)$$

The inputs for the model have now been fully defined. Figure 6.7 summarises the inputs and outputs of the model.

$[H_2O]$
$[HOAc]_0$
Initial AGU composition
Temperature
Rate constants

MODEL

$DP_n(t)$
$DS(t)$
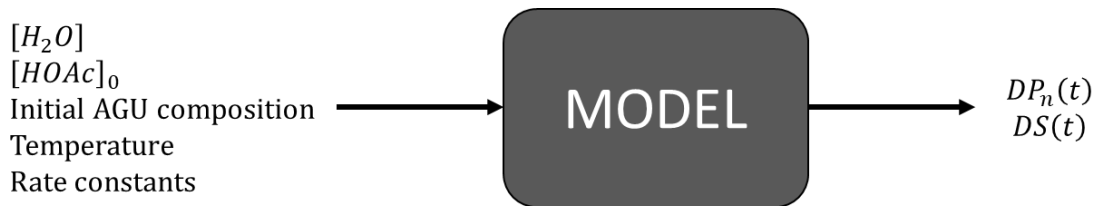
Figure 6.7 Model inputs and outputs.

6.4 RESULTS AND DISCUSSION

6.4.1 Training

The models were trained on all the data ($n = 17$), obtaining the results in Figure 6.8 and Table 6.5.
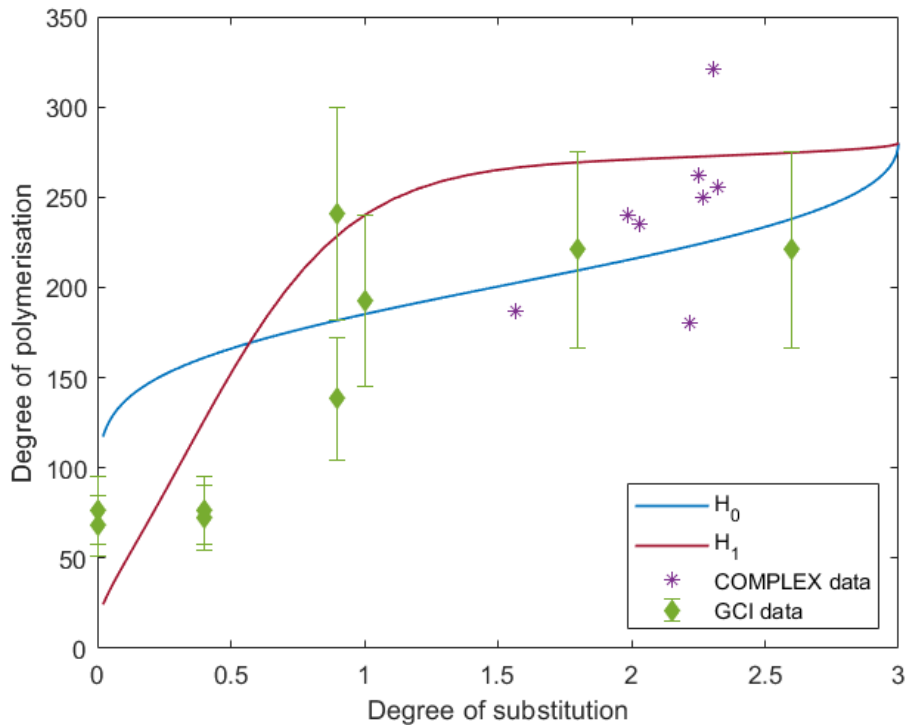
Figure 6.8 DP_n vs. DS of models fitted on all $n = 17$ data points, and the data.

Table 6.5 Fitted parameters.

Parameter	H_0	H_1
$CSRR$	1*	171.28
F	2.98	56.2

*Specified as a constant; not a fitted parameter.

Figure 6.9 shows the simulated DP_n vs. time for the two models. In Figure 6.10, chain end concentration and cellulose AGU mole fraction are plotted against time. The cellulose AGU mole fraction is the same for both models. The simulations of DS and pH vs. time are the same for both models (Figure 6.11), as they have identical deacetylation models.
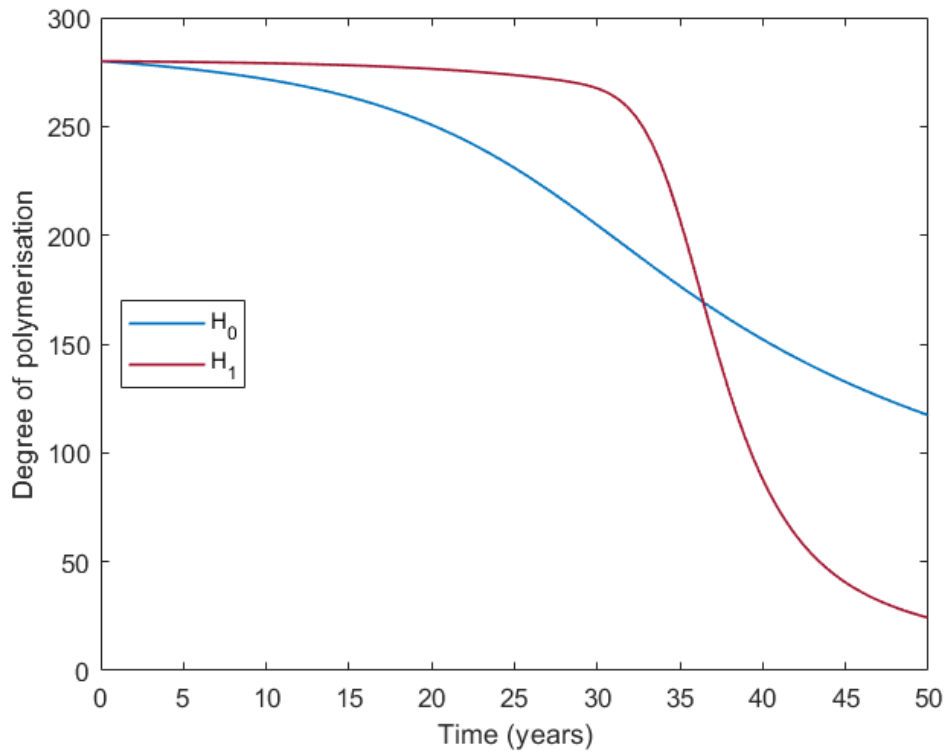
Figure 6.9 Simulated degree of polymerisation vs. time.
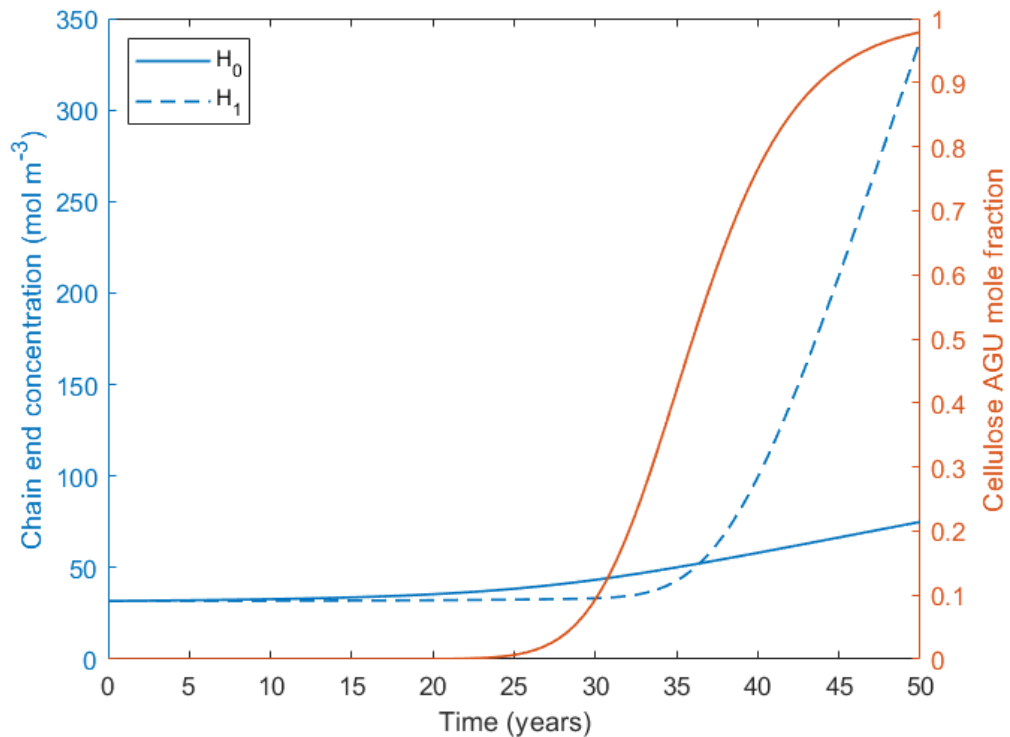
Figure 6.10 Simulated chain end concentration and cellulose AGU mole fraction vs. time. The cellulose AGU mole fractions (orange line) for H_0 and H_1 coincide as they have the same deacetylation model.

141
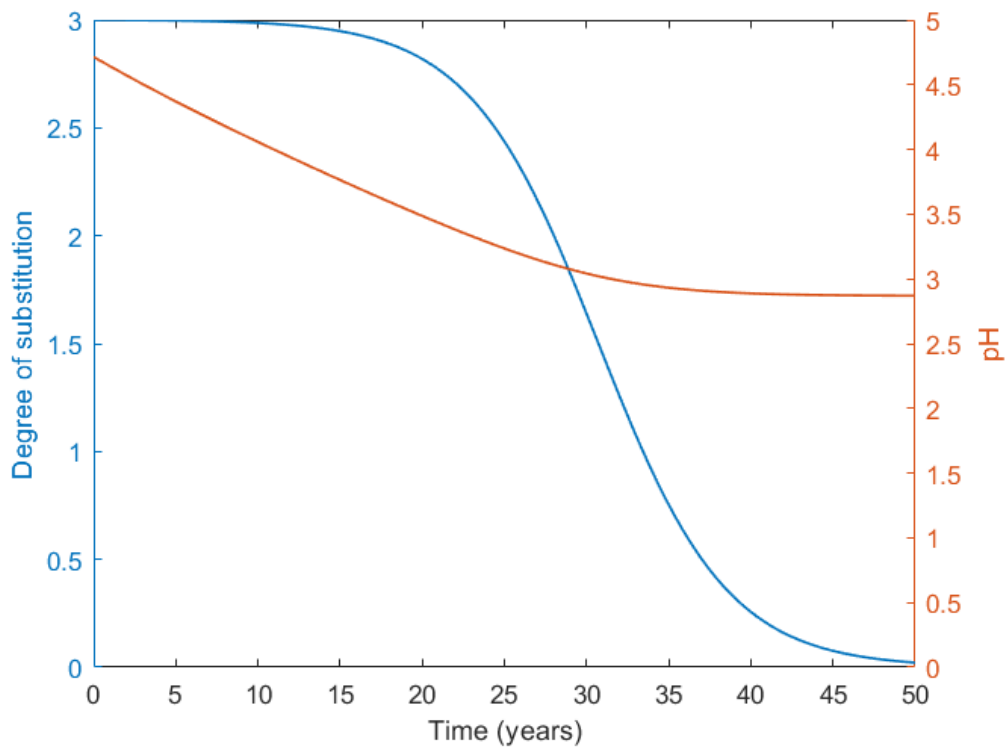
Figure 6.11 Simulated degree of substitution and pH vs. time.

In Figure 6.9, H₀ predicts a consistent, continual decline in DP_n, while H₁ predicts that DP_n appears stable for a prolonged period (about 32 years, in this example) before declining rapidly over a relatively short period (about a decade). Thus, by H₁, most of the degradation occurs in a timespan that is short relative to the lifetime of the material.

Chain ends are the products of chain scission. Chain end concentration corresponds to the yield of the chain scission reaction, and the gradient with respect to time of chain end concentration is proportional to the rate of chain scission. In Figure 6.10, the chain end concentration of H₀ appears more linear throughout than H₁. The reason it is not perfectly linear is because k_{cc}^* is not quite constant in H₀, it varies with the pH. As pH decreases over time, k_{cc}^* increases slightly. The rate of chain scission in H₁ increases following the rise in cellulose AGU mole fraction, as cellulose-cellulose bonds are more susceptible to chain scission in this model.

Based on the trained parameters, H₀ and H₁ have different implications for how the model of the rate of chain scission in paper cellulose compares to the model of the rate of chain scission in CA. H₀ finds that k_{cc} is an underestimate; $F = 2.98 > 1$. So, the rate of chain scission in H₀, which is the same for all types of chain bonds, is predicted to be about three times as much as initially estimated using Equation 6.21. In H₁, $F = 56.2 > 1$ also says that Equation 6.21 significantly underestimates the rate of chain scission in cellulose-cellulose bonds in CA. However, $k_{xx}^*/k_{cc} = F/CSRR = 56.2/171.28 = 0.33 < 1$. Therefore, H₁ predicts that Equation 6.21 overestimates the rate of chain scission between non-(cellulose-cellulose) bonds, while for H₀, Equation 6.21 underestimates it. These findings show that the direction (overestimate or underestimate) of the error of approximation, which is what Equation 6.21 is, depends on the assumptions of the model.

The result in H₁ that $CSRR \gg 1$ is consistent with the original hypothesis that cellulose-cellulose bonds are more susceptible to chain scission than non-(cellulose-cellulose) bonds, i.e., the rate of chain scission of non-(cellulose-cellulose) bonds is less than the rate of chain scission of cellulose-cellulose bonds. The concept of $CSRR$ is novel, with nothing analogous found in the literature review. It is therefore not possible to compare the result in Table 6.5 with any reference values, as there appear to be no precedents. Clearly from Figure 6.8, $CSRR = 171.28$ produces a noticeably different relationship between DP_n and DS, from $CSRR = 1$. From a qualitative perspective, H₁ appears to be better at simulating the sharp downtrend in DP_n that occurs below DS $= 1$. H₀ is not able to simulate this behaviour. Furthermore, this difference is explainable in terms of the theory and assumptions underlying the models.

6.4.2 Validation

To evaluate the models' performance, one needs the out-of-sample (OOS) error when the model makes a prediction on samples not used to train the model. In Chapter 4, this was the model's error on the test dataset. Because the data for the models in this chapter are limited, it was not possible to have a test dataset. However, it is possible to obtain the cross-validation (CV) errors by splitting the training dataset and comparing the CV errors of H₀ and H₁. To generate the CV

folds, the Leave One Out procedure was used. Each of the 17 CV datasets consisted of the original data but omitting one of the datapoints. For each CV fold, the models were trained on only 16 datapoints. The models then make a prediction for the datapoint omitted in the training. The root square error (RSE) of this prediction is the CV fold error. Figure 6.12 shows the results of this.
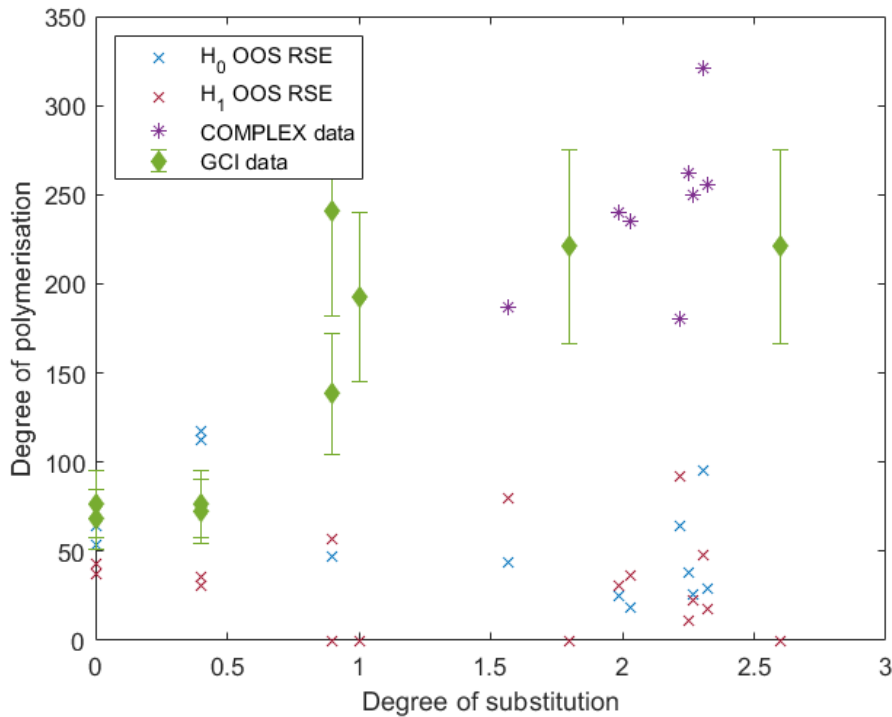
Figure 6.12 Out-of-sample errors of each model on each data point that was left out of the ($n = 16$) training. The RSE has the same units as DP_n, as it is the error on the DP_n prediction. The errors are plotted against the DS of the data point on which the OOS prediction was made.

Table 6.6 Results of Leave-One-Out cross-validation.

Statistics	H_0	H_1
Mean OOS RSE	43.2	31.9
Std. OOS RSE	37.9	27.1
% max OOS RSE	47.1	29.4
Mean $CSRR$	1*	158.4
Std. $CSRR$	0*	55.9
Mean F	2.34	62.5
Std. F	0.73	10.5

*Specified as a constant; not a fitted parameter.

144

Due to the uncertainty in the GCI data, it was feasible to obtain RSE = 0 on these datapoints. In these cases, the errors for both models coincide, and only one marker may appear in Figure 6.12. Table 6.6 compares the distributions of the errors of the models, as well as statistics for $CSRR$ and F. The % max OOS RSE is the percent of CV folds in which each model had the highest OOS RSE. Because sometimes both models had RSE = 0, the values in this column add up to less than unity. Excluding the CV folds where the models had the same RSE, the revised % max OOS RSE is 61.6 and 38.4, for H_0 and H_1 respectively. Based on H_0 achieving higher mean OOS RSE than H_1 (43.2 vs. 31.9) and having a higher RSE than H_1 for a larger proportion of folds (47.1% vs. 29.4% over all folds, 61.6% vs. 38.4% excluding cases where the models were tied), the quantitative results suggest that H_1 may be a better fit for modelling this data than H_0.

6.5 CONCLUSIONS

To investigate the hypothesis that deacetylation leads to chain scission by increasing the prevalence of cellulose-cellulose bonds (which are believed to be more susceptible to chain scission), a novel mathematical framework was developed. The framework uses the outputs of the deacetylation models of Chapters 4-5, which provides the concentration of cellulose AGUs. A probabilistic model estimates the expected frequency of cellulose-cellulose bonds based on the concentration of cellulose AGUs. The parameter $CSRR$ (chain scission rate ratio) quantifies how much more susceptible the cellulose-cellulose bonds are to chain scission than non-(cellulose-cellulose) bonds. By either setting $CSRR = 1$ or allowing it to vary (by fitting to data), the mathematical framework can express two models, a benchmark H_0 (cellulose-cellulose bonds are same as other bonds) and the proposed H_1 (cellulose-cellulose bonds could have different susceptibility to chain scission than other bonds). When the models were trained on cross-sectional DP_n vs. DS data from samples of naturally aged historical CA objects, H_1 obtained the result $CSRR = 171.28$, showing that according to this model, cellulose-cellulose bonds could have chain scission rate constants 171.28 times bigger than the chain scission rate constants of non-(cellulose-cellulose) bonds. From a qualitative perspective, H_1 is better at simulating the plateau behaviour at higher DS with sharp reduction in DP_n at lower DS. H_0 cannot simulate this sharp

decline. Cross-validation indicated that H_1 outperforms H_0 on predictions made on unseen data, suggesting that this new model could be more representative of reality than the old benchmark.

In general, coupling depolymerisation to deacetylation by a dependence on AGU composition appears to be a promising direction, based on these simulations. The interpretation and significance of the modelling research in the context of heritage conservation is the topic of the following chapter.

7 IMPLICATIONS FOR HERITAGE CONSERVATION

This chapter is written for heritage scientists and conservation professionals interested in understanding the implications of the modelling research for heritage conservation. It discusses:

- *innovative features of the models, in non-technical terms*
- *predictions of cellulose triacetate film permanence*
- *practical aspects of developing models of cultural heritage artefacts*
- *how biases in data could affect modelling research*
- *whether models can be expected to have significant implications for heritage conservation.*

The chapter includes materials from a paper I authored and published (178), which is the same paper referred to at the start of Chapter 4.

7.1 INTRODUCTION

"All models are wrong, but some are useful." (227)

In the last three chapters, the technical details of models of cellulose acetate (CA) polymer degradation were developed in great depth and detail. The performances of the models were tested using objective methods to assess accuracy, or it was demonstrated in principle how one might do so were more data to become available. This chapter aims to address the more subjective aspects of the models: Are these models useful? How? What (if any) consequences do they have for decision-making in museums and archives? The chapter also discusses some of the challenges of developing "useful" models for heritage conservation, and the risks and limitations of modelling itself to the heritage field.

A high-level summary of the models and their key innovations benefits the discussion. The research focused on modelling chemical reactions which alter (degrade) the CA polymer molecule, deacetylation, and chain scission. Deacetylation, associated with the vinegar syndrome, is (under certain circumstances) a self-accelerating process due to the production of acetic acid,

which may increase the rate of degradation when it stays in the object. This is known as autocatalysis and is represented as a *positive feedback* loop in the mathematics of the models (see Figure 7.1). As deacetylation advances, CA monomers are transformed into cellulose monomers. Chain scission, associated with brittleness and mechanical damage, tends to follow deacetylation. Empirical evidence as well as hypotheses proposed by other researchers suggest that this could be due to changes in monomer composition caused by deacetylation, leading to more susceptible links between the monomers (100,101,104). Links between cellulose monomers may be more susceptible to chain scission than links between CA monomers (108). When chain bonds between monomers break, the bonds are converted to chain ends, and the average size of the polymer molecules decreases as bigger molecules split into smaller ones. The relationship between the outputs of deacetylation to the inputs of chain scission characterises a *cascade process* (see Figure 7.1).

The models represent causal relationships between these processes which take place *inside* the object. This is a departure from earlier modes of analysis in heritage science, which focus on the effects of the *external* environment e.g., temperature and relative humidity (Figure 7.2).
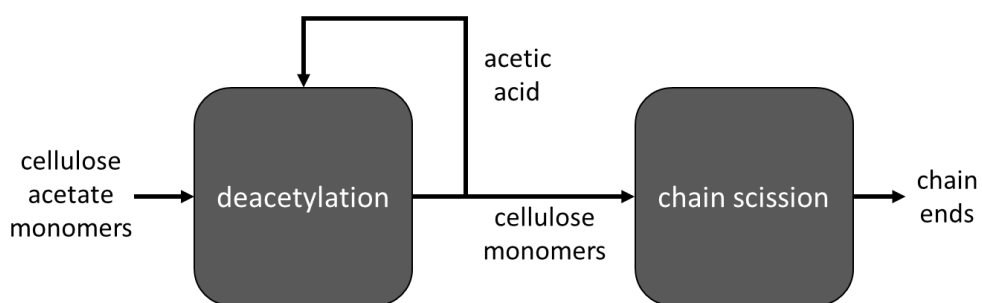
Figure 7.1 Model representing internal structure of the system. Deacetylation involves a positive feedback loop, due to the effect of acetic acid autocatalysis. Outputs from deacetylation are inputs to chain scission, illustrating the causal link between the processes.
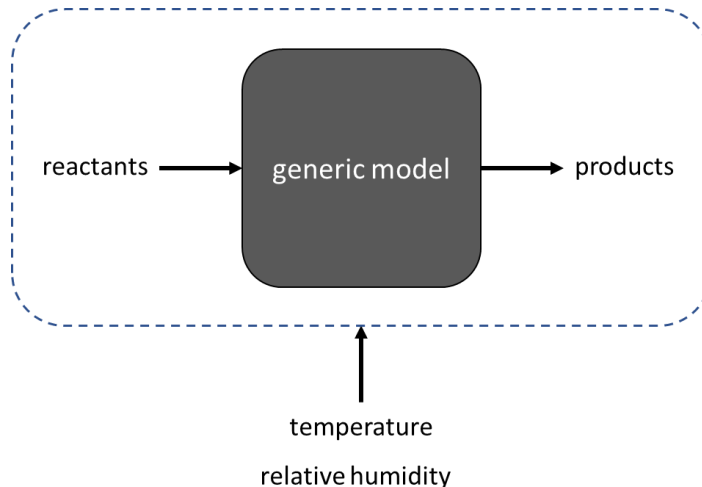
Figure 7.2 Model representing effects of external factors on the system. The internal structure of the system itself is a "black-box".

The impact of exogenous factors on deterioration has obvious relevance for decision-making in preventive conservation, as these are independent variables which could be controlled by a conservator to reduce the rate of degradation in objects in a collection. Why study the internal workings of the system?

One independent variable which is implicit in both the representations in Figures 7.1-2 is time. Outer-focused models have tended to assume that the extent of degradation is approximately proportional to time elapsed, all other factors (e.g., temperature and relative humidity) being constant. This property is known as linearity. It means the rate of degradation is constant. In a non-linear system, the rate of degradation could vary over time, even when temperature and relative humidity are the same. The inner-focused models developed in this thesis can model non-linear degradation. More importantly, unlike a "black-box" representation of non-linearity, these models provide physical insight and knowledge required to alter the relationship between input and output. While this may sound theoretical, the application of these concepts has profound implications for practical assessment of collection risk.

7.2 CELLULOSE TRIACETATE FILM PERMANENCE

Guidelines for cellulose triacetate (CTA) cinematographic film conservation provide estimates for film permanence in terms of the number of years for fresh

film to reach a free acidity of 0.5, when stored under specified temperature and RH (14). These are intended as "worst-case scenario" estimates, where it is assumed that the maximum amount of acetic acid is retained in the film base, as these were the conditions from which the guidelines extrapolated. However, the guidelines assumed a constant rate of reaction during the induction phase and did not take into account catalysis by newly generated acetic acid. The assumption of maximum acid retention is necessary for the guidelines because it permits the free acidity to be used as a direct measure of the extent of the reaction, not because the effect of acid on the reaction rate is modelled. The data used for training the autocatalytic model (Chapter 4) are from the same experiments on which the guidelines are based, therefore any differences between the model's predictions and the guidelines are due to the theory that was applied in each. The values for the film permanence predicted by using the autocatalytic model and by the guidelines as a function of temperature are shown in Figure 7.3, with initial moisture-conditioning at 20, 40 and 60% RH. No equation is provided by the guidelines, so the tabulated point values are plotted instead.
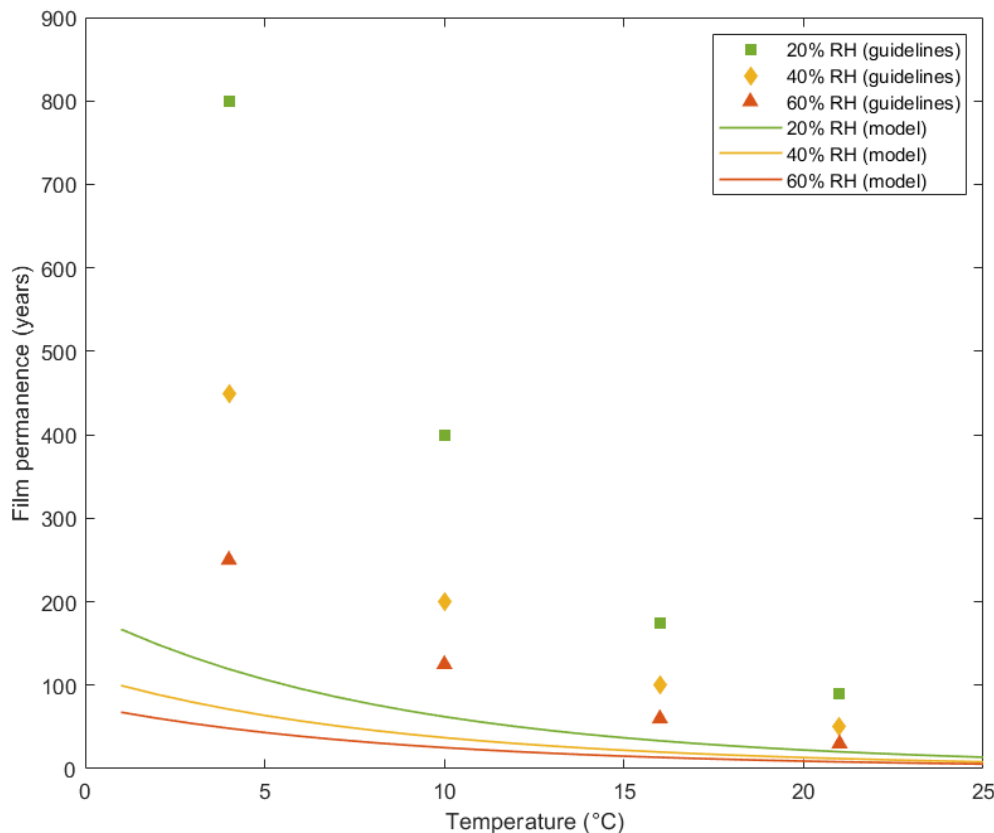
Figure 7.3 Model and guideline predictions of CTA film permanence.

The model predicts that the film permanence is less than what is stated by the guidelines at every RH and temperature, with the magnitude of the gap increasing at lower temperatures. For example, at 40% RH and 21 °C the guidelines say the film permanence is 50 years and the model predicts 12.1 years (37.9 years difference, or 75.8% less), but at 40% RH and 4 °C, the guidelines say the film permanence is 450 years and the model predicts 71.2 years (378.8 years difference, or 84.2% less).

Most likely, the reason that the model and the guidelines do not agree is that the model accounts for the effect of autocatalysis, while the guidelines do not. Other possible differences between the model and the guidelines, for example in the assumptions about moisture content, cannot explain the discrepancy between the two sets of predictions. Because the guidelines are based on the extrapolation of data of film conditioned at 21 °C and the specified RH prior to sealing in an air-tight enclosure, it was assumed that the initial moisture content in the model corresponds to that at 21 °C, rather than the equilibrium moisture content at the storage temperature (14). This is the "best-case scenario" with respect to moisture, as moisture content increases with lower temperature (121). Moreover, if the moisture content was maintained at constant levels while somehow ensuring maximum acid-trapping, this would result in higher moisture content throughout, as it would counter the depletion of water that otherwise occurs in the closed system. Either of these assumptions—moisture-conditioning at the storage temperature, or constant moisture levels—increases the reaction rate, reducing the predicted film permanence further.

Another important difference between the model and the guidelines, which is a consequence of accounting for autocatalysis vs. not doing so, is that the model and the guidelines have different sensitivity to temperature. The apparent activation energy E_a is a parameter that determines how degradation rate (and so film permanence) varies with temperature. With the autocatalysis model, the activation energy is 70.7 ± 10.1 kJ mol^{-1}. The activation energies for the guidelines are 87.9-92.0 kJ mol^{-1}. The larger activation energy is why the guidelines predict that temperature reduction has a greater effect on film permanence than the autocatalytic model does—the guidelines have higher temperature sensitivity.

Several factors are believed to influence the rate of CTA film degradation. These were already discussed in Chapter 2 and are summarised in Table 7.1 for convenience. It is not well-established how much these factors contribute to degradation relative to temperature and RH, nor are the complex interactions between different factors well-characterised.

Table 7.1 Factors that affect CTA film degradation (deacetylation). Exogenous factors refer to external or environmental causes, such as those that may be implemented by conservation professionals. Endogenous factors refer to attributes of the material/object.

Factors	Examples of effects
Exogenous factors	
Temperature	Increasing the temperature increases the deacetylation rate constant.
Relative humidity	Water is a reactant in the hydrolysis of CTA.
Enclosure design	Tightly sealed storage containers have been found to prevent acetic acid from escaping from the film, increasing the potential for autocatalysis (12,93); ventilated containers facilitate the escape of acetic acid (129).
Enclosure material	Iron cans accelerate the degradation rate compared with other materials, for example glass (26).
Reel winding tension	In ventilated or open enclosure designs, which permit acetic acid to escape, the acid is able to diffuse faster out of the film if the reel is wound less tightly (31).
Acid-neutralising inserts	These contain a base such as calcium carbonate which reacts with acetic acid to neutralise it (31).
Acid or moisture adsorbents	Molecular sieves can aid in the removal of acid from the film, or protect it from RH fluctuations (31,129).
Endogenous factors	
Residual process reagents	Impurities which come from processing reagents may help to catalyse the reaction (13).
Residual manufacturing impurities	For example, sulphuric acid (13).
Emulsion layer	Based on gelatine, the emulsion layer may act as an acid-scavenger (26).

It is widely recommended that cold storage is the best option to prolong the life of film, which implies that temperature has the greatest impact relative to other (exogenous) factors, or that it is the most cost-effective (10,120,133). This may be true, and the model does not necessarily dispute this. Controlling the macroenvironment is often the cheapest option, next to doing nothing (70,228). In many cases, this will make it the only option that conservators can realistically pursue. However, the model suggests that the impact of cold storage (and low RH) on prolonging the life of film is less than what is set out by the guidelines. This should be of critical interest to CTA film archivists who are using these guidelines to inform the preservation strategy for their collections.

Bearing in mind the model errors and the variability in real collections compared with the idealised model system, the magnitudes of the predicted film lifetimes are notable, compared to the guidelines, for three reasons. First, cellulose acetate has only existed for about 150 years (33). It is therefore impossible to validate the accuracy of any predictions which exceed this timeframe. The model predictions are within a timeframe that make it possible to test against real collections. Second, based on the model, there are archives which are already or very soon will be past the point of vinegar syndrome, much earlier than expected even with cold storage. This risk should be addressed immediately. Third, the timescales of the model predictions are within the scale of the human lifetime, the age of an institutional archive, and even the duration of employment for a film conservator. This compels the responsibility of present-day custodians of film collections to initiate alternative long-term strategies, for example digitisation, as it may not be an option to leave this to their successors.

7.3 What is important to model about cultural heritage artefacts?

The threshold of 0.5 free acidity is somewhat arbitrary as it is underpinned by the notion that deacetylation is autocatalytic before this point, a notion that the model proposed in this thesis rejects. However, the threshold facilitates comparison between the relative rates of degradation predicted by the model and the guidelines. It may be worth establishing other criteria or values-based functions to

evaluate film fitness-for-use, or even a range of options of such, since there are several types of damage that could render film "unfit", and they may occur at different rates depending on the film characteristics and storage environment. For example, the models in this thesis have been combined with a model of plasticiser loss from CA developed by COMPLEX researcher Argyro Gili, to predict deacetylation and plasticiser loss simultaneously. I recommend the development of values-based functions and/or fitness-for-use thresholds which are independent from the assumptions of the degradation model. This modular approach would make it easier to change the degradation model (for example, by accounting for autocatalysis throughout) without it affecting the validity of the fitness-for-use threshold (for example, the relevance of free acidity $= 0.5$ as a critical point). This could also benefit the study of the effects of environmental factors when these are specified in the degradation model assumptions. For example, the 0.5 free acidity cut-off is only meaningful for a closed storage container where all the acetic acid is retained in the object.

While the autocatalytic model is conceptually general, the parameters were fitted on CTA film data, and it may not be reliable for predicting deacetylation in objects made from thicker films or CA sheets, such as sculptures or fashion accessories. Such objects tend to be made of lower-DS CA such as cellulose diacetate (CDA) and may have different plasticisers or additives. The model may be less accurate for predicting CDA permanence. In terms of the deacetylation model, which includes autocatalysis (Chapter 4) and AGU composition (Chapter 5), while in theory it is applicable to modelling any kind of CA artefacts, in practice, the parameters of the model should be fitted to data collected from samples that are most like the types of objects one wishes to make predictions about. This may include training the model separately on CTA and CDA photographic film data. It would probably also make sense to train the model separately for non-film CDA objects and CDA photographic films.

There are several other differences between modelling degradation in CA films and non-film artefacts which affect the practical application of modelling methods. Besides objective differences in physical and chemical characteristics, there are differences in what qualities are subjectively valued in films and non-film artefacts.

Films are typically valued for their information-storing qualities. There is the option of transferring the information to another medium (such as digital) if not the same medium (a fresh CA film base), although this is typically cost-prohibitive in the short- to medium-term. Films have a certain fungibility. On the other hand, mitigating image deterioration is very important, as this would prohibit the original information from being preserved via duplication. Most of the forms of damage that are relevant to non-film objects—yellowing, warping, cracking, blooming—would also likely harm the image-storing performance of films, but non-film objects do not need to store images. Here, physical change due to chemical deterioration also precludes faithful duplication of films. However, non-film objects are valued for other properties, which may also vary widely between different objects. So, not only would it possibly be harder to train a CA degradation model to create a dose-response function for non-film CA artefacts, due to larger variation in objective physical qualities, but it would also likely be complicated to develop values-based functions for these objects, due to the variety in subjective qualities of value.

Films and non-film artefacts are stored and accessed in different ways. The microenvironment and the physical shape of CA artefacts can impact mass transport processes such as diffusion, evaporation, and absorption. To model the objects as having uniform composition, assumptions were made about the microenvironment and the shape of the objects, such as the use of sealed enclosures with negligible air volume inside the enclosure (the object volume is large relative to the total volume inside the enclosure). These assumptions are probably most consistent with cinematographic film reels stored inside cans. The reaction terms of the models may still be used in mass balances account for mass transport processes, among other things, although this adds complexity.

7.4 LIMITATIONS OF DATA

I have presented evidence to argue that the non-linear models I developed fit the data better than simpler linear models. However, it is possible that features of the data are caused not by some underlying phenomenon, but by other factors that bias the shape of the data considered for study. This is particularly true for non-

empirical data such as the cross-sectional studies included in Chapter 6. One aspect of the data in Figure 6.6 that is not explained/simulated by this model is the plateau around DP = 70, which appears to be reached by around DS = 0.4.

In a condition survey of archival paper, DP < 300 was identified as the approximate limit below which the materials become "unfit for use" (155). What such a limit would mean in the context of CA artefacts is unclear—as discussed in Section 7.3, this depends not only on the material properties but also the desired use of the object. For CA these uses are diverse—CA artefacts include archival records such as photographic film, (formerly) functional objects such as combs and cutlery, and objects of artistic value such as sculptures. If there exist objective physical criteria (i.e., critical DP threshold) which define the state at which an artefact is considered subjectively "unfit for use", these are likely to vary considerably between the many types of objects which are made of cellulose acetate. Regardless, there likely exists a limiting DP below which an object is too damaged to remain part of a collection or is otherwise excluded from sampling. An interesting possibility is that if this is the case, then there may be few or no empirical observations of degraded CA artefacts with DP below this threshold, as it may no longer be feasible to make measurements or gather data on these samples.

DP as low as 31 has been measured for cellulose acetate degraded in solution of acetic anhydride, but as the polymer was already dissolved, it was not a selection criterion that the polymer with this DP possessed mechanical integrity or a "fitness for use" beyond fitness for the measurement method (viscometry) (180). This reasoning could explain the apparent plateau in DP around this level in surveys of naturally aged objects. This kind of "survivorship bias" should be considered when evaluating the data obtained by condition surveys, particularly when analysing patterns at the extreme end of degradation. More generally, data obtained by non-empirical means, such as cross-sectional studies, are susceptible to selection bias. However, similar issues may still arise when models are based on empirical data, for example samples may be rejected for measurement. Individuals interested in interpreting model predictions should be alert to overfitting patterns in data that may have been caused by selection bias, rather than some underlying degradation process.

7.5 MARGINAL UTILITY OF MODELLING

As the previous example shows, there is a risk of overfitting when non-linear behaviour is attributed to non-linear dynamics, rather than to outside forces that could bias the data. If this is a case of "false positive" (non-linearity) error, the "false negative" error is another risk. This means modelling as linear dynamics when non-linearity is observed, and (mis)attributing endogenous non-linearity to exogenous factors. For example, the artist Naum Gabo blamed the unexpected rapid deterioration of his sculpture *Construction in Space: Two Cones* (1927) on the Philadelphia Museum of Art, where the artwork had been stored (18). Yet the replica he made, which is kept at Tate today, also suffered from severe deterioration (19). Based on what is known about CA degradation today, it is far more likely that the instability of Gabo's artworks was due to the inherent instability of the materials, not the perceived lack of care from conservators.

Steps to avoid both types of errors include having awareness of the errors and what causes them; understanding of where the data came from and how it was collected; having a scientific hypothesis (prior belief) about cause and effect that can be updated with more data; and applying sensible statistical modelling practices such as estimating test errors on a test dataset separate from the training dataset.

As the CTA film permanence predictions demonstrate, accounting for non-linearity can also change the predicted effects of exogenous factors. For example, cold storage is not predicted to prolong film life as much as the guidelines would suggest. This is mainly because the autocatalytic model found a reduced temperature sensitivity, compared with the linear model (guidelines). Thus, the inner-focused modelling perspective (Figure 7.1) has implications for the outer-focused perspective (Figure 7.2).

Assuming the models are not overfit, are more complex models always better? Are they more *useful?* More complex models tend to involve a greater cost than simpler ones, in terms of resources required to develop them. They may also require more resources to be used, for example knowledge of more inputs. There is a trade-off between accuracy and effort.

One might therefore ask, what is the marginal utility (where utility may be defined subjectively) gained from more complex models? If a simple model and a complex model make similar predictions of permanence, then it is more economical to use the simple model, as the additional resources required to use the complex model do not yield additional utility. If they differ, then the *direction* in which a simple and a complex model's predictions of risk differ also matters. In the case of CTA film permanence, the autocatalytic model predicted *increased* risk compared to the benchmark model (guidelines). Underestimation of risk is usually a more concerning issue than overestimation of risk in heritage conservation.

For chain scission (Chapter 6), although the benchmark and the proposed model make discernible predictions on the training dataset, it is not possible at this stage to make any recommendations based on this. First, without a values-based function or fitness-for-use definition, it is not possible to interpret the two models as making different predictions for permanence even on the training datasets. While there is, broadly speaking, agreement that more degradation is correlated with diminishing value, the nature of the values-based function and fitness definition depending on DP (and/or DS) does not yet exist for CA artefacts. The models make similar predictions down to a DS of about 0.9, where the curves intersect, before diverging. The condition survey which was carried out on the samples included in the training data does not clearly suggest a threshold DP or DS (or combination thereof) that could be used to define permanence (222). So, although the models clearly represent different degradation rates, particularly in later stages of degradation, it is not possible to say from the training data alone whether they might predict different lifetimes. Secondly, without reliable data at different (known) temperatures, it is not possible to fit the activation energies for each model, which gives the temperature sensitivity. As was seen with the vinegar syndrome model, the difference between the non-linear model and the linear benchmark may be magnified when the models are extrapolated to lower temperatures, due to the difference in the temperature sensitivity implied by each.

7.6 CONCLUSIONS

Models of CA polymer degradation which focus on endogenous factors are innovative in heritage science, but their utility for practical applications is not guaranteed. In the case of the autocatalytic deacetylation model, the existence of a well-established benchmark (IPI guidelines) to compare against makes it possible to conclude that the autocatalytic model has marginal utility, because it implies, to a significant degree, that current policies (i.e., cold storage) are not as effective at reducing risk as was previously believed. The main issues limiting application of the chain scission model are lack of experimental data, values-based functions, and fitness-for-use definitions. There are numerous challenges in collecting data on deterioration in CA cultural heritage artefacts, which will be necessary to further develop the chain scission model and any future models of CA degradation. However, complex models risk overfitting training data. Even if this is avoided, improvements in collections care may not necessarily be achieved by increasing the accuracy of model predictions, as the information provided by the models may not make any practical difference when it comes to selecting between policies of action. Such models could enhance scientific understanding of degradation phenomena, but heritage scientists and conservation professionals interested in using models to influence decision-making in museums and archives should manage their expectations and prioritise the allocation of resources accordingly.

8 CONCLUSIONS

This research project set out to mathematically model the dynamics of deacetylation and chain scission in cellulose acetate (CA) artefacts. Based on empirical evidence and hypotheses put forth by earlier researchers in the field, autocatalysis in deacetylation and increased susceptibility of deacetylated anhydroglucose units (AGUs) to chain scission were identified as underlying phenomena which could lead to non-linear degradation dynamics. The mathematical models proposed in this thesis succeed as representations of existing knowledge about how CA polymer degradation works. In this sense, these models on their own do not tell us anything fundamentally new from a scientific perspective. However, the models facilitate the generation of hypotheses which may be tested against experimental data, including that not yet available, as was demonstrated at various points. Furthermore, predictions based on the models may be used to inform decisions made by conservation professionals.

The focus on modelling relationships between degradation processes, rather than the effect of the environment on degradation, is a novel mode of analysis in the context of heritage conservation. While acid-catalysed models of deacetylation have been proposed previously, this is the first time that an autocatalytic model of deacetylation was trained, tested, and used to make predictions for CTA film lifetimes. These predictions suggest that the current guidelines significantly underestimate the risk to archival film collections. The principles of the AGU composition-deacetylation model are not new, but the use of this type of model to connect deacetylation to chain scission is original. Furthermore, the chain scission model is the first model of deacetylation-dependent chain scission that can predict degree of polymerisation over time.

While it was not possible (due to lack of data) to apply the AGU composition-deacetylation model to samples or conditions more similar to those found in museums, the application of the AGU composition-deacetylation model to published lab data nevertheless had some interesting outputs. First, lower DS does not appear to (consistently) increase the propensity for remaining acetyl groups on an AGU to react. This casts doubt over the role of steric hindrance in

160

deacetylation, or at least, demands a more nuanced explanation. Second, the results disagree with the original interpretation by the authors of the study where the data came from, which attributed the apparent order of reactions to the order of electron density of the hydroxyl groups of cellulose. The mathematical model showed that under closer examination this order of preference for reacting at certain positions was not conserved; therefore, another explanation is required.

The role of substitutions on depolymerisation of cellulose derivatives is a broad topic with extensive applications ranging from medicine to green plastics. In Chapter 6, this thesis proposes the first ever mathematical model to couple two degradation processes in a cellulose derivative, the substitution reaction, and the chain scission reaction, modelling the kinetics of both simultaneously. The model has already obtained promising results by outperforming the benchmark (which does not couple these two reactions) on cross-sectional data of naturally aged historical CA objects.

While effects of environmental conditions on CA degradation was not the focus of the research, the models made some connections to these. First, the models assumed that all acetic acid was retained in the object, which requires a closed storage enclosure. This was an essential assumption to study the kinetics of autocatalysis. Therefore, the predictions only apply to systems in which this environmental condition is met. Second, the autocatalytic model of deacetylation found a reduced temperature sensitivity in terms of lower activation energy E_a, compared with the non-autocatalytic model as implied by the Image Permanence Institute guidelines. This showed that modelling interactions between the internal structure of the system (see Figure 7.1) has consequences for predicting the effects of external factors (see Figure 7.2).

As discussed in Chapter 7, the potential benefits of these models to heritage conservation are complicated. The discovery that risk to CTA film may be underestimated is an important result of the autocatalytic model of deacetylation, with urgent consequences for film conservation. Modelling of AGU composition and chain scission were comparatively limited due to lack of experimental data (and could thus be benefitted by more data), but the effects of these types of degradation on value is less quantified. As we have seen, the use of the threshold

"free acidity = 0.5" for evaluating the impact on value due to deacetylation is somewhat arbitrary under the assumption that autocatalysis is present before and after the threshold. It would be more useful to define fitness-for-use thresholds independently from the assumptions of the degradation model. Although there is ample evidence that deacetylation and chain scission are associated with tangible damage, diminishing the perceived value of CA artefacts, a more quantitative analysis of the relationship between CA degradation and damage, for example values-based functions and fitness-for-use thresholds, would increase the potential utility of degradation models for conservation of CA cultural heritage conservation.

BIBLIOGRAPHY

1. de la Torre M. Values and Heritage Conservation. Heritage & Society. 2013;6(2):155–66.

2. Strlič M, Thickett D, Taylor J, Cassar M. Damage functions in heritage science. Studies in Conservation. 2013;58(2):80–7.

3. Bell N, Cassar M, Strlič M. Evidence for Informed Preservation Planning and Advocacy: A Synoptic View. Studies in Conservation. 2018;63(sup1):8–14.

4. Allen NS, Edge M, Appleyard JH, Jewitt TS, Horie C v., Francis D. Degradation of historic cellulose triacetate cinematographic film: The vinegar syndrome. Polymer Degradation and Stability. 1987;19(4):379–87.

5. Horvath DG. The Acetate Negative Survey: Final Report. Holden MS, editor. Vol. 2, Topics in Photographic Preservation. Photographic Materials Group of the American Institute for Conservation of Historic & Artistic Works; 1988.

6. Shashoua Y. Inhibiting the inevitable; current approaches to slowing the deterioration of plastics. Macromolecular Symposia. 2006;238:67–77.

7. Edge M, Allen NS, Williams DAR, Thompson F, Horie V. Methods for predictive stability testing of archival polymers: A preliminary assessment of cellulose triacetate based motion picture film. Polymer Degradation and Stability. 1992;35(2):147–55.

8. Adelstein PZ, Reilly JM, Nishimura DW, Erbland CJ, Bigourdan JL. Stability of cellulose ester base photographic film: part V - recent findings. Society of Motion Picture & Television Engineers Journal. 1995;104(7):439–47.

9. Williams RS. Care of Plastics: Malignant plastics. WAAC Newsletter [Internet]. 2002 [cited 2019 Aug 8];24(1). Available from: http://cool.conservation-us.org/waac/wn/wn24/wn24-1/wn24-102.html

10. Adelstein PZ, Reilly JM, Nishimura DW, Erbland CJ. Stability of cellulose ester base photographic film: part I - laboratory testing procedures. Society of Motion Picture & Television Engineers Journal. 1992;101(5):336–46.

11. Adelstein PZ, Reilly JM, Nishimura DW, Erbland CJ. Stability of cellulose ester base photographic film: part II - practical storage

considerations. Society of Motion Picture & Television Engineers Journal. 1992;101(5):347–53.

12. Allen NS, Edge M, Appleyard JH, Jewitt TS, Horie C v., Francis D. Acid-catalysed degradation of historic cellulose triacetate, cinematographic film: Influence of various film parameters. European Polymer Journal. 1988;24(8):707–12.

13. Edge M, Allen NS, Jewitt TS, Horie C v. Fundamental aspects of the degradation of cellulose triacetate base cinematograph film. Polymer Degradation and Stability [Internet]. 1989;25(2–4):345–62. Available from: http://dx.doi.org/10.1016/S0141-3910(89)81016-X

14. Reilly JM. IPI Storage Guide for Acetate Film. Rochester, NY: Image Permanence Institute, Rochester Institute of Technology; 1993.

15. Schorsch K. Vinegar Syndrome is Eating Away Cook County History. WBEZ [Internet]. 2019 Jun 12; Available from: https://www.wbez.org/stories/vinegar-syndrome-is-eating-away-cook-county-history/b7cb51f3-faee-4532-b710-3f9d5597fd90

16. Thompson M. Cash-strapped archive struggles to preserve indigenous history. The Conversation [Internet]. 2012 Jan 24; Available from: https://theconversation.com/cash-strapped-archive-struggles-to-preserve-indigenous-history-5015

17. Mazurek J, Laganà A, Dion V, Etyemez S, Carta C, Schilling MR. Investigation of cellulose nitrate and cellulose acetate plastics in museum collections using ion chromatography and size exclusion chromatography. Journal of Cultural Heritage [Internet]. 2018;35:263–70. Available from: https://doi.org/10.1016/j.culher.2018.05.011

18. Rankin E. A Betrayal of Material: Problems of Conservation in the Constructivist Sculpture of Naum Gabo and Antoine Pevsner. Leonardo. 1988;21(3):285–90.

19. Lodder C. Naum Gabo and the Quandaries of the Replica. Tate Papers [Internet]. 2007;8:1–5. Available from: https://www.tate.org.uk/research/publications/tate-papers/08/naum-gabo-and-the-quandaries-of-the-replica

20. Kearney M, Parkin I, Townsend JH, Hidalgo M, Curran K. Characterisation of VOCs Surrounding Naum Gabo's Construction in Space 'Two Cones ', (Tate) by in situ SPME GC-MS Monitoring . Studies in Conservation. 2018;63(sup1):369–71.

21. Keneghan B. The Popart project. V&A Conservation Journal [Internet]. 2011;(59):28–9. Available from: http://www.vam.ac.uk/

22. Keneghan B, van Oosten T, Laganà A, Wagenaar M, Barabant G, Balcar N, et al. 2.1 In what condition are my artefacts? Case studies. In: Lavédrine B, Fournier A, Martin G, editors. Preservation of Plastic Artefacts in Museum Collections. Comité Des Travaux Historiques Et Scientifiques; 2012. p. 109–37.

23. Barabant G. Appendix 2. Degradation associated with some plastics found during surveys of three French collections. In: Lavédrine B, Fournier A, Martin G, editors. Preservation of Plastic Artefacts in Museum Collections. Comité Des Travaux Historiques Et Scientifiques; 2012. p. 298–301.

24. degradation. In: Collins English Dictionary - Complete & Unabridged 2012 Digital Edition [Internet]. HarperCollins; 2012. Available from: https://www.dictionary.com/browse/degradation

25. degradation [Internet]. Dictionary.com. 2021 [cited 2021 Mar 9]. Available from: https://www.dictionary.com/browse/degradation

26. Allen NS, Edge M, Appleyard JH, Jewitt TS, Horie CV, Francis D. Degradation of cellulose triacetate cinematographic film: Prediction of archival life. Polymer Degradation and Stability. 1989;23(1):43–50.

27. Groom S. Foundry Welding Goggles and Lenses: A Case Study in Cellulose Acetate Degradation. AICCM Bulletin. 1999;24(1):29–38.

28. Giachet MT, Schilling M, McCormick K, Mazurek J, Richardson E, Khanjian H, et al. Assessment of the composition and condition of animation cels made from cellulose acetate. Polymer Degradation and Stability [Internet]. 2014;107:223–30. Available from: http://dx.doi.org/10.1016/j.polymdegradstab.2014.03.009

29. Shinagawa Y, Murayama M, Sakaino Y. Investigation of the archival stability of cellulose triacetate film: The effect of additives to CTA support. In: Allen NS, Edge M, Horie C v., editors. Polymers in Conservation. Cambridge, UK: Royal Society of Chemistry; 1992. p. 138–50.

30. Littlejohn D, Pethrick RA, Quye A, Ballany JM. Investigation of the degradation of cellulose acetate museum artefacts. Polymer Degradation and Stability [Internet]. 2013;98(1):416–24. Available from: http://dx.doi.org/10.1016/j.polymdegradstab.2012.08.023

31. Bigourdan JL, Reilly JM. Environment and Enclosures in Film Preservation. 1997.

32. Bao CY, Long DR, Vergelati C. Miscibility and dynamical properties of cellulose acetate/plasticizer systems. Carbohydrate Polymers [Internet]. 2015;116:95–102. Available from: http://dx.doi.org/10.1016/j.carbpol.2014.07.078

33. Wisniak J. Paul Schützenberger. Educacion Quimica [Internet]. 2015;26(1):57–65. Available from: http://dx.doi.org/10.1016/S0187-893X(15)72100-2

34. Schützenberger P. Action de l'acide acétique anhydre sur la cellulose, les sucres, la mannite et ses congénères. Comptes Rendus de l'Académie des Sciences. 1865;61:485–6.

35. Chanda M, Roy S. Industrial Polymers. In: Plastics Technology Handbook. 4th ed. Boca Raton, FL: CRC Press, Taylor & Francis; 2007. p. 128–32.

36. Heinze T, Liebert T. Characteristics of celllose acetates— Chemical characteristics of cellulose acetate. Macromolecular Symposia. 2004;208:167–237.

37. Zugenmaier P. Characteristics of cellulose acetates— Characterization and physical properties of cellulose acetates. Macromolecular Symposia [Internet]. 2004 Mar;208(1):81–166. Available from: http://doi.wiley.com/10.1002/masy.200450407

38. Carollo P, Grospietro B. Plastic materials. Macromolecular Symposia [Internet]. 2004 Mar;208(1):335–52. Available from: http://doi.wiley.com/10.1002/masy.200450414

39. Rustemeyer P. History of CA and evolution of the markets. Macromolecular Symposia. 2004;208:1–6.

40. Saka S. The raw materials of CA— Wood as natural raw materials for cellulose acetate production. Macromolecular Symposia [Internet]. 2004 Mar;208(1):7–28. Available from: http://doi.wiley.com/10.1002/masy.200450402

41. Saka S. The raw materials of CA—Cotton fibers as natural raw materials for cellulose acetate production. Macromolecular Symposia [Internet]. 2004 Mar;208(1):29–36. Available from: http://doi.wiley.com/10.1002/masy.200450403

42. Steinmeier H. Acetate manufacturing, process and technology— Chemistry of cellulose acetylation. Macromolecular Symposia [Internet]. 2004 Mar;208(1):49–60. Available from: http://doi.wiley.com/10.1002/masy.200450405

43. Hummel A. Acetate manufacturing, process and technology— Industrial processes. Macromolecular Symposia [Internet]. 2004 Mar;208(1):61–80. Available from: http://doi.wiley.com/10.1002/masy.200450406

44. Bao C. Cellulose acetate / plasticizer systems : structure, morphology and dynamics. 2015.

45.   King R, Grau-Bové J, Curran K. Plasticiser loss in heritage collections: its prevalence, cause, effect, and methods for analysis. Heritage Science [Internet]. 2020;8(1):1–17. Available from: https://doi.org/10.1186/s40494-020-00466-0

46.   Schilling M, Bouchard M, Khanjian H, Learner T, Phenix A, Rivenc R. Application of chemical and thermal analysis methods for studying cellulose ester plastics. Accounts of Chemical Research. 2010;43(6):888–96.

47.   Law RC. Cellulose acetate in textile application. Macromolecular Symposia. 2004;208:255–66.

48.   "You Can't See the Join!" - Recovering Morecambe and Wise (Part 1) [Internet]. BBC Research and Development. 2017 [cited 2021 Mar 12]. Available from: https://www.bbc.co.uk/rd/blog/2017-12-morecambe-wise-video-film-archive-restoration

49.   Appeal bid to save Graham Herbert's Dorset photographs. BBC [Internet]. 2017 Nov 8; Available from: https://www.bbc.co.uk/news/uk-england-dorset-41914141

50.   Fordyce CR. Improved Safety Motion Picture Film Support. Journal of the Society of Motion Picture Engineers [Internet]. 1948 Oct;51(4):331–50. Available from: http://ieeexplore.ieee.org/lpdocs/epic03/wrapper.htm?arnumber=7250944

51.   Cummings JW, Hutton AC, Silfin H. Spontaneous Ignition of Decomposing Cellulose Nitrate Film. Journal of the Society of Motion Picture and Television Engineers [Internet]. 1950 Mar;54(3):268–74. Available from: http://ieeexplore.ieee.org/lpdocs/epic03/wrapper.htm?arnumber=7251200

52.   Ciliberto E, Gemmellaro P, Iannuso V, la Delfa S, Urso RG, Viscuso E. Characterization and Weathering of Motion-picture Films with Support of Cellulose Nitrate, Cellulose Acetate and Polyester. Procedia Chemistry [Internet]. 2013;8:175–84. Available from: http://dx.doi.org/10.1016/j.proche.2013.03.023

53.   BFI Master Film Store [Internet]. AJ Buildings Library. 2011 [cited 2021 Mar 12]. Available from: https://www.ajbuildingslibrary.co.uk/projects/display/id/4219

54.   Edwards HGM, Johnson AF, Lewis IR, Turner P. Raman spectroscopic studies of "Pedigree Doll disease." Polymer Degradation and Stability. 1993;41(3):257–64.

55.   Cruse J. The Comb: Its History and Development. London: Robert Hale; 2007.

56.   Shashoua Y. Conservation of Plastics. Routledge; 2008.

57.   Rainey J. Plastic straw ban? Cigarette butts are the single greatest source of ocean trash. NBC News [Internet]. 2018 Aug 27; Available from: https://www.nbcnews.com/news/us-news/plastic-straw-ban-cigarette-butts-are-single-greatest-source-ocean-n903661

58.   Shibata T. Cellulose acetate in separation technology. Macromolecular Symposia. 2004;208:353–70.

59.   Puls J, Wilson SA, Hölter D. Degradation of Cellulose Acetate-Based Materials: A Review. Journal of Polymers and the Environment. 2011;19(1):152–65.

60.   Quintana R, Persenaire O, Lemmouchi Y, Sampson J, Martin S, Bonnaud L, et al. Enhancement of cellulose acetate degradation under accelerated weathering by plasticization with eco-friendly plasticizers. Polymer Degradation and Stability [Internet]. 2013;98(9):1556–62. Available from: http://dx.doi.org/10.1016/j.polymdegradstab.2013.06.032

61.   Hanson JA. Functional group chemistry. Cambridge, UK: Royal Society of Chemistry; 2001. 11 p.

62.   de Freitas RRM, Senna AM, Botaro VR. Influence of degree of substitution on thermal dynamic mechanical and physicochemical properties of cellulose acetate. Industrial Crops and Products [Internet]. 2017;109(March):452–8. Available from: http://dx.doi.org/10.1016/j.indcrop.2017.08.062

63.   Hiller Jr. LA. The reaction of cellulose acetate with acetic acid and water. Journal of Polymer Science. 1953;10(4):385–423.

64.   Derham M, Edge M, Williams DAR, Williamson DM. The degradation of cellulose triacetate studied by nuclear resonance spectroscopy and molecular modeling. In: Allen NS, Edge M, Horie C v., editors. Polymers in Conservation. Royal Society of Chemistry; 1992. p. 125–37.

65.   Kono H, Oka C, Kishimoto R, Fujita S. NMR characterization of cellulose acetate: Mole fraction of monomers in cellulose acetate determined from carbonyl carbon resonances. Carbohydrate Polymers [Internet]. 2017;170:23–32. Available from: http://dx.doi.org/10.1016/j.carbpol.2017.04.061

66.   Samios E, Dart RK, Dawkins J v. Preparation, characterization and biodegradation studies on cellulose acetates with varying degrees of substitution. Polymer (Guildf). 1997;38(12):3045–54.

67. Goodlett VW, Dougherty JT, Patton HW. Characterization of cellulose acetates by nuclear magnetic resonance. Journal of Polymer Science Part A-1: Polymer Chemistry. 1971;9(1):155–61.

68. Zhang K, Feldner A, Fischer S. FT Raman spectroscopic investigation of cellulose acetate. Cellulose. 2011;18(4):995–1003.

69. He J, Tang Y, Wang SY. Alkaline treatment of diacetate fibers and subsequent cellulase degradation. Journal of Applied Polymer Science [Internet]. 2008 Feb 15;107(4):2466–74. Available from: http://doi.wiley.com/10.1002/app.27373

70. Shenton H. Addressing Cellulose Acetate Microfilm from a British Library perspective. LIBER Quarterly. 2005;15(2).

71. Hacke M, Willey J, Mitchell G, Rushworth ID, Higgitt C, Gibson LT. Investigation of long term storage solutions for rubber garments. Journal of the Institute of Conservation [Internet]. 2014 Jul 3;37(2):179–96. Available from: https://www.tandfonline.com/doi/full/10.1080/19455224.2014.931 872

72. Hackney S. Colour measurement of acid-detector strips for the quantification of volatile organic acids in storage conditions. Studies in Conservation. 2016;61:55–69.

73. Ballany JM. An Investigation of the Factors Affecting the Degradation of Cellulose Acetate Artefacts in Museum Collections. 2000.

74. Curran K, Underhill M, Gibson LT, Strlic M. The development of a SPME-GC/MS method for the analysis of VOC emissions from historic plastic and rubber materials. Microchemical Journal [Internet]. 2016;124:909–18. Available from: http://dx.doi.org/10.1016/j.microc.2015.08.027

75. Kammer J, Truong F, Boissard C, Soulié AL, Dupont AL, Simon L, et al. Quantitative and qualitative assessment of VOCs emitted from cellulose acetate movie films by PTR-ToF-MS. Journal of Cultural Heritage [Internet]. 2020;(xxxx). Available from: https://doi.org/10.1016/j.culher.2020.09.004

76. Adelstein PZ, Reilly JM, Nishimura DW, Erbland CJ. Stability of cellulose ester base photographic film: part III - measurement of film degradation. Society of Motion Picture & Television Engineers Journal. 1995;104(5):281–91.

77. Parekh VJ, Rathod VK, Pandit AB. Substrate Hydrolysis. In: Comprehensive Biotechnology. 2nd ed. Elsevier; 2011. p. 103–18.

78. Knight B. Lack of evidence for an autocatalytic point in the degradation of cellulose acetate. Polymer Degradation and Stability

[Internet]. 2014;107:219–22. Available from: http://dx.doi.org/10.1016/j.polymdegradstab.2013.12.002

79. Curran K, Underhill M, Grau-Bové J, Fearn T, Gibson LT, Strlič M. Classifying Degraded Modern Polymeric Museum Artefacts by Their Smell. Angewandte Chemie - International Edition. 2018;57(25):7336–40.

80. Curran K, Možir A, Underhill M, Gibson LT, Fearn T, Strlič M. Cross-infection effect of polymers of historic and heritage significance on the degradation of a cellulose reference test material. Polymer Degradation and Stability [Internet]. 2014;107:294–306. Available from: http://dx.doi.org/10.1016/j.polymdegradstab.2013.12.019

81. Sutherland K, Schwarzinger C, Price BA. The application of pyrolysis gas chromatography mass spectrometry for the identification of degraded early plastics in a sculpture by Naum Gabo. Journal of Analytical and Applied Pyrolysis [Internet]. 2012;94:202–8. Available from: http://dx.doi.org/10.1016/j.jaap.2011.12.016

82. Vos KD, Burris FO, Riley RL. Kinetic study of the hydrolysis of cellulose acetate in the pH range of 2–10. Journal of Applied Polymer Science. 1966;10(5):825–32.

83. Stephens CH. Effect of residual sulfur content on the degradation behavior of cellulose acetate. Journal of the American Institute for Conservation [Internet]. 2018;57(4):221–8. Available from: https://doi.org/10.1080/01971360.2018.1535029

84. Yarsley V, Flavell W, Adamson P, Perkins N. Cellulosic plastics: cellulose acetate; cellulose ethers; regenerated cellulose; cellulose nitrate. London: Illiffe Books Ltd.; 1964. 3–7 p.

85. Wadsworth L, Daponte D. No Title. In: Nevell T, Zernonian S, editors. Cellulose chemistry and it's applications. Chichester: Ellis Horwood Ltd.; 1985. p. 344–62.

86. Lipscomb A. Cellulose acetate, it's manufacture and applications. London: Ernest Benn Ltd.; 1933.

87. Ram AT, McCrea JL. Stability of Processed Cellulose Ester Photographic Films. SMPTE Journal [Internet]. 1988 Jun;97(6):474–83. Available from: http://ieeexplore.ieee.org/lpdocs/epic03/wrapper.htm?arnumber=7270932

88. Rudnik E. Compostable Polymer Materials: Definitions, Structures, and Methods of Preparation. Handbook of Biopolymers and Biodegradable Plastics [Internet]. 2013 Jan 1 [cited 2019 Nov 6];189–211. Available from:

https://www.sciencedirect.com/science/article/pii/B978145572834
3000100

89. Olaru N, Andriescu A, Olaru L. On the hydrolysis of cellulose acetate in toluene/acetic acid/water system. European Polymer Journal. 2001;37(4):865–7.

90. Mayes HB, Broadbelt LJ. Unraveling the reactions that unravel cellulose. Journal of Physical Chemistry A. 2012;116(26):7098–106.

91. Cabiac A, Guillon E, Chambon F, Pinel C, Rataboul F, Essayem N. Cellulose reactivity and glycosidic bond cleavage in aqueous phase by catalytic and non catalytic transformations. Applied Catalysis A: General [Internet]. 2011;402(1–2):1–10. Available from: http://dx.doi.org/10.1016/j.apcata.2011.05.029

92. Hosono K, Kanazawa A, Mori H, Endo T. Photodegradation of cellulose acetate film in the presence of benzophenone as a photosensitizer. Journal of Applied Polymer Science [Internet]. 2007 Sep 15;105(6):3235–9. Available from: http://doi.wiley.com/10.1002/app.26386

93. Edge M, Allen NS, Jewitt TS, Horie C v. The inhibition of oxidative and hydrolytic degradation pathways in archival cellulose-triacetate base cinematograph films. Polymer Degradation and Stability. 1990;29(1):31–48.

94. Staudinger H, Heuer W. Über hochpolymere Verbindungen, 33. Mitteilung: Beziehungen zwischen Viscosität und Molekulargewicht bei Poly-styrolen. Berichte der deutschen chemischen Gesellschaft (A and B Series) [Internet]. 1930 Jan 8;63(1):222–34. Available from: http://doi.wiley.com/10.1002/cber.19300630129

95. Liu L, Gong D, Bratasz L, Zhu Z, Wang C. Degradation markers and plasticizer loss of cellulose acetate films during ageing. Polymer Degradation and Stability [Internet]. 2019;168:108952. Available from: https://doi.org/10.1016/j.polymdegradstab.2019.108952

96. Wakeman H. Mechanical Properties of Cellulose and Its Derivatives. In: Ott E, Spurlin HM, Grafflin MW, editors. Cellulose and Cellulose Derivatives, Part III. 2nd ed. New York: Interscience Publishers; 1955. p. 1247–355.

97. Jane Ballany, David Littlejohn, Richard A. Pethrick, Anita Quye. Probing the Factors That Control Degradation in Museum Collections of Cellulose Acetate Artefacts. In: Historic Textiles, Papers, and Polymers in Museums [Internet]. 2000. p. 145–65. Available from: http://dx.doi.org/10.1021/bk-2001-0779.ch012

98. Tsang J sun, Madden O, Coughlin M, Maiorana A, Watson J, Little NC, et al. Degradation of "Lumarith" Cellulose Acetate: Examination and Chemical Analysis of a Saleseman's Sample Kit. Studies in Conservation. 2009;54(2):90–105.

99. Lawton TS, Nason HK. Effect of Ultraviolet Light on Cellulose Acetate and Nitrate. Industrial & Engineering Chemistry. 2005;36(12):1128–30.

100. Ram AT. Archival preservation of photographic films - A perspective. Polymer Degradation and Stability. 1990;29(1):3–29.

101. Williamson DM. The degradation of cellulose acetate base motion picture film. 1994.

102. Mu B, Xu H, Yang Y. Accelerated hydrolysis of substituted cellulose for potential biofuel production: Kinetic study and modeling. Bioresource Technology [Internet]. 2015;196:332–8. Available from: http://dx.doi.org/10.1016/j.biortech.2015.07.093

103. Karst DT, Yang Y, Tanaka G. An explanation of increased hydrolysis of the β-(1,4)-glycosidic linkages of grafted cellulose using molecular modeling. Polymer (Guildf). 2006;47(18):6464–71.

104. Rosenthal AJ. Kinetics of the acid-catalyzed degradation of cellulose esters. Journal of Polymer Science. 1961;51(155):111–22.

105. Namchuk MN, Mccarter JD, Becalski A, Andrews T, Withers SG. The Role of Sugar Substituents in Glycoside Hydrolysis. J Am Chem Soc. 2000;(10):1270–7.

106. Lure BA, Valishina ZT, Svetlov BS. Kinetics and mechanism of the chemical transformation of nitrocellulose under the action of aqueous sulphuric acid solutions. Polymer Science USSR. 1991;33(1):99–106.

107. Tsygankova NG, Kaputskii FN, Grinshnap DD. No Title. Khimiya drevesiny [Chemistry of Wood]. 1983;70.

108. Malm CJ, Glegg RE, Salzer JT, Ingerick DF, Tanghe LJ. Hydrolysis of cellulose esters. Industrial and Engineering Chemistry Process Design and Development. 1966;5(1):81–7.

109. Robertson RM, Thomas WC, Suthar JN, Brown DM. Accelerated degradation of cellulose acetate cigarette filters using controlled-release acid catalysis. Green Chemistry. 2012;14(8):2266–72.

110. Pan X, Gilkes N, Saddler JN. Effect of acetyl groups on enzymatic hydrolysis of cellulosic substrates. Holzforschung. 2006;60(4):398–401.

111. Kovačić T, Mrklić Ž. The kinetic parameters for the evaporation of plasticizers from plasticized poly(vinyl chloride). Thermochimica Acta. 2002;381(1):49–60.

112. Calvert PD, Billingham NC. Loss of additives from polymers: A theoretical model. Journal of Applied Polymer Science. 1979;24(2):357–70.

113. Rambaldi DC, Suryawanshi C, Eng C, Preusser FD. Effect of thermal and photochemical degradation strategies on the deterioration of cellulose diacetate. Polymer Degradation and Stability [Internet]. 2014;107:237–45. Available from: http://dx.doi.org/10.1016/j.polymdegradstab.2013.12.004

114. Richardson E, Truffa Giachet M, Schilling M, Learner T. Assessing the physical stability of archival cellulose acetate films by monitoring plasticizer loss. Polymer Degradation and Stability [Internet]. 2014;107:231–6. Available from: http://dx.doi.org/10.1016/j.polymdegradstab.2013.12.001

115. Michalski S. Double the life for each five-degree drop, more than double the life for each halving of relative humidity. Thirteenth Triennial meeting ICOM-CC. 2002;(3):66–72.

116. Truhlar DG, Garrett BC, V BB, K- MS, Klippenstein SJ. Current Status of Transition-State Theory. Journal of Physical Chemistry. 1996;100(31):12771–800.

117. Arrhenius S. On the reaction rate of the inversion of non-refined sugar upon souring. Z Phys Chem. 1889;4:226–48.

118. Laidler KJ. The Development of the Arrhenius Equation. Journal of Chemical Education. 1984;61(6):494–8.

119. Shashoua Y. Modern Plastics: Do They Suffer From the Cold? Studies in Conservation. 2004;49(sup2):91–5.

120. Bigourdan JL. Stability of Acetate Film Base: Accelerated-Aging Data Revisited. Journal of Imaging Science and Technology. 2006;50(5):494–501.

121. Adelstein PZ, Bigourdan JL, Reilly JM. Moisture Relationships of Photographic Film. Journal of the American Institute for Conservation. 1997;36(3):193.

122. Shashoua Y. Storing plastics in the cold - more harm than good? In: Verger I, editor. Preprints of the 14th ICOM-CC Triennial Meeting. The Hague: James & James Ltd.; 2005. p. 358–64.

123. Feller RL. Theoretical Aspects of Photochemical Deterioration. In: Berland D, editor. Accelerated Aging: Photochemical and Thermal Aspects. The Getty Conservation Institute; 1994. p. 45–62.

124. Pastorelli G, Strlič M. 2.3 Development of dose-response functions for historic plastic materials. In: Lavédrine B, Fournier A, Martin G, editors. Preservation of Plastic Artefacts in Museum Collections. Comité Des Travaux Historiques Et Scientifiques; 2012. p. 151–5.

125. Goodman TM. International standards for colour [Internet]. Second Edi. Colour Design: Theories and Applications: Second Edition. Elsevier Ltd.; 2012. 417–452 p. Available from: http://dx.doi.org/10.1016/B978-0-08-101270-3.00018-7

126. Pickett JE. Reversible post-exposure yellowing of weathered polymers. Polymer Degradation and Stability. 2004;85(1):681–7.

127. Feller RL, Curran M, Colaluca V, Bogaard J, Bailie C. Photochemical deterioration of poly(vinylbutyral) in the range of wavelengths from middle ultraviolet to the visible. Polymer Degradation and Stability. 2007;92(5):920–31.

128. Morris RA, Prejean TG, Green JG. Dark time yellowing of white rigid vinyl outdoor weatherable compounds. Journal of Vinyl Technology. 1986;8(2):86–93.

129. Bigourdan J louis, Reilly JM. Effectiveness of Storage Conditions in Controlling the Vinegar Syndrome: Preservation Strategies for Acetate Base Motion-Picture Film Collections. In: Aubert M, Billeaud R, editors. Image and Sound Archiving and Access: the Challenges of the 3rd Millenium, proceedings of the Joint Technical Symposium. Paris; 2000. p. 14–34.

130. Gehlen MH. Kinetics of autocatalytic acid hydrolysis of cellulose with crystalline and amorphous fractions. Cellulose. 2010;17(2):245–52.

131. Curran K, Zimmermann N. The Dynamics of Collaboration in Heritage Science. Studies in Conservation [Internet]. 2021;0(0):1–14. Available from: https://doi.org/10.1080/00393630.2021.1875175

132. Saunders D. Museum Lighting: A Guide for Conservators and Curators. Getty Publications; 2020.

133. Nishimura D. Strategies for the storage of cellulose acetate film. AIC News. 2015;40(6):1–5.

134. Padfield T. Condensation in film containers during cooling and warming. In: Nissen D, Larsen LR, Christensen T, Johnsen JS, editors. Postprints of Preserve, then Show. Copenhagen: The Danish Film Institute; 2002. p. 1–9.

135. Ram AT, Holtz CF, Sehlin RC, Kopperl DF. Method for improving the archival properties of a processed photographic film in a storage assembly for achieving the same. United States; US5215192A, 1993.

136. Ligterink FJ. Notes on the use of acid absorbents in storage of cellulose acetate-based materials. Contributions to conservation. 2002. p. 64–73.

137. Viggiani MA. Film archival storage and preservation system. United States; US20020108876A1, 2002.

138. Matsui K, Ishii T, Hashimoto A. Film deterioration preventing material and acidic gas removing agent. EP3357557A1, 2016.

139. Sawaguchi T, Yano S, Morimatsu Y, Sakaki M. Method of removing acid component in deteriorated acetate film. United States; US7144461B2, 2006.

140. Quye A. Care Advice Summary. In: Quye A, Williamson CJ, editors. Plastics: Collecting and Conserving. NMS Publishing Ltd.; 1999. p. 136–7.

141. Kansou K, Rémond C, Paës G, Bonnin E, Tayeb J, Bredeweg B. Testing scientific models using Qualitative Reasoning: Application to cellulose hydrolysis. Scientific Reports. 2017;7(1):1–18.

142. Reilly JM, Nishimura DW, Zinn E. New Tools for Preservation: Assessing Long-Term Environmental Effects on Library and Archives Collections. Washington, D.C.: The Commission on Preservation and Access; 1995.

143. Gagliardi M, Lenarda P, Paggi M. A reaction-diffusion formulation to simulate EVA polymer degradation in environmental and accelerated ageing conditions. Solar Energy Materials and Solar Cells [Internet]. 2017;164(October 2016):93–106. Available from: http://dx.doi.org/10.1016/j.solmat.2017.02.014

144. Emsley AM. The kinetics and mechanisms of degradation of cellulosic insulation in power transformers. Polymer Degradation and Stability. 1994;44(3):343–9.

145. Bernstein R, Gillen KT. Nylon 6.6 accelerating aging studies: II. Long-term thermal-oxidative and hydrolysis results. Polymer Degradation and Stability [Internet]. 2010;95(9):1471–9. Available from: http://dx.doi.org/10.1016/j.polymdegradstab.2010.06.018

146. Laycock B, Nikolić M, Colwell JM, Gauthier E, Halley P, Bottle S, et al. Lifetime prediction of biodegradable polymers. Progress in Polymer Science. 2017;71:144–89.

147. Knab TD, Little SR, Parker RS. A systems approach to modeling drug release from polymer microspheres to accelerate in vitro to in vivo translation. Journal of Controlled Release [Internet]. 2015;211:74–84. Available from: http://dx.doi.org/10.1016/j.jconrel.2015.04.045

148. Peppas NA, Narasimhan B. Mathematical models in drug delivery: How modeling has shaped the way we design new drug delivery systems. Journal of Controlled Release [Internet]. 2014;190:75–81. Available from: http://dx.doi.org/10.1016/j.jconrel.2014.06.041

149. Sackett CK, Narasimhan B. Mathematical modeling of polymer erosion: Consequences for drug delivery. International Journal of Pharmaceutics [Internet]. 2011;418(1):104–14. Available from: http://dx.doi.org/10.1016/j.ijpharm.2010.11.048

150. Tosin M, Pischedda A, Degli-Innocenti F. Biodegradation kinetics in soil of a multi-constituent biodegradable plastic. Polymer Degradation and Stability [Internet]. 2019;166:213–8. Available from: https://doi.org/10.1016/j.polymdegradstab.2019.05.034

151. Chinaglia S, Tosin M, Degli-Innocenti F. Biodegradation rate of biodegradable plastics at molecular level. Polymer Degradation and Stability [Internet]. 2018;147(October 2017):237–44. Available from: https://doi.org/10.1016/j.polymdegradstab.2017.12.011

152. Waller R, Michalski S. Effective Preservation: From Reaction to Prediction. The Getty Conservation Institute Newsletter [Internet]. 2004;19(1):4–9. Available from: http://repositorio.unan.edu.ni/2986/1/5624.pdf

153. Strlič M, Grossi CM, Dillon C, Bell N, Fouseki K, Brimblecombe P, et al. Damage function for historic paper. Part I: Fitness for use. Heritage Science. 2015;3(1):1–12.

154. Strlič M, Grossi CM, Dillon C, Bell N, Fouseki K, Brimblecombe P, et al. Damage function for historic paper. Part II: Wear and tear. Heritage Science. 2015;3(1):1–11.

155. Strlič M, Grossi CM, Dillon C, Bell N, Fouseki K, Brimblecombe P, et al. Damage function for historic paper. Part III: Isochrones and demography of collections. Heritage Science. 2015;3(1):1–11.

156. Ekenstam A. The behaviour of cellulose in mineral acid solutions: kinetic study of the decomposition of cellulose in acid solutions. Berichte der deutschen chemischen Gesellschaft. 1936;69:553.

157. Fenech A, Fearn T, Strlic M. Use of Design-of-Experiment principles to develop a dose-response function for colour photographs. Polymer Degradation and Stability [Internet]. 2012;97(4):621–5. Available from: http://dx.doi.org/10.1016/j.polymdegradstab.2012.01.012

158. Zou X, Uesaka T, Gurnagul N. Prediction of paper accelerated aging I. aging process permanence by Kinetic analysis of the aging process. Cellulose [Internet]. 1996;3:243–67. Available from: https://link-springer-com.libproxy.ucl.ac.uk/content/pdf/10.1007%2FBF02228805.pdf

159. American Society of Heating, Refrigerating and Air-Conditioning Engineers Inc (ASHRAE). Museums, galleries, archives, and libraries. In: American Society of Heating, Refrigerating and Air-Conditioning Engineers Inc (ASHRAE), editor. 2019 ASHRAE® Handbook Heating, Ventilating, and Air-Conditioning Applications (S-I Edition). American Society of Heating, Refrigerating and Air-Conditioning Engineers, Inc. (ASHRAE); 2019.

160. Sebera DK. Isoperms: An Environmental Management Tool [Internet]. 1994. Available from: https://www.clir.org/pubs/reports/isoperm/isoperm/

161. Nishimura DW. Understanding Preservation Metrics [Internet]. Rochester, NY; 2007. Available from: https://www.imagepermanenceinstitute.org/webfm_send/536

162. Collections Environmental Monitoring [Internet]. Image Permanence Institute. [cited 2021 Oct 6]. Available from: https://www.imagepermanenceinstitute.org/research/environmental.html

163. Ankersmit B, Stappers MHL, Kramer R. Guideline in Jeopardy: Observations on the Application of the ASHRAE Chapter on Climate Control in Museums. Studies in Conservation. 2018;63(sup1):1–7.

164. Lavédrine B. Photographs of the Past: Process and Preservation. Second Edi. Getty Publications; 2009. 278 p.

165. Zou X, Uesaka T, Gurnagul N. Prediction of paper permanence by accelerated aging II. Comparison of the predictions with natural aging results. Cellulose. 2005;3(1):269–79.

166. Liu Y, Kralj Cigić I, Strlič M. Kinetics of accelerated degradation of historic iron gall ink-containing paper. Polymer Degradation and Stability. 2017;142:255–62.

167. Ligterink F, di Pietro G. The limited impact of acetic acid in archives and libraries. Heritage Science [Internet]. 2018;6(1):1–12. Available from: https://doi.org/10.1186/s40494-018-0225-y

168. Shahani CJ, Harrison G. Spontaneous Formation of Acids in the Natural Aging of Paper. Studies in Conservation. 2014;47(sup3):189–92.

169. Duran-Casablancas C, Strlič M, Beentjes G, de Bruin G, van der Burg J, Grau-Bové J. A Comparison of Preservation Management Strategies for

Paper Collections. Studies in Conservation [Internet]. 2020;0(0):1–9. Available from: https://doi.org/10.1080/00393630.2020.1790264

170. Spurlin HM. Arrangement of Substituents in Cellulose Derivatives. J Am Chem Soc. 1939;61(8):2222–7.

171. Richardson S, Gorton L. Characterisation of the substituent distribution in starch and cellulose derivatives. Analytica Chimica Acta. 2003;497(1–2):27–65.

172. Salmi T, Damlin P, Mikkola JP, Kangas M. Modelling and experimental verification of cellulose substitution kinetics. Chemical Engineering Science [Internet]. 2011;66(2):171–82. Available from: http://dx.doi.org/10.1016/j.ces.2010.10.013

173. Salmi T, Damlin P, Mikkola JP, Kangas M. A chemical engineering approach to cellulose substitution kinetics. Chemical Engineering Transactions. 2011;24:151–6.

174. Salmi T, Valtakari D, Paatero E, Holmbom B, Sjöholm R. Kinetic Study of the Carboxymethylation of Cellulose. Industrial and Engineering Chemistry Research. 1994;33(6):1454–9.

175. Mischnick P, Hennig C. A new model for the substitution patterns in the polymer chain of polysaccharide derivatives. Biomacromolecules. 2001;2(1):180–4.

176. Carvalho-Silva VH, Coutinho ND, Aquilanti V. Temperature dependence of rate processes beyond Arrhenius and Eyring: Activation and transitivity. Frontiers in Chemistry. 2019;7(May):1–11.

177. al Mohtar A, Nunes S, Silva J, Ramos AM, Lopes J, Pinto ML. First-Principles Model to Evaluate Quantitatively the Long-Life Behavior of Cellulose Acetate Polymers. ACS Omega. 2021;

178. Ahmad IR, Cane D, Townsend JH, Triana C, Mazzei L, Curran K. Are we overestimating the permanence of cellulose triacetate cinematographic films? A mathematical model for the vinegar syndrome. Polymer Degradation and Stability [Internet]. 2020 Feb;172:109050. Available from: https://doi.org/10.1016/j.polymdegradstab.2019.109050

179. Kuhn W. Über die Kinetik des Abbaues hochmolekularer Ketten. Berichte der deutschen chemischen Gesellschaft (A and B Series) [Internet]. 1930;63(6):1503–9. Available from: https://onlinelibrary.wiley.com/doi/abs/10.1002/cber.19300630631

180. Mark H, Simha R. Degradation of Long Chain Molecules. Transactions of the Faraday Society. 1940;35:611–8.

181. Montroll EW, Simha R. Theory of Depolymerization of Long Chain Molecules. The Journal of Chemical Physics. 1940;8:721–6.

182. Johansen AM. Monte Carlo methods. In: International Encyclopedia of Education. Elsevier Ltd.; 2010. p. 296–303.

183. Definition of randomness [Internet]. Dictionary.com. [cited 2021 Oct 15]. Available from: https://www.dictionary.com/browse/randomness

184. Stepto RFT. Dispersity in polymer science (IUPAC Recommendations 2009). Pure and Applied Chemistry. 2009;81(2):351–3.

185. Guaita M, Chiantore O, Luda MP. Monte Carlo Simulations of Polymer Degradations. 1. Degradations Without Volatilization. Macromolecules. 1990;23(7):2087–92.

186. Nishida H, Yamashita M, Nagashima M, Hattori N, Endo T, Tokiwa Y. Theoretical prediction of molecular weight on autocatalytic random hydrolysis of aliphatic polyesters. Macromolecules. 2000;33(17):6595–601.

187. Emsley AM, Heywood RJ. Computer modelling of the degradation of linear polymers. Polymer Degradation and Stability. 1995;49(1):145–9.

188. Bose SM, Git Y. Mathematical modelling and computer simulation of linear polymer degradation: Simple scissions. Macromolecular Theory and Simulations. 2004;13(5):453–73.

189. Lyu SP, Schley J, Loy B, Lind D, Hobot C, Sparer R, et al. Kinetics and time-temperature equivalence of polymer degradation. Biomacromolecules. 2007;8(7):2301–10.

190. Calvini P. What went wrong with the kinetics of cellulose degradation? In: Lejeune A, Deprez T, editors. Cellulose : Structure and Properties , Derivatives and Industrial Uses. Nova Science Publishers, Inc.; 2010. p. 417–26.

191. Zervos S. Natural and accelerated ageing of cellulose and paper : A literature review. In: Cellulose: Structure and Properties, Derivatives and Industrial Uses. Nova Science Publishers, Inc.; 2010.

192. Zou X, Gurnagul N, Uesaka T, Bouchard J. Accelerated aging of papers of pure cellulose: mechanism of cellulose degradation and paper embrittlement. Polymer Degradation and Stability. 1994;43(3):393–402.

193. Gehlen MH. Approximate solution of the autocatalytic hydrolysis of cellulose. Cellulose. 2009;16:1069–73.

194. Calvini P, Gorassini A, Merlani AL. On the kinetics of cellulose degradation: Looking beyond the pseudo zero order rate equation. Cellulose. 2008;15(2):193–203.

195. Calvini P, Gorassini A, Luigimerlani A. Autocatalytic degradation of cellulose paper in sealed vessels. Restaurator. 2007;28(1):47–54.

196. Zervos S, Moropoulou A. Cotton cellulose ageing in sealed vessels. Kinetic model of autocatalytic depolymerization. Cellulose. 2005;12(5):485–96.

197. Calvini P. The Influence of Levelling-off Degree of Polymerisation on the Kinetics of Cellulose Degradation. Cellulose. 2005;12(4):445–7.

198. Sharples A. Acid hydrolysis and Alcoholysis. In: Bikales NM, Segal I, editors. High Polymer, Degradation of Cellulose and Its Derivatives Part V. 2nd ed. New York: Wiley-Interscience; 1971.

199. Sharples A. The hydrolysis of cellulose part II. Acid sensitive linkages in egyptian cotton. Journal of Polymer Science. 1954;14(73):95–104.

200. Sharples A, Laboratories HG. The hydrolysis of cellulose and its relation to structure. 1957;3–7.

201. Daruwalla EH, Narsian MG. Detection and identification of acid-sensitive linkages in cellulose fibre substances. Tappi. 1966;49(3):106.

202. Agarwal N, McKean WT, Gustafson RR. Cellulose degradation kinetics in alkaline pulping. In: Proc 6th Intl Symp Wood Pulping Chem. Melbourne, Australia; 1991. p. 213–20.

203. Feller RL, Lee SB, Bogaard J. The kinetics of cellulose deterioration.

204. McBurney LF. Cellulose and Cellulose Derivatives. Part I. 2nd ed. Ott E, Spurlin HM, Grafflin UW, editors. New York: Wiley-Interscience; 1954. 99–176 p.

205. Samios E, Dart RK, Dawkins J v., Vlachonikolis IG. A theoretical examination of the biodegradation of cellulose acetate. Biomedical Letters. 1996;53:105–13.

206. Emsley AM, Stevens GC. Kinetics and mechanisms of the low-temperature degradation of cellulose. Cellulose. 1994;1(1):26–56.

207. Wang Y, Pan J, Han X, Sinka C, Ding L. A phenomenological model for the degradation of biodegradable polymers. Biomaterials. 2008;29(23):3393–401.

208. Han X, Pan J. A model for simultaneous crystallisation and biodegradation of biodegradable polymers. Biomaterials [Internet].

2009;30(3):423–30. Available from:
http://dx.doi.org/10.1016/j.biomaterials.2008.10.001

209. Gleadall A, Pan J, Kruft MA, Kellomäki M. Degradation mechanisms of bioresorbable polyesters. Part 1. Effects of random scission, end scission and autocatalysis. Acta Biomaterialia [Internet]. 2014;10(5):2223–32. Available from: http://dx.doi.org/10.1016/j.actbio.2013.12.039

210. Gleadall A, Pan J, Kruft MA, Kellomäki M. Degradation mechanisms of bioresorbable polyesters. Part 2. Effects of initial molecular weight and residual monomer. Acta Biomaterialia [Internet]. 2014;10(5):2233–40. Available from: http://dx.doi.org/10.1016/j.actbio.2014.01.017

211. Simha R. Kinetics of Degradation and Size Distribution of Long Chain Polymers. Journal of Applied pHysics. 1941;12:569–78.

212. Karst D, Yang Y. Molecular modeling study of the resistance of PLA to hydrolysis based on the blending of PLLA and PDLA. Polymer (Guildf). 2006;47(13):4845–50.

213. Pitt CG, Chasalow FI, Hibionada YM, Klimas DM, Schindler A. Aliphatic polyesters. I. The degradation of poly(ϵ-caprolactone) in vivo. Journal of Applied Polymer Science. 1981;26(11):3779–87.

214. Brownlee J. What is the Difference Between Test and Validation Datasets? [Internet]. Machine Learning Mastery. 2017 [cited 2021 Nov 22]. Available from: https://machinelearningmastery.com/difference-test-validation-datasets/

215. Sata H, Murayama M, Shimamoto S. Properties and applications of cellulose triacetate film. Macromolecular Symposia [Internet]. 2004 Mar;208(1):323–34. Available from: http://doi.wiley.com/10.1002/masy.200450413

216. (MathWorks). goodnessOfFit [Internet]. R2019a Documentation. 2019 [cited 2019 Jul 10]. Available from: https://uk.mathworks.com/help/ident/ref/goodnessoffit.html

217. Schmitt EA, Flanagan DR, Linhardt RJ. Importance of Distinct Water Environments in the Hydrolysis of Poly(dl-lactide-co-glycolide). Macromolecules. 1994;27(3):743–8.

218. da Ros S, Aliev AE, del Gaudio I, King R, Pokorska A, Kearney M, et al. Characterising plasticised cellulose acetate-based historic artefacts by NMR spectroscopy: A new approach for quantifying the degree of substitution and diethyl phthalate contents. Polymer Degradation and Stability. 2021;183.

219. Kono H. Chemical shift assignment of the complicated monomers comprising cellulose acetate by two-dimensional NMR spectroscopy. Carbohydrate Research [Internet]. 2013;375:136–44. Available from: http://dx.doi.org/10.1016/j.carres.2013.04.019

220. Kono H, Hashimoto H, Shimizu Y. NMR characterization of cellulose acetate: Chemical shift assignments, substituent effects, and chemical shift additivity. Carbohydrate Polymers [Internet]. 2015;118:91–100. Available from: http://dx.doi.org/10.1016/j.carbpol.2014.11.004

221. Kono H, Yunoki S, Shikano T, Fujiwara M, Erata T, Takai M. CP/MAS 13C NMR study of cellulose and cellulose derivatives. 1 . Complete assignment of the CP/MAS 13C NMR spectrum of the native cellulose. J Am Chem Soc. 2002;124(25):7506–11.

222. Mazurek J, Laganà A, Dion V, Etyemez S, Carta C, Schilling MR. Investigation of cellulose nitrate and cellulose acetate plastics in museum collections using ion chromatography and size exclusion chromatography. Appendix A Supplementary Data. Journal of Cultural Heritage [Internet]. 2018 Jan;35:263–70. Available from: https://linkinghub.elsevier.com/retrieve/pii/S1296207418301055

223. ISO. Imaging materials - Processed imaging materials - Albums, framing and storage materials ISO 18902. International Organization for Standardization; 2013.

224. Harned HS, Ehlers RW. The dissociation constant of acetic acid from 0 to 60° centigrade. J Am Chem Soc. 1933;55(2):652–6.

225. Petrucci RH, Harwood WS, Herring FG. General Chemistry. 8th ed. Prentice Hall; 2002. 648–653 p.

226. Ghareeb HO. Development of New Analytical Methods To Characterize the Heterogeneity of Cellulose Acetates [Internet]. 2013. Available from: http://tuprints.ulb.tu-darmstadt.de/3333/1/HewaOthmanGhareebDissertation.pdf

227. Box GEP. Science and Statistics. J Am Stat Assoc [Internet]. 1976 Dec;71(356):791–9. Available from: http://www.tandfonline.com/doi/abs/10.1080/01621459.1976.10480949

228. Field C. Forum, Round Table and Vinegar: Managing the Cellulose Acetate Microfilm Challenge. LIBER Quarterly. 2005;15(2).

APPENDIX

A. ANALYTICAL SOLUTION OF EQUATION 4.11

The equation to be integrated is:

$$\int_{[HOAc]_0}^{[HOAc]} \frac{1}{(a-x)(b-x)x}\,dx = \int_0^t k\,d\tau \tag{A.1}$$

The term to be integrated on the left-hand side can be simplified by separating the factors in the denominator, introducing α, β and γ as constants in the numerators.

$$\frac{1}{(a-x)(b-x)x} \equiv \frac{\alpha}{x-a} + \frac{\beta}{x-b} + \frac{\gamma}{x} \tag{A.2}$$

$$\alpha(x^2 - bx) + \beta(x^2 - ax) + \gamma(x^2 - (a+b)x + ab) = 1 \tag{A.3}$$

Equation A.3 must be true for all values of $0 < x < a, b$. Write the following balance for terms that are multiples of x^2:

$$\alpha + \beta + \gamma = 0 \tag{A.4}$$

For terms that are multiples of x (but not x^2):

$$-\alpha b - \beta a - \gamma(a+b) = 0 \tag{A.5}$$

For terms that are not multiples of x:

$$\gamma ab = 1 \tag{A.6}$$

Equation A.4-A.6 define a system of three equations for three unknowns α, β and γ. The solution to this system is:

$$\alpha = \frac{1}{a(b-a)} \tag{A.7}$$

$$\beta = \frac{1}{b(b-a)} \tag{A.8}$$

$$\gamma = \frac{1}{ab} \tag{A.9}$$

With these solutions for the constants in Equation A.2, make a substitution in Equation A.1 to solve the integration problem:

$$\int_{[HOAc]_0}^{[HOAc]} \left(\frac{\alpha}{x-a} + \frac{\beta}{x-b} + \frac{\gamma}{x}\right) dx = \int_0^t k \, d\tau \tag{A.10}$$

$$[\alpha \ln(x-a) + \beta \ln(x-b) + \gamma \ln x]_{[HOAc]_0}^{[HOAc]} = kt \tag{A.11}$$

$$\alpha \ln\left(\frac{[HOAc]-a}{[HOAc]_0-a}\right) + \beta \ln\left(\frac{[HOAc]-b}{[HOAc]_0-b}\right) + \gamma \ln\left(\frac{[HOAc]}{[HOAc]_0}\right) = kt \tag{A.12}$$

B. CONVERTING BETWEEN FREE ACIDITY AND CONCENTRATION

Free acidity is measured by the millilitres of 0.1 M NaOH required to neutralise 1 g of cellulose triacetate film base. Acid is extracted from 1 g of sample using the water-leaching method (76). This method is assumed to give an accurate measurement of how much acetic acid is present in the sample, when used with the appropriate indicator for this acid (metacresol purple) (76). A free acidity of 1 corresponds to 0.001 L × 0.1 M NaOH = 0.0001 mol NaOH, which can neutralise 0.0001 mol of acetic acid. The density of cellulose triacetate is 1.3 g cm^{-3}, so the concentration of acetic acid is 0.0001 mol g^{-1} × 1.3 × 10^6 g m^{-3} = 130 mol m^{-3} (36). Hence free acidity is converted to acetic acid concentration in mol m^{-3} by multiplying by 130.

C. PROCESSING OF LITERATURE DATA USED IN CHAPTER 5

AGU composition was calculated from the Integral values (I_i) in the carbonyl carbon resonances of progressively deacetylated cellulose acetate, HCA 1-3 (65). Assignment of the carbonyl carbons are labelled as i_j, where i is the position of the substituted acetyl group (i = 2, 3, or 6), and subscript j is the AGU. For j, I use the AGU notation defined in chapter 6, Table 6.3. For example, 6_{206} indicates the carbonyl carbon resonance of the 6-position of the 2,6-diacetate AGU. Tables C.1-2 show the original data. The composition of the starting cellulose triacetate was based on an earlier study (220) by the same authors. The DS of each sample was also provided. Although the paper (65) states that the sum of I_1-I_{12} was set to 1, this appears to be an error, as the sum is approximately the DS. This is shown in Table C.3.

Table C.1 Original data from (65).

Sample	Line number	1	2	3	4	5	6
	Assignment	6_{206}	6_{236}	6_{006}	6_{036}	3_{030}	3_{036}
CTA		0	0.915	0	0	0	0
HCA 1		0.12	0.51	0.07	0.09	0.1	0.09
HCA 2		0.07	0.22	0.4	0.06	0.08	0.08
HCA 3		0.06	0.06	0.45	0.09	0.07	0.09

Table C.2 Original data from (65).

Sample	Line number	7	8	9	10	11	12
	Assignment	3_{236}	3_{230}	2_{230}	2_{236}	2_{206}	2_{200}
CTA		0.915	0.085	0.085	0.915	0	0
HCA 1		0.49	0.1	0.1	0.49	0.12	0.02
HCA 2		0.22	0.17	0.19	0.22	0.05	0.05
HCA 3		0.06	0.12	0.12	0.06	0.05	0.04

Table C.3 Nominal DS of CA samples and sum of carbonyl carbon resonances.

Sample	Nominal DS	$\sum I_i$
CTA	2.92	2.915
HCA 1	2.31	2.30
HCA 2	1.81	1.81
HCA 3	1.28	1.27

It was assumed that the sum of I_1-I_{12} should equal exactly the DS, the error is a typo, and the numerical discrepancy is a rounding error. In Tables C.4-5, the data in Table C.1 were normalised so that the sum of I_1-I_{12} add up to the DS.

Table C.4 Processed data following normalisation.

Sample	Line number Assignment	1 6_{206}	2 6_{236}	3 6_{006}	4 6_{036}	5 3_{030}	6 3_{036}
CTA		0	0.91657	0	0	0	0
HCA 1		0.12052	0.51222	0.0703	0.09039	0.10043	0.09039
HCA 2		0.07	0.22	0.4	0.06	0.08	0.08
HCA 3		0.06047	0.06047	0.45354	0.09071	0.07055	0.09071

Table C.5 Processed data following normalisation.

Sample	Line number Assignment	7 3_{236}	8 3_{230}	9 2_{230}	10 2_{236}	11 2_{206}	12 2_{200}
CTA		0.91657	0.08515	0.08515	0.91657	0	0
HCA 1		0.49213	0.10043	0.10043	0.49213	0.12052	0.02009
HCA 2		0.22	0.17	0.19	0.22	0.05	0.05
HCA 3		0.06047	0.12094	0.12094	0.06047	0.05039	0.04031

The following equations were used to obtain the mole fractions χ of the eight AGUs, and are based on Equations 1-8 in (65):

$$\chi_{200} = I_{12} \tag{C.1}$$

$$\chi_{030} = I_5 \tag{C.2}$$

$$\chi_{006} = I_3 \tag{C.3}$$

$$\chi_{230} = (I_8 + I_9)/2 \tag{C.4}$$

$$\chi_{206} = (I_1 + I_{11})/2 \tag{C.5}$$

$$\chi_{036} = (I_4 + I_6)/2 \tag{C.6}$$

$$\chi_{236} = (I_2 + I_7 + I_{10})/3 \tag{C.7}$$

$$\chi_{000} = 1 - (\chi_{200} + \chi_{030} + \chi_{006} + \chi_{230} + \chi_{206} + \chi_{036} + \chi_{236}) \tag{C.8}$$

Negative values of χ_{000} were changed to 0 (Equation 5.17). The final outputs used to train the models are in Table C.6, including the reaction times corresponding to each sample.

Table C.6 Data used for model training.

Sample	Time (min^{-1})	χ_{200}	χ_{030}	χ_{006}	χ_{230}	χ_{206}	χ_{036}	χ_{236}	χ_{000}
CTA	0	0	0	0	0.0852	0	0	0.9166	0
HCA 1	10	0.0201	0.1004	0.0703	0.1004	0.1205	0.0904	0.4988	0
HCA 2	40	0.05	0.08	0.4	0.18	0.06	0.07	0.22	0
HCA 3	70	0.0403	0.0706	0.4535	0.1209	0.0554	0.0907	0.0605	0.1080

D. INTEGRATION OF EQUATIONS 5.1-7

The equations to be integrated are

$$\frac{d[2,3,6\text{ tri}]}{dt} = -(k_I + k_{II} + k_{III})[2,3,6\text{ tri}] \tag{D.1}$$

$$\frac{d[3,6\text{ di}]}{dt} = k_I[2,3,6\text{ tri}] - (k_{IV} + k_V)[3,6\text{ di}] \tag{D.2}$$

$$\frac{d[2,6\text{ di}]}{dt} = k_{II}[2,3,6\text{ tri}] - (k_{VI} + k_{VII})[2,6\text{ di}] \tag{D.3}$$

$$\frac{d[2,3\text{ di}]}{dt} = k_{III}[2,3,6\text{ tri}] - (k_{VIII} + k_{IX})[2,3\text{ di}] \tag{D.4}$$

$$\frac{d[6\text{ mono}]}{dt} = k_{IV}[3,6\text{ di}] + k_{VI}[2,6\text{ di}] - k_X[6\text{ mono}] \tag{D.5}$$

$$\frac{d[2\text{ mono}]}{dt} = k_{VII}[2,6\text{ di}] + k_{VIII}[2,3\text{ di}] - k_{XI}[2\text{ mono}] \tag{D.6}$$

$$\frac{d[3\text{ mono}]}{dt} = k_V[3,6\text{ di}] + k_{IX}[2,3\text{ di}] - k_{XII}[3\text{ mono}] \tag{D.7}$$

Integrating Equation D.1 is straightforward:

$$\int_{[2,3,6\text{ tri}]_0}^{[2,3,6\text{ tri}]} \frac{1}{x}\, dx = -\int_0^t (k_I + k_{II} + k_{III})\, d\tau \tag{D.8}$$

$$\ln\left(\frac{[2,3,6\text{ tri}]}{[2,3,6\text{ tri}]_0}\right) = -(k_I + k_{II} + k_{III})t \tag{D.9}$$

$$[2,3,6\text{ tri}] = [2,3,6\text{ tri}]_0 \exp(-(k_I + k_{II} + k_{III})t) \tag{D.10}$$

Next, solve Equation D.2 substituting Equation D.10 for [2,3,6 tri]:

$$\frac{d[3,6 \text{ di}]}{dt} = k_I[2,3,6 \text{ tri}]_0 \exp(-(k_I + k_{II} + k_{III})t) - (k_{IV} + k_V)[3,6 \text{ di}] \qquad \text{(D.11)}$$

$$\frac{d[3,6 \text{ di}]}{dt} + (k_{IV} + k_V)[3,6 \text{ di}] \qquad \text{(D.12)}$$
$$= k_I([2,3,6 \text{ tri}]_0 \exp(-(k_I + k_{II} + k_{III})t))$$

Equation D.12 has the form

$$\frac{dx}{dt} + p(t)x(t) = q(t) \qquad \text{(D.13)}$$

where $x = [3,6 \text{ di}]$. This can be solved by multiplying by an integrating factor $\mu(t)$:

$$\mu(t)\frac{dx}{dt} + \mu(t)p(t)x(t) = \mu(t)q(t) \qquad \text{(D.14)}$$

which satisfies

$$\mu(t)p(t) = \frac{d\mu}{dt} \qquad \text{(D.15)}$$

so that the left-hand side of Equation D.14 becomes

$$\frac{d}{dt}(\mu(t)x(t)) = \mu(t)q(t) \qquad \text{(D.16)}$$

The integrating factor is

$$\mu(t) = \exp\left(\int p(t)\,dt\right) \qquad \text{(D.17)}$$

With reference to Equation D.12, the terms are

$$p(t) = k_{IV} + k_V \qquad \text{(D.18)}$$

$$q(t) = k_I[2,3,6 \text{ tri}]_0 \exp(-(k_I + k_{II} + k_{III})t) \qquad \text{(D.19)}$$

$$\mu(t) = \exp\left(\int p(t)\, dt\right) = \exp\left((k_{IV} + k_V)t\right) \qquad \text{(D.20)}$$

Substitute the terms into Equation D.16 and integrate:

$$\frac{d}{dt}\left(\exp\left((k_{IV} + k_V)t\right) x(t)\right) \qquad \text{(D.21)}$$
$$= \exp\left((k_{IV} + k_V)t\right)$$
$$\times k_I[2{,}3{,}6 \text{ tri}]_0 \exp\left(-(k_I + k_{II} + k_{III})t\right)$$

$$\int \frac{d}{dt}\left(\exp\left((k_{IV} + k_V)t\right) x(t)\right) dt \qquad \text{(D.22)}$$
$$= c$$
$$+ k_I[2{,}3{,}6 \text{ tri}]_0 \int \exp\left((k_{IV} + k_V\right.$$
$$\left. - (k_I + k_{II} + k_{III}))t\right) dt$$

$$\exp\left((k_{IV} + k_V)t\right) x(t) \qquad \text{(D.23)}$$
$$= c$$
$$+ \frac{k_I[2{,}3{,}6 \text{ tri}]_0}{k_{IV} + k_V - (k_I + k_{II} + k_{III})} \exp\left((k_{IV} + k_V\right.$$
$$\left. - (k_I + k_{II} + k_{III}))t\right)$$

where c is a constant.

$$x(t) = c \exp\left(-(k_{IV} + k_V)t\right) \qquad \text{(D.24)}$$
$$+ \frac{k_I[2{,}3{,}6 \text{ tri}]_0}{k_{IV} + k_V - (k_I + k_{II} + k_{III})} \exp\left(-(k_I + k_{II} + k_{III})t\right)$$

Solve for c:

$$x(0) = [3{,}6 \text{ di}]_0 = c + \frac{k_I[2{,}3{,}6 \text{ tri}]_0}{k_{IV} + k_V - (k_I + k_{II} + k_{III})} \qquad \text{(D.25)}$$

$$c = [3{,}6 \text{ di}]_0 - \frac{k_I[2{,}3{,}6 \text{ tri}]_0}{k_{IV} + k_V - (k_I + k_{II} + k_{III})} \qquad \text{(D.26)}$$

Writing out the full solution for Equation D.2:

$$[3,6 \text{ di}] = \left([3,6 \text{ di}]_0 - \frac{k_I[2,3,6 \text{ tri}]_0}{k_{IV} + k_V - (k_I + k_{II} + k_{III})} \right) \exp(-(k_{IV} + k_V)t) \qquad \text{(D.27)}$$

$$+ \frac{k_I[2,3,6 \text{ tri}]_0}{k_{IV} + k_V - (k_I + k_{II} + k_{III})} \exp(-(k_I + k_{II} + k_{III})t)$$

The solutions for Equation D.3-4 ([2,6 di] and [2,3 di]) are obtained in a similar fashion:

$$[2,6 \text{ di}] = \Bigg([2,6 \text{ di}]_0 \qquad\qquad\qquad\qquad\qquad\qquad\qquad \text{(D.28)}$$

$$- \frac{k_{II}[2,3,6 \text{ tri}]_0}{k_{VI} + k_{VII} - (k_I + k_{II} + k_{III})} \Bigg) \exp(-(k_{VI} + k_{VII})t)$$

$$+ \frac{k_{II}[2,3,6 \text{ tri}]_0}{k_{VI} + k_{VII} - (k_I + k_{II} + k_{III})} \exp(-(k_I + k_{II} + k_{III})t)$$

$$[2,3 \text{ di}] = \Bigg([2,3 \text{ di}]_0 \qquad\qquad\qquad\qquad\qquad\qquad\qquad \text{(D.29)}$$

$$- \frac{k_{III}[2,3,6 \text{ tri}]_0}{k_{VIII} + k_{IX} - (k_I + k_{II} + k_{III})} \Bigg) \exp(-(k_{VIII} + k_{IX})t)$$

$$+ \frac{k_{III}[2,3,6 \text{ tri}]_0}{k_{VIII} + k_{IX} - (k_I + k_{II} + k_{III})} \exp(-(k_I + k_{II} + k_{III})t)$$

Notice that the form of solution for each diacetate $D(t)$ follows the format

$$D(t) = \left(D_0 - \frac{C_D[2,3,6 \text{ tri}]_0}{P_D - Q} \right) \exp(-P_D t) + \frac{C_D[2,3,6 \text{ tri}]_0}{P_D - Q} \exp(-Qt) \qquad \text{(D.30)}$$

where subscript D is used to distinguish between diacetates, C_D is the rate constant for the reaction of 2,3,6-triacetate that yields D, P_D is the sum of the rate constants for the deacetylation reactions that deplete D, and $Q = k_I + k_{II} + k_{III}$. For example, when $D = [3,6 \text{ di}]$, $C_D = k_I$ and $P_D = k_{IV} + k_V$. To solve Equations D.5-7, notice that these derivatives of the monoacetates $M(t)$ take the form

$$\frac{dM}{dt} = A_1 D_1(t) + A_2 D_2(t) - B_M M(t) \tag{D.31}$$

where subscripts 1 and 2 denote the deacetylation reactions that produce M from diacetates D_1 and D_2, respectively, A_1 and A_2 are the rate constants for those reactions, and B_M is the rate constant for the deacetylation (depletion) of M. For example, when $M(t) = $ [6 mono], $D_1 = $ [3,6 di], $D_2 = $ [2,6 di], $A_1 = k_{IV}$, $A_2 = k_{VI}$, and $B_M = k_X$. Equation D.31 rearranges to:

$$\frac{dM}{dt} + B_M M(t) = A_1 D_1(t) + A_2 D_2(t) \tag{D.32}$$

which resembles the format of Equation D.13. Using the same approach as before (multiplying by an integrating factor), it can be shown that

$$M(t) = \exp(-B_M t)\left\{\int \exp(B_M t)A_1 D_1(t)\, dt + \int \exp(B_M t)A_2 D_2(t)\, dt + c\right\} \tag{D.33}$$

where c is a constant. Consider (either) one of the integral terms:

$$\int \exp(Bt)AD(t)\, dt \tag{D.34}$$

$$= \int \exp(Bt)A\left\{\left(D_0 - \frac{C[2,3,6\ \text{tri}]_0}{P - Q}\right)\exp(-Pt)\right.$$
$$\left. + \frac{C[2,3,6\ \text{tri}]_0}{P - Q}\exp(-Qt)\right\} dt$$

$$= \frac{AC[2,3,6\ \text{tri}]_0}{P - Q}\int \exp\big((B - Q)t\big)\, dt \tag{D.35}$$
$$+ A\left\{D_0 - \frac{C[2,3,6\ \text{tri}]_0}{P - Q}\right\}\int \exp\big((B - P)t\big)\, dt$$

$$= \frac{AC[2,3,6\ \text{tri}]_0 \exp\big((B - Q)t\big)}{(P - Q)(B - Q)} + A\left\{D_0 - \frac{C[2,3,6\ \text{tri}]_0}{P - Q}\right\}\frac{\exp\big((B - P)t\big)}{B - P} \tag{D.36}$$

Substitute Equation D.36 into Equation D.33 and solve for c:

$$M(0) = M_0 = c \tag{D.37}$$

$$+ \sum_{n=1}^{2} \left(\frac{A_n C_n [2,3,6 \text{ tri}]_0}{(P_n - Q)(B - Q)} \right.$$

$$\left. + \frac{A_n}{B - P_n} \left\{ D_n(0) - \frac{C_n [2,3,6 \text{ tri}]_0}{P_n - Q} \right\} \right)$$

$$c = M_0 - \sum_{n=1}^{2} \left(\frac{A_n C_n [2,3,6 \text{ tri}]_0}{(P_n - Q)(B - Q)} + \frac{A_n}{B - P_n} \left\{ D_n(0) - \frac{C_n [2,3,6 \text{ tri}]_0}{P_n - Q} \right\} \right) \tag{D.38}$$

The full solutions for Equations D.5-7 are thus:

[6 mono] (D.39)

$$= [6 \text{ mono}]_0 \exp(-k_X t)$$

$$+ \{ \exp(-(k_I + k_{II} + k_{III})t)$$

$$- \exp(-k_X t) \} \left\{ \frac{k_{IV} k_I [2,3,6 \text{ tri}]_0}{(k_{IV} + k_V - k_I - k_{II} - k_{III})(k_X - k_I - k_{II} - k_{III})} \right\}$$

$$+ \{ \exp(-(k_{IV} + k_V)t) - \exp(-k_X t) \} \left\{ \frac{k_{IV}}{k_X - k_{IV} - k_V} \right\} \left\{ [3,6 \text{ di}]_0 \right.$$

$$\left. - \frac{k_I [2,3,6 \text{ tri}]_0}{(k_{IV} + k_V - k_I - k_{II} - k_{III})} \right\}$$

$$+ \{ \exp(-(k_I + k_{II} + k_{III})t)$$

$$- \exp(-k_X t) \} \left\{ \frac{k_{VI} k_{II} [2,3,6 \text{ tri}]_0}{(k_{VI} + k_{VII} - k_I - k_{II} - k_{III})(k_X - k_I - k_{II} - k_{III})} \right\}$$

$$+ \{ \exp(-(k_{VI} + k_{VII})t) - \exp(-k_X t) \} \left\{ \frac{k_{VI}}{k_X - k_{VI} - k_{VII}} \right\} \left\{ [2,6 \text{ di}]_0 \right.$$

$$\left. - \frac{k_{II} [2,3,6 \text{ tri}]_0}{(k_{VI} + k_{VII} - k_I - k_{II} - k_{III})} \right\}$$

[2 mono] (D.40)

$$= [2 \text{ mono}]_0 \exp(-k_{XI} t)$$

$$+ \{ \exp(-(k_I + k_{II} + k_{III})t)$$

$$- \exp(-k_{XI} t) \} \left\{ \frac{k_{VII} k_{II} [2,3,6 \text{ tri}]_0}{(k_{VI} + k_{VII} - k_I - k_{II} - k_{III})(k_{XI} - k_I - k_{II} - k_{III})} \right\}$$

$$+ \{\exp(-(k_{VI} + k_{VII})t) - \exp(-k_{XI}t)\}\left\{\frac{k_{VII}}{k_{XI} - k_{VI} - k_{VII}}\right\}\left\{[2,6 \text{ di}]_0\right.$$

$$\left. - \frac{k_{II}[2,3,6 \text{ tri}]_0}{(k_{VI} + k_{VII} - k_I - k_{II} - k_{III})}\right\}$$

$$+ \{\exp(-(k_I + k_{II} + k_{III})t)$$

$$- \exp(-k_{XI}t)\}\left\{\frac{k_{VIII}k_{III}[2,3,6 \text{ tri}]_0}{(k_{VIII} + k_{IX} - k_I - k_{II} - k_{III})(k_{XI} - k_I - k_{II} - k_{III})}\right\}$$

$$+ \{\exp(-(k_{VIII} + k_{IX})t) - \exp(-k_{XI}t)\}\left\{\frac{k_{VIII}}{k_{XI} - k_{VIII} - k_{IX}}\right\}\left\{[2,3 \text{ di}]_0\right.$$

$$\left. - \frac{k_{III}[2,3,6 \text{ tri}]_0}{(k_{VIII} + k_{IX} - k_I - k_{II} - k_{III})}\right\}$$

$$[3 \text{ mono}] \tag{D.41}$$

$$= [3 \text{ mono}]_0 \exp(-k_{XII}t)$$

$$+ \{\exp(-(k_I + k_{II} + k_{III})t)$$

$$- \exp(-k_{XII}t)\}\left\{\frac{k_V k_I[2,3,6 \text{ tri}]_0}{(k_{IV} + k_V - k_I - k_{II} - k_{III})(k_{XII} - k_I - k_{II} - k_{III})}\right\}$$

$$+ \{\exp(-(k_{IV} + k_V)t) - \exp(-k_{XII}t)\}\left\{\frac{k_V}{k_{XII} - k_{VI} - k_{VII}}\right\}\left\{[3,6 \text{ di}]_0\right.$$

$$\left. - \frac{k_I[2,3,6 \text{ tri}]_0}{(k_{IV} + k_V - k_I - k_{II} - k_{III})}\right\}$$

$$+ \{\exp(-(k_I + k_{II} + k_{III})t)$$

$$- \exp(-k_{XII}t)\}\left\{\frac{k_{IX}k_{III}[2,3,6 \text{ tri}]_0}{(k_{VIII} + k_{IX} - k_I - k_{II} - k_{III})(k_{XII} - k_I - k_{II} - k_{III})}\right\}$$

$$+ \{\exp(-(k_{VIII} + k_{IX})t) - \exp(-k_{XII}t)\}\left\{\frac{k_{IX}}{k_{XII} - k_{VIII} - k_{IX}}\right\}\left\{[2,3 \text{ di}]_0\right.$$

$$\left. - \frac{k_{III}[2,3,6 \text{ tri}]_0}{(k_{VIII} + k_{IX} - k_I - k_{II} - k_{III})}\right\}$$